FINAL DESIGN REPORT
FOR
HIGH SENSITIVITY INFRARED 10.6-MICROMETER HETERODYNE RECEIVER DEVELOPMENT

April 1972

Contract No.: NAS5-11665

AIL Report 8783-3

Prepared by

AIL, a division of CUTLER-HAMMER
Melville, New York 11746

For

Goddard Space Flight Center
Greenbelt, Maryland 20771

FINAL DESIGN REPORT
FOR
HIGH SENSITIVITY INFRARED 10.6-MICROMETER HETERODYNE RECEIVER DEVELOPMENT

April 1972

Contract No. : NAS5-11665

Goddard Space Flight Center
Contracting Officer: Kent Cockerham
Technical Monitor: John McElroy

Prepared by

AIL, a division of CUTLER-HAMMER
Melville, New York 11746

Project Manager: B. Peyton

For

Goddard Space Flight Center
Greenbelt, Maryland 20771

TABLE OF CONTENTS

		Page
I.	Introduction	1
II.	Functional Performance Measurements on the Optical Receiver Subsystem (ORS)	5
	A. Optical Receiver Subsystem	5
	B. Spatial Acquisition Sequence	7
	C. Conical-Scan Tracking	25
	D. Video Group Delay Measurements	38
	E. Conclusions	41
III.	Performance Measurements on PV HgCdTe Photomixer/Preamplifier Combination	43
	A. Mixer Quantum Efficiency	43
	B. Current/Voltage Characteristics	48
	C. Photomixer Frequency Response	51
	D. Noise Equivalent Power	52
	E. Receiver Sensitivity	55
IV.	Temperature and dc Bias Cycling of PV HgCdTe Photomixers	60
	A. Photomixer 1	60
	B. Photomixer 2	64
	C. Conclusions	66
V.	Design Considerations for an Operational 10.6-Micrometer Heterodyne Receiver	67
	A. Laser Local Oscillator Power Requirements	67
	B. Heat Loads of Photomixer Cooler	72
	C. Photomixer Uniformity	76
	D. Photomixer/Preamplifier Impedance Match	81

		Page
VI.	10.6-Micrometer Heterodyne Detection Using p-Type HgCdTe Photomixers	99
	A. Analysis of Mixing in p-Type HgCdTe	99
	B. Measurement Data	111
VII.	Conclusions	123
VIII.	References	127
Appendixes:		
	A--High-Sensitivity Receiver for Infrared Laser Communications	129
	B--Photomixer Housing	131

LIST OF ILLUSTRATIONS

Figure		Page
1	Simplified Block Diagram of 10.6-Micrometer Infrared Communications Receiver	2
2	Optical Receiver Subsystem Block Diagram	6
3	Acquisition Sequence of Optical Receiver Subsystem	8
4	Functional Diagram of Acquisition Sequence of ORS	11
5	Laboratory Setup for ORS Measurements	12
6	Block Diagram of Test Setup for Electronic Acquisition Measurements	13
7	Probability of Encounter Versus Threshold with IF SNR as a Parameter	17
8	Measured Time Delay Between Optical Acquisition and Electronic Encounter Pulse	18
9	Probability of Encounter Confirm Pulse as a Function of Threshold Level	19
10	Block Diagram of Digitized Raster Drive Circuitry	20
11	Block Diagram of Experimental Setup for Acquisition Encounter Measurements	21
12	Measured Acquisition Sequence of ORS	23
13	Measured Acquisition Sequence with "Stop" Command	24
14	Measured Acquisition Sequence with "Stop" and "Readdress" Commands	26
15	Block Diagram of Test Setup for Direct Detection Tracking Measurements	27
16	Optical Field Patterns With and Without Nutation	29
17	Error Voltage Output of E/W, N/S Synchronous Detectors	30
18	Dc Tracking Error Voltage as a Function of Receiver Boresight Offset	31
19	Postdetection Video Output Level as a Function of Receiver Boresight Offset for IF SNR = -1 dB	33

Figure		Page
20	Composite Plot of System Voltage Levels for Open- and Closed-Loop Operation	35
21	Postdetection Video Output Level as a Function of Boresight Offset for IF SNR = -10 dB	36
22	Postdetection Video Output Level as a Function of Boresight Offset for IF SNR = -20 dB	37
23	Block Diagram of Test Setup for Video Group Delay Measurements	39
24	Measured Time Delay and Amplitude Response of ORS	40
25	Photomixer Housing	44
26	Measured Quantum Efficiency of a HgCdTe Photomixer as a Function of Operating Temperature	45
27	Dynamically Measured Quantum Efficiency of a HgCdTe Photomixer as a Function of Operating Temperature	47
28	I-V Curves for Various Temperatures With/Without LO Illumination	49
29	Reverse Slope Resistance of a PV HgCdTe Photomixer as a Function of Operating Temperature	50
30	Cutoff Frequency Versus Bias Voltage for HgCdTe Photodiode	53
31	Shot Noise Spectrum of HgCdTe Photodiode	54
32	Receiver Sensitivity Versus Mixer Temperature	57
33	Measured Receiver NEP as a Function of Oscillator Power	59
34	Measured Spectral Response of PV HgCdTe Photomixer 1 at the Beginning of Test Period	63
35	Measured Spectral Response of PV HgCdTe Photomixer 1 at the Conclusion of Test Period	63
36	Current-Voltage Characteristics of Photomixer 1 Over a 9-Month Test Period	65
37	Heterodyne Signal-To-Noise Ratio as a Function of Lateral Displacement of LO Laser Beam in Focal Plane with f-Number of Local Oscillator Beam as a Parameter	70

Figure		Page
38	Experimental Setup for Measurement of Laser LO Heat Load	74
39	Block Diagram of Measurement Setup used to Determine Photomixer Uniformity	77
40	Spatial Pattern of Focused CO_2 Laser Beam	79
41	Responsivity Profile of PV HgCdTe Photomixer at Y = 0.025 Position	82
42	Responsivity Profile of HgCdTe Photomixer at Y = 0.017 Position	83
43	Measured Responsivity Contours for HgCdTe Photomixer	85
44	Photomicrograph of PV HgCdTe Mixer	85
45	Engineering Sketch of PV HgCdTe Photomixer	85
46	Norton Equivalent for PV HgCdTe Mixer/Preamplifier	87
47	Total Receiver Noise Versus LO Induced Photocurrent for PV HgCdTe Photomixer	91
48	Equivalent Circuit for Mixer with Finite Dark Conductance	99
49	Theoretical Conductance Ratio Versus LO Power for p-Type HgCdTe (Auger Recombination)	103
50	Measured Mixer Conductance Ratio Versus Applied LO Power in p-Type HgCdTe	112
51	Contact (1/f) Noise Versus IF Frequency in p-Type HgCdTe Dector	115
52	Mixer Noise Power Versus dc Bias Power in p-Type HgCdTe Photomixer	116
53	G-R Noise Spectrum of p-Type HgCdTe Photomixer	117
54	Measured NEP Versus Applied dc Bias Power in p-Type HgCdTe Photomixer	120
55	Elevation Monopulse Antenna Patterns for a 2 by 2 p-Type HgCdTe Photomixer Array	122
56	10.6-Micrometer Optical Receiver Subsystem Breadboard	125

ACKNOWLEDGMENTS

AIL staff members, A. Di Nardo and R. Cardwell have made significant technical contributions to various phases of this program. In addition, M. Aita, F. Anderson, G. Kanischak, R. Lange, E. Sard, and J. Wolczok of AIL have also contributed.

We wish to express our appreciation for the technical direction of Mr. John McElroy of the Advanced Data Systems Division, NASA, Goddard Space Flight Center, Greenbelt, Maryland.

ABSTRACT

This report presents the results of a study on the design of an infrared 10.6-micrometer quantum-noise-limited optical receiver subsystem (ORS).

Laboratory measurements of the ORS demonstrated that:

- Heterodyne receiver sensitivities of less than 10^{-19} W/Hz over the 15 to 40 MHz IF band was achieved for mixer temperatures between 85 and 115 K
- The acquisition sequence could be successfully completed for IF signal-to-noise ratios as low as -24 dB
- The time delay during acquisition was approximately 14 ms and the spatial overshoot was 1 photomixer width
- Spatial tracking was successfully achieved over 11 photomixer widths
- The ORS amplitude variation was ± 0.4 dB and the time delay variation was ± 10 ns over the 26 to 36 MHz IF band

Performance measurements of the HgCdTe photomixer preamplifier combination were carried out for photomixer temperatures up to 152 K and a photomixer frequency response of up to 420 MHz was obtained. Results of temperature and bias cycling of HgCdTe photomixers are reported.

Design considerations for an operational 10.6 micrometer heterodyne receiver are presented in this report. These considerations consist of design data on required laser LO illumination, heat load levels for photomixer cooler, photomixer uniformity and the effects of photomixer impedance match on receiver sensitivity.

Analysis and measurements of 10.6 micrometer heterodyne detection in an extrinsic photoconductive (p-type) HgCdTe photomixer are presented.

I. INTRODUCTION

This Final Design Report of Contract NAS-5-11665 presents design and measurement data on a wide IF bandwidth, infrared 10.6-micrometer quantum-noise-limited optical receiver subsystem (ORS). This subsystem employs a cooled HgCdTe photomixer, a conical scanner for spatial tracking, an acquisition channel for spatial search and station alignment, an automatic frequency control channel to maintain a fixed laser frequency offset, and a communications channel for the heterodyne detection, amplification and demodulation of a frequency-modulated incident signal beam.

Although direct detection is useful in 10.6 micrometer systems when simplicity is desired, heterodyne detection is preferred in many applications because it combines high sensitivity with wide electrical bandwidth, and preserves the phase and frequency characteristics of the infrared signal. Coherent (heterodyne) detection is most practical at the long wavelengths due to reduced quantum noise, easier alignment of signal and local oscillator, and greater diffraction-limited field of view. Also, the CO_2 laser has proven practical as an efficient single-frequency stabilized source for the transmitter and local oscillator (reference 1), and operates in a cooperative atmospheric window. The potential of 10.6 micrometer heterodyne detection has been previously established (references 2 through 7). The infrared receiver system (Figure 1) consists principally of an infrared mixer/preamplifier, associated optical components, and signal processing electronics. Its functions are described in the following paragraphs.

The communications channel includes all circuits from the IF preamplifier to the video output buffer amplifier. Due to the relatively narrow tuning range of the CO_2 LO laser, an IF center frequency of 30 MHz

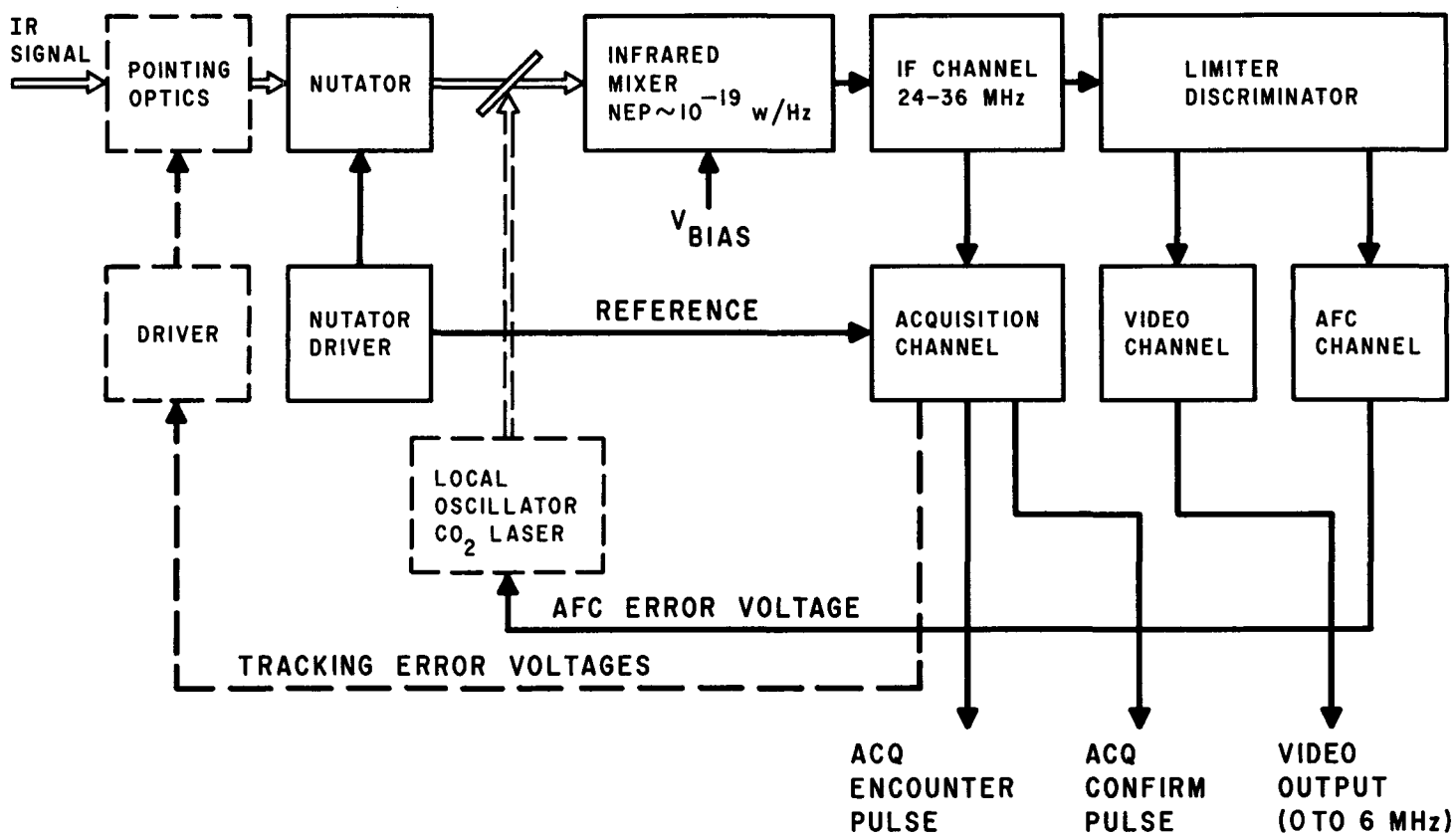

V71-1249R2

FIGURE 1. SIMPLIFIED BLOCK DIAGRAM OF 10.6-MICROMETER INFRARED COMMUNICATIONS RECEIVER

was employed. The FM signal is demodulated in an unusually wide (40-percent bandwidth), highly linear limiter/discriminator. When the frequency separation between the incoming signal and LO frequencies is not exactly 30 MHz, an AFC error voltage is applied to a piezoelectric stack which displaces one of the reflectors of the LO laser thereby changing its output frequency and correcting the error in the frequency offset.

Key technical parameters for laser communication systems are the reliable acquisition of the transmit signal and accurate station tracking.

During the acquisition sequence, the receiver field of view is scanned in an X-Y raster pattern. A narrowband acquisition encounter channel extracts the received signal pulse from noise when the scanning receiver beam intersects the transmit beam located in the search volume dictated by the initial uncertainty of transmitter location. The encounter channel consists of a narrow IF band-pass filter, AM detector, matched filter, and threshold detector which triggers an electronic acquisition pulse. An acquisition confirm channel, which operates at the second harmonic of the conical scan frequency, provides a positive indication of acquisition.

A conical scanner which nutates the received infrared beam to develop east/west and north/south tracking error signals has been demonstrated. The error signals drive receiver pointing optics to maintain the ORS on boresight.

This unique 10.6-micrometer heterodyne receiver has been used in a simulated laser communications link. Measurements have been carried out to determine the effectiveness of the communications, tracking, acquisition, and AFC channels of the ORS. During this testing, system parameters were evaluated under operational conditions. Among these parameters were:

- Probability of encounter
- Probability of confirm

- ORS time delays and the uncertainty of the delay in the generation of the acquisition encounter and confirm pulses
- Selection of threshold voltages for acquisition and confirm channels
- Receiver video group delay
- Closed loop spatial tracking

II. FUNCTIONAL PERFORMANCE MEASUREMENTS ON THE OPTICAL RECEIVER SUBSYSTEM (ORS)

The laboratory measurements aimed at determining system performance of the ORS under simulated operating conditions were carried out to determine the ability of the 10.6-micrometer infrared heterodyne receiver to:

- Acquire weak CO_2 laser transmitter signals
- Discriminate against noise pulses in order to minimize acquisition time
- Spatially track the transmit signal by correcting for spatial changes in attitude or position during the acquisition (or communication) mode
- Maintain a fixed frequency offset between the incoming signal and LO laser by means of automatic frequency control (AFC) channel
- Provide high quality signal processing in the communications channel by impedance matching, and minimizing system group delay with a specially designed delay equalizer

A. OPTICAL RECEIVER SUBSYSTEM

A more detailed block diagram of the electronic portion of the optical receiver subsystem (fabricated and tested at AIL) is shown in Figure 2. As shown, received laser energy is focused onto a photovoltaic HgCdTe photomixer which is also illuminated by a CO_2 laser local oscillator (LO). The IF ($\nu_{sig} - \nu_{LO}$) signal produced by the signal and LO mixing process is amplified, filtered and processed to provide outputs from the acquisition, video and AFC channels. The video channel contains the wideband (6 MHz) communications information. The AFC channel develops

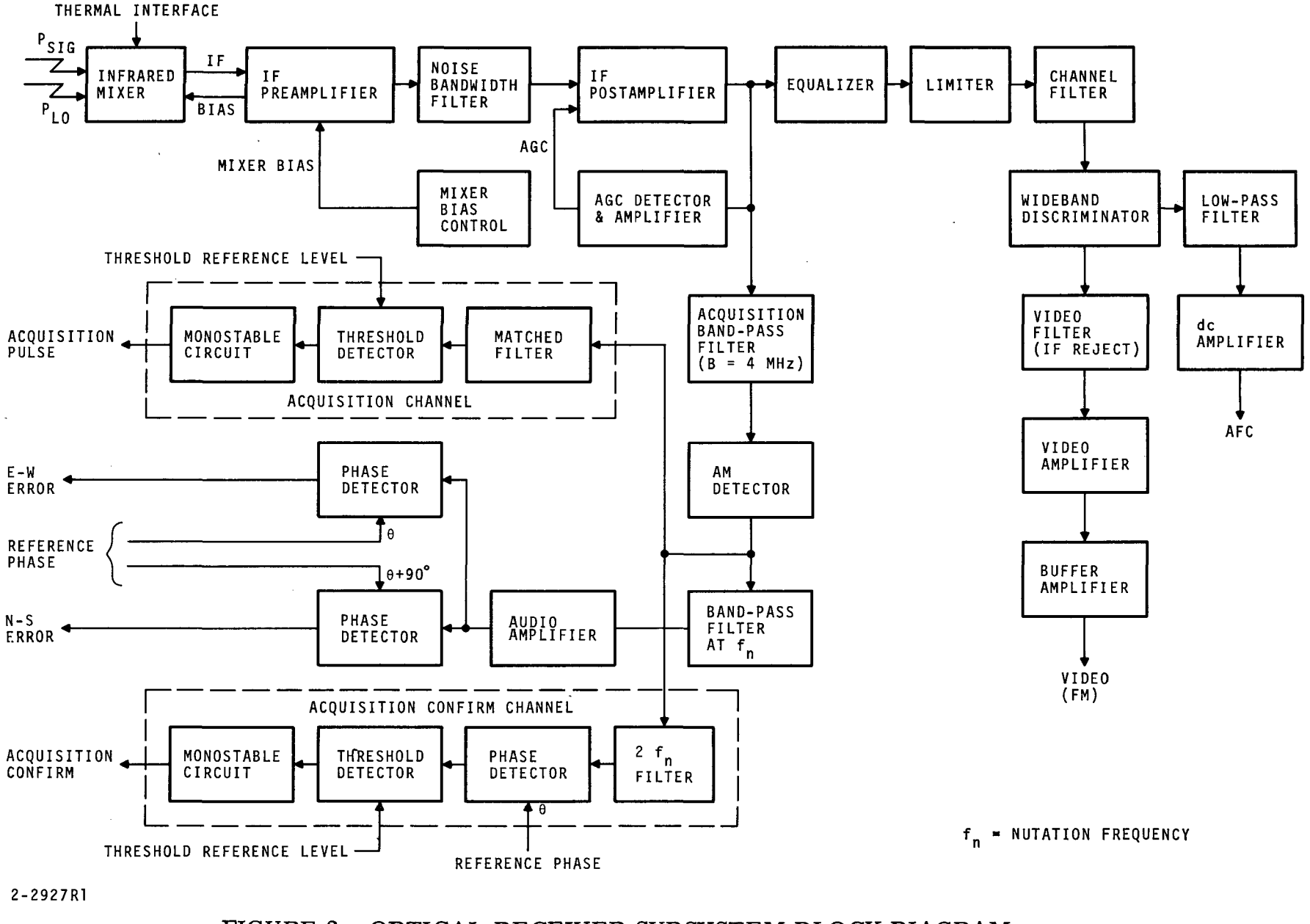

FIGURE 2. OPTICAL RECEIVER SUBSYSTEM BLOCK DIAGRAM

the required error voltage to maintain the desired IF offset (30 MHz) between the two lasers. The acquisition channel is a novel electro-optical network which enables signal acquisition and confirmation with a negative IF signal-to-noise ratio (SNR). In addition, tracking of the spatial position of the signal source is accomplished after initial signal acquisition by means of a conical scan of the heterodyne receiver field of view*.

B. SPATIAL ACQUISITION SEQUENCE

Any uncertainty in the attitude and position of the two remote stations, such as a synchronous satellite to ground link, requires an acquisition sequence to align the optics in the two transceivers within some specified acquisition time. The spatial search to achieve acquisition in the ORS uses a digitized X-Y raster scan pattern of the receiving optics at one station, while the transmit beam of the other station is broadened sufficiently to ensure illumination of the receiving station consistent with any spatial uncertainties (references 8 and 9).

During the acquisition sequence, a predetection filter is used in the acquisition channel to reduce the IF bandwidth to 4 MHz (the uncertainty of the laser frequency fixes the upper limit of the filter bandwidth). A matched filter following an AM detector is used to maximize the acquisition channel SNR when the receiver's scanning optics sweeps through the transmit signal beam.

The acquisition sequence of the optical receiver subsystem (Figure 3) has been demonstrated using a laboratory simulation of the communications link. On receiving an optical encounter pulse with an amplitude which exceeds a preselected threshold, an electronic acquisition pulse is generated and used to terminate the raster scan and initiate a 100-Hz conical scan.

---

*Some details of ORS performance are available in a published paper included as Appendix A to this report.

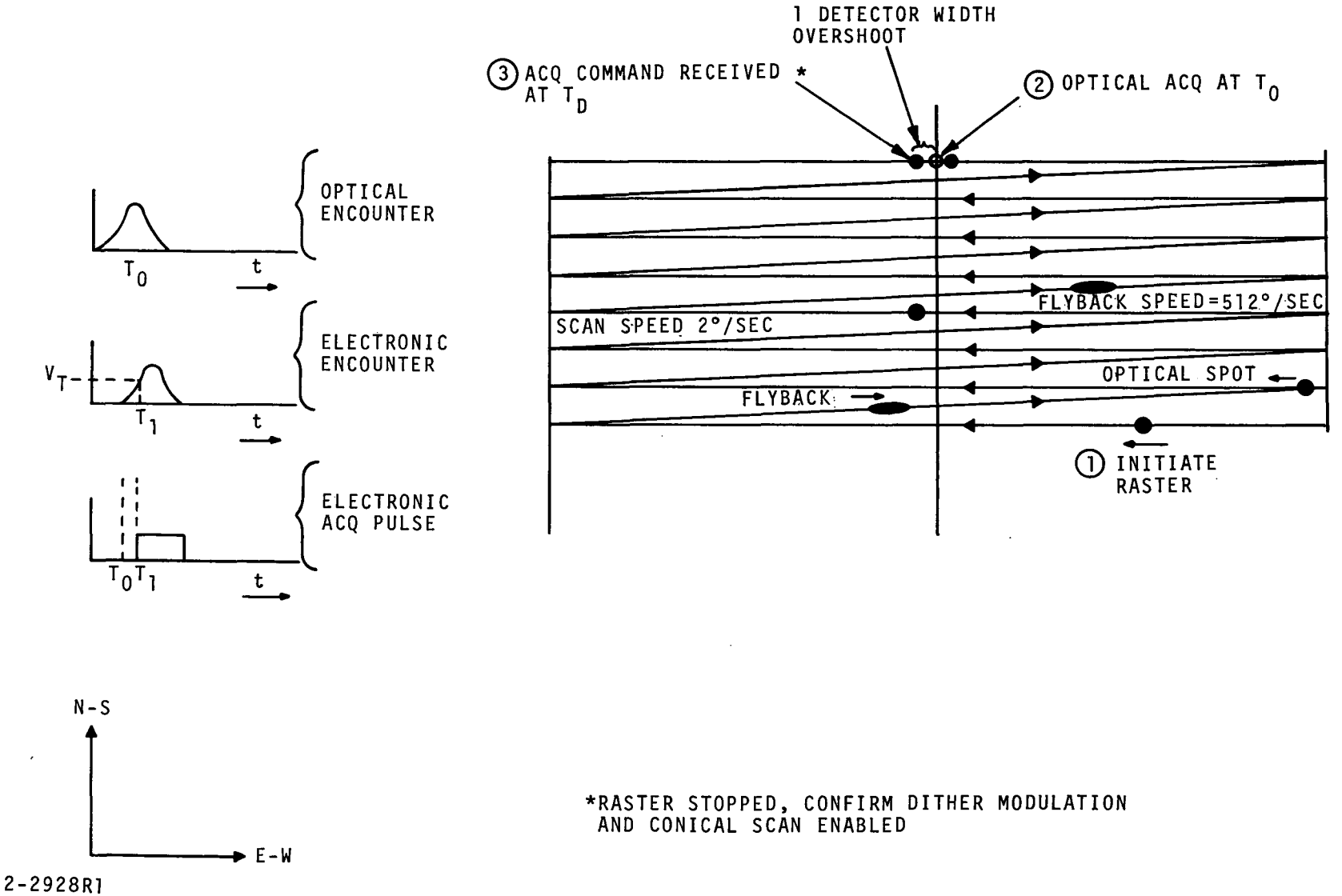

FIGURE 3. ACQUISITION SEQUENCE OF OPTICAL RECEIVER SUBSYSTEM

Due to the time delay between the intercept of the incoming optical signal and the generation of the electronic acquisition pulse there is an overshoot of approximately one detector spot size before the raster search scan is terminated. The overshoot of the raster scan depends on the scan speed, receiver time constants, signal amplitude, and the comparator threshold setting. Since the overshoot is a function of non-varying system constants, it can be corrected by readdressing the receiver field of view by a preprogrammed command after initial acquisition. During the readdress sequence, a 200-Hz dither modulation is superimposed on one axis of the conical scan. The confirm channel detects the presence of this one axis dither and generates an acquisition confirm signal which is particularly insensitive to random noise spikes. When acquisition is confirmed, the 200-Hz dither is automatically terminated and the 100-Hz conical scan is maintained to provide spatial tracking. After both stations have completed their acquisition sequences, the transmit beams are narrowed and communication is established.

1. ELECTRONIC MEASUREMENTS

Measurements of the probability of obtaining an acquisition pulse were carried out by introducing 20 RF pulses (pulse width = 60 ms) into the IF channel over a 10-second time interval. A simplified block diagram of the instrumentation used for these acquisition measurements is shown in Figure 4. A photograph of the laboratory setup, which includes a signal and local oscillator CO_2 laser, is shown in Figure 5.

In order to establish and vary the IF SNR's for these measurements, white noise was added to the IF preamplifier to simulate the noise generated in the photomixer. The amount of additional noise was determined as follows:

The heterodyne receiver NEP is 10^{-19} watts/Hz. The noise contributed by the HgCdTe photomixer = N_D = (NEP) $\times B_N$*

$N_D = 0.8\ (10)^{-10}$ mW = -101 dBm.

The noise contributed by the preamplifier (F_{IF} = 2 dB) is

$$N_{AMP} = -114 + 10 \log (B \text{ in MHz}) + \text{Noise Figure (preamplifier)}$$

$$= -114 + 9 + 2 = -103 \text{ dBm} = 0.5\ (10)^{-10} \text{ mW}$$

Since the HgCdTe photomixer was not used for the RF measurements, the infrared mixer shot noise was simulated by a separate noise source (Figure 6), the increase in the IF noise power due to the shot noise contribution from the HgCdTe detector is:

$$\Delta L = \frac{N_D + N_{AP}}{N_{AP}} = \frac{0.8 + 0.5}{0.5} = 2.6 = 4 \text{ dB} \qquad (1)$$

Unity SNR was established by:

- Deenergizing the pulse simulator and increasing the additive noise until the IF noise level was increased by 4 dB, simulating the shot noise of the HgCdTe photomixer
- The pulse simulator was turned on and adjusted until the IF noise level was doubled.

The IF SNR was varied by adjusting the attenuator at the output of the RF pulse simulator.

---

* B_N is the system noise bandwidth for an acquisition filter of 4 MHz at the 0.5 dB points and a 12 dB/octave roll-off, 8 MHz is the noise bandwidth.

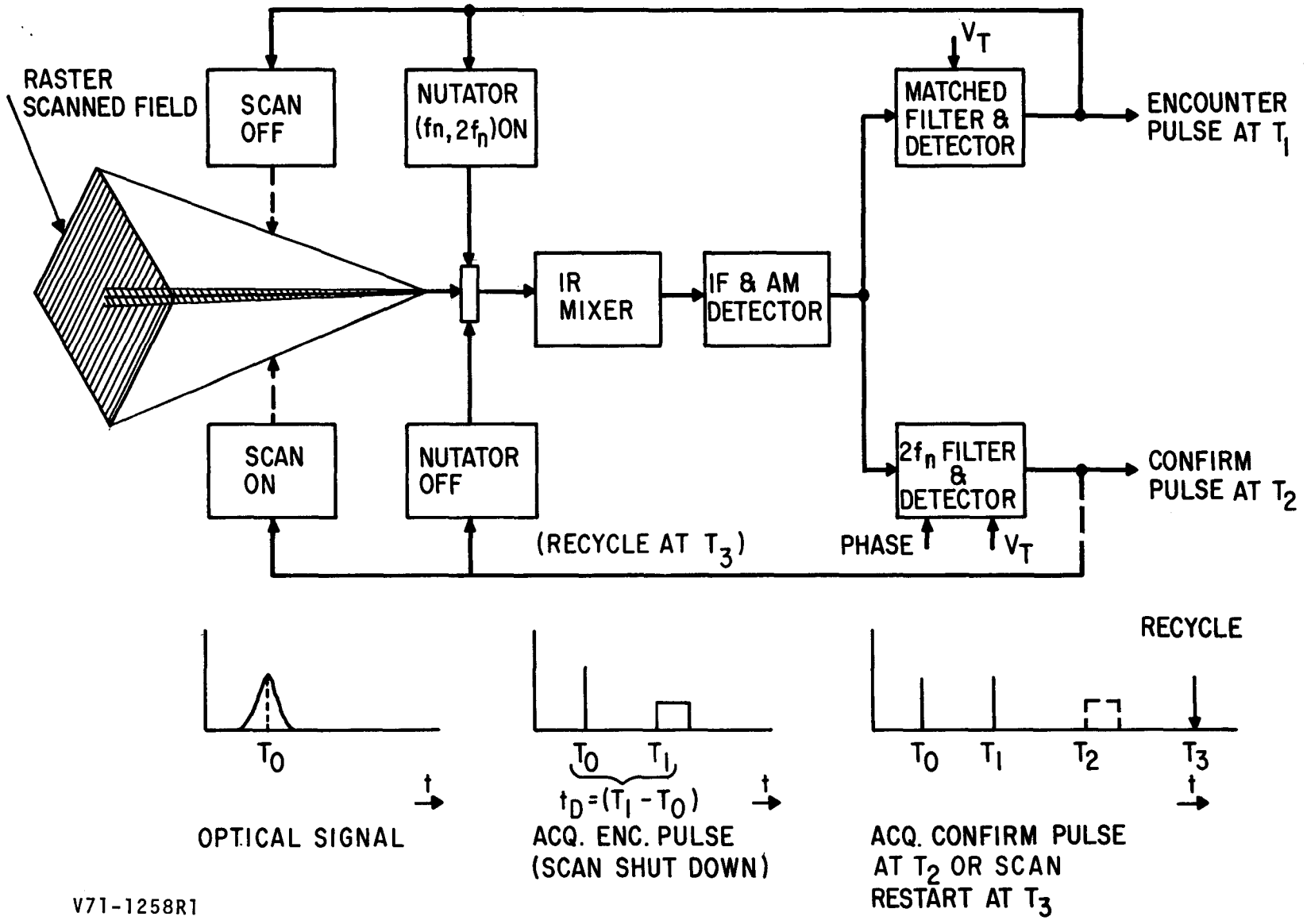

FIGURE 4. FUNCTIONAL DIAGRAM OF ACQUISITION SEQUENCE OF ORS

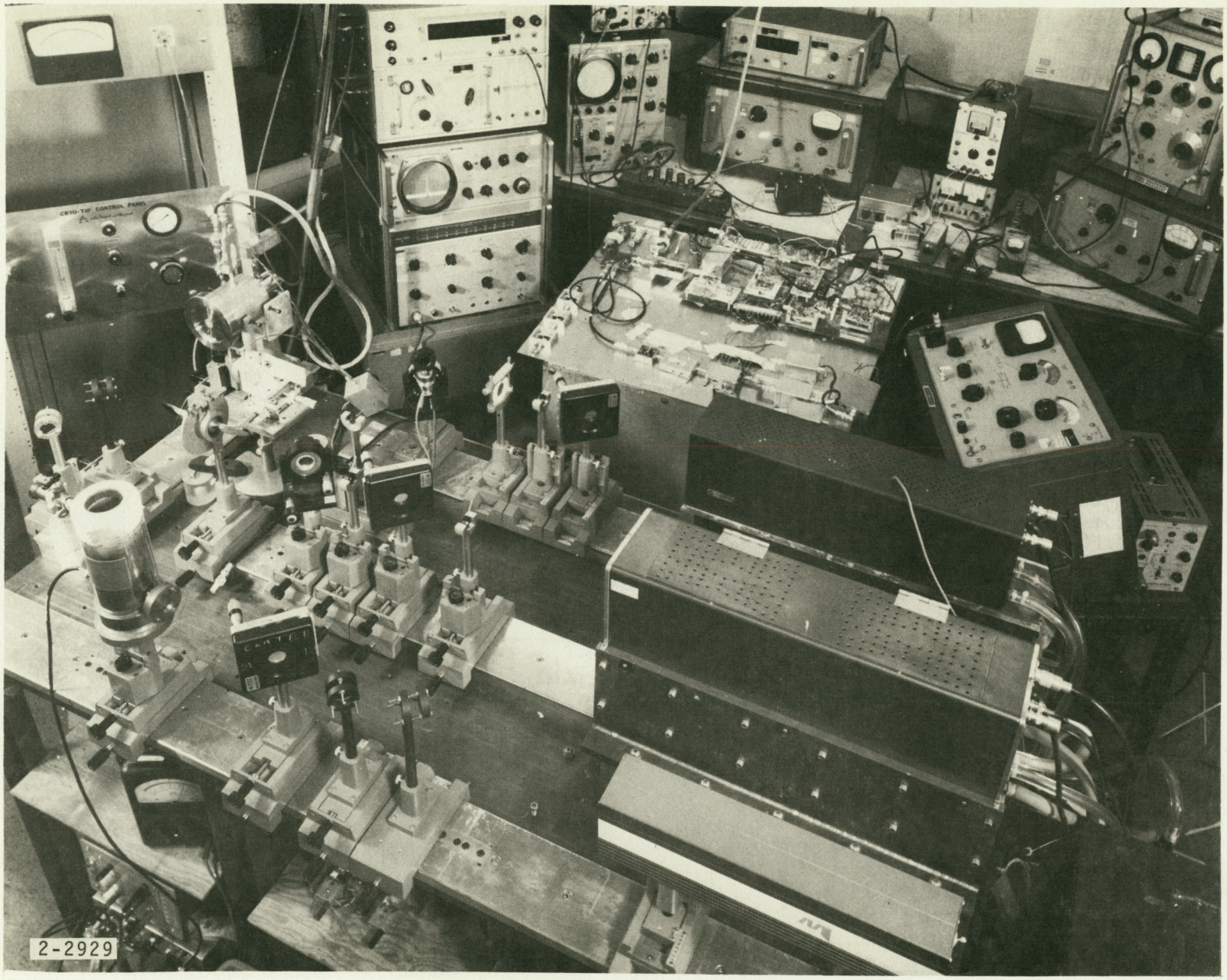

FIGURE 5. LABORATORY SETUP FOR ORS MEASUREMENTS

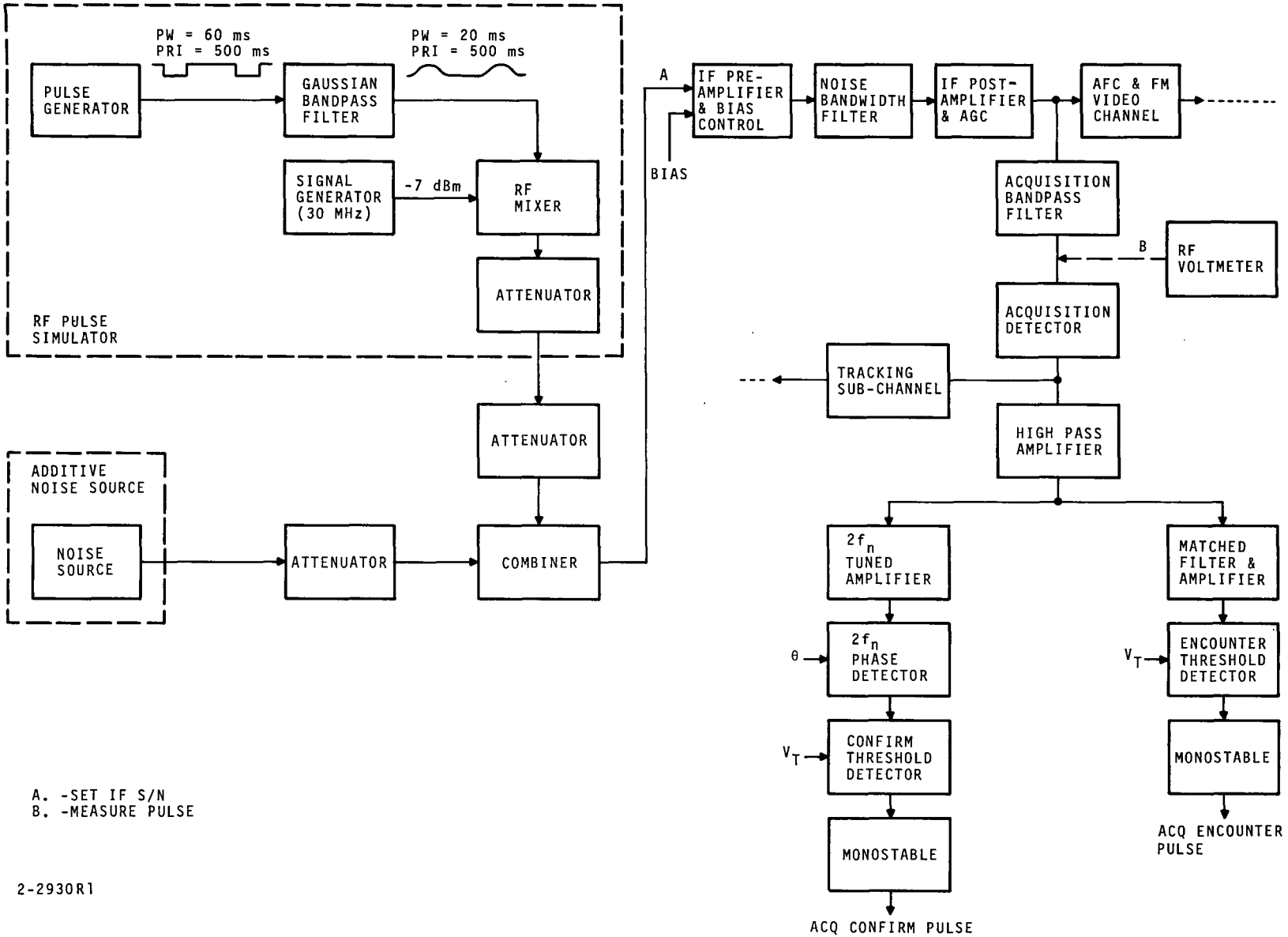

FIGURE 6. BLOCK DIAGRAM OF TEST SETUP FOR ELECTRONIC ACQUISITION MEASUREMENTS

The probability of generating an encounter pulse was measured as a function of encounter threshold voltage (V_t) for IF SNR's between -21 and -26 dB. The results of these measurements are given in Figure 7. It can be seen that V_t must be lowered as the IF SNR is reduced in order to maintain a high probability of encounter. For V_t = 1.5 V and an IF SNR = -23 dB and larger, the probability of encounter is 1. For an IF SNR = -24 dB, the probability of encounter is 0.85, and for an IF SNR = -25 dB, the probability of encounter drops to 0.40. For a threshold setting of 0.5 V and below, noise generates erroneous encounter pulses by false triggering of the threshold detector. As can be seen from Figure 7, a threshold voltage near 1 volt is desirable.

The generation of the electronic encounter pulse in the ORS is delayed by an amount T_D from actual optical acquisition (Figure 3). The delay represents the propagation time of the signal through the IF and acquisition channels. Measurements of the time required for the output of the matched filter to rise to the threshold value from its base line were carried out at IF. The time delay consists of two parts: the delay at IF and the delay in the acquisition channel. The major portion of the delay is due to the bandwidth of the matched filter in the acquisition channel. In addition, the delay changes with the signal strength during the acquisition sequence, the threshold setting, and the noise level riding on the acquisition signal. However, the change in time delay due to these considerations is small compared to the delay caused by the matched filter. The filter in the acquisition channel is matched to the incoming signal pulse duration and shape, and the maximum response is obtained by taking the convolution integral of the two time domain system variables:

$$V(t) = \int f(\tau)\, h(t - \tau)\, d\tau \qquad (2)$$

where

f(t) = time domain representation of the input signal

h(t) = matched filter response

For the case h(t) = f(t), maximum response is obtained at $t = T_{max}$ where T_{max} is the duration of f(t).

Measurements of the time delay through the ORS were carried out as a function of IF SNR with acquisition threshold setting as a parameter. The results are given in Figure 8. For the expected IF SNR's of -20 dB (during acquisition) and a threshold voltage of 1 V, the ORS time delay is approximately 14 ms.

Measurements of the probability of obtaining an acquisition confirm pulse were carried out as a function of IF SNR and threshold voltage. The acquisition confirm circuit consists of a very narrow band-pass filter centered at 200 Hz followed by an AM detector/integrator. The presence of 200 Hz AM modulation on the incoming signal (due to the dither on one axis of the conical scanner) is detected, integrated and compared to a threshold setting. When the integrated signal level crosses the confirm threshold reference, a pulse is triggered which confirms that the ORS has acquired the transmitter (Figure 9). The probability of confirm versus the threshold voltage setting for IF SNR's as low as -29 dB is given in Figure 9 for dither modulation of 70 and 15 percent. For a 1 V threshold setting, a positive confirm will be obtained for IF SNR's = -27 dB or greater at a 70 percent dither modulation. This is a favorable result.

2. ELECTRO-OPTIC MEASUREMENTS

Laboratory measurements of the acquisition capability of the ORS operating under simulated operating conditions have been carried out. Digital drive circuitry which:

- Develops the raster search scan with digitized control
- Provides logic commands to (a) initiate the search scan, (b) stop search and start nutation, (c) digitally readdress the signal beam, and (d) initiate and terminate the confirm sequence
- Shapes the scan drive voltages to eliminate ringing and minimize mechanical overshoot

has been developed for the ORS (Figure 10). The pulse generator provides pulses at a desired rate while a decision gate enables a 14 bit counter which drives two D/A converters. The output of the converters is shaped so that the rise and fall times match the frequency response of the optical scanner. The amplitude shaping circuits are designed to:

- Eliminate ringing during search scan and/or flyback
- Minimize time delay when the stop scan command (acquisition) is encountered

The field of view of the photomixer was swept through the laser transmit beam at the acquisition search rate, so that the bandwidth of the acquisition matched filter maximizes the output SNR. Start/stop and readdress of the receiver field of view can be automatically accomplished by simple logic commands generated in the ORS. A schematic of the essential instrumentation used for the optical acquisition measurements is shown in Figure 11.

Under constant laser LO illumination, the photo-inducted shot noise is higher than the total thermal noise of the receiving electronics so that the receiver is nearly quantum noise limited (NEP $\approx 10^{-19}$ W/Hz). The signal beam is focused by the lens to a spot-size comparable to the sensitive area of the photomixer. As the signal spot is swept across the mixer, the IF output produces a 30 MHz Gaussian shaped pulse of duration T_{max} (a function of mixer size, optical spot size and sweep speed).

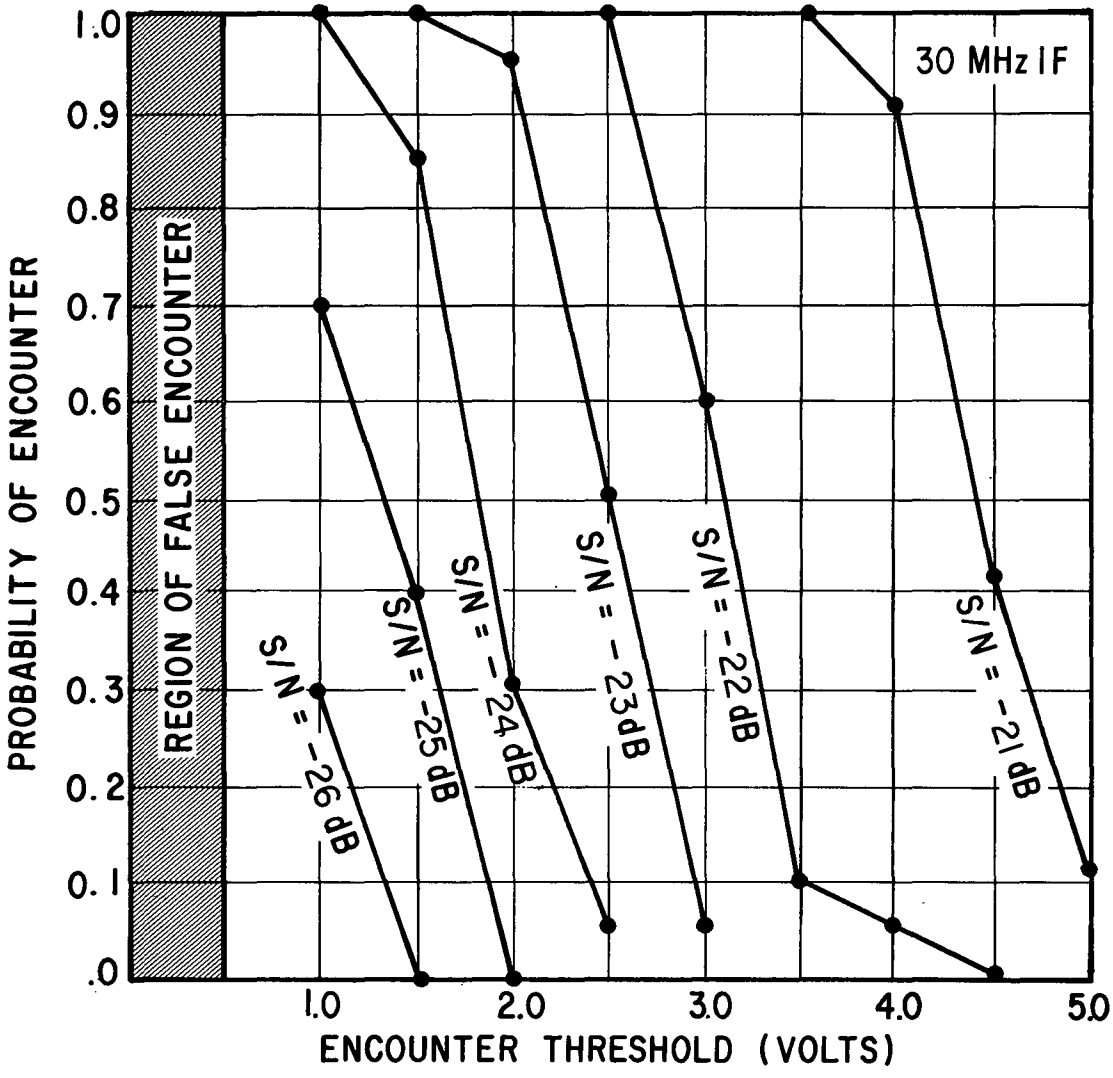

V71-1256R1

FIGURE 7. PROBABILITY OF ENCOUNTER VERSUS THRESHOLD WITH IF SNR AS A PARAMETER

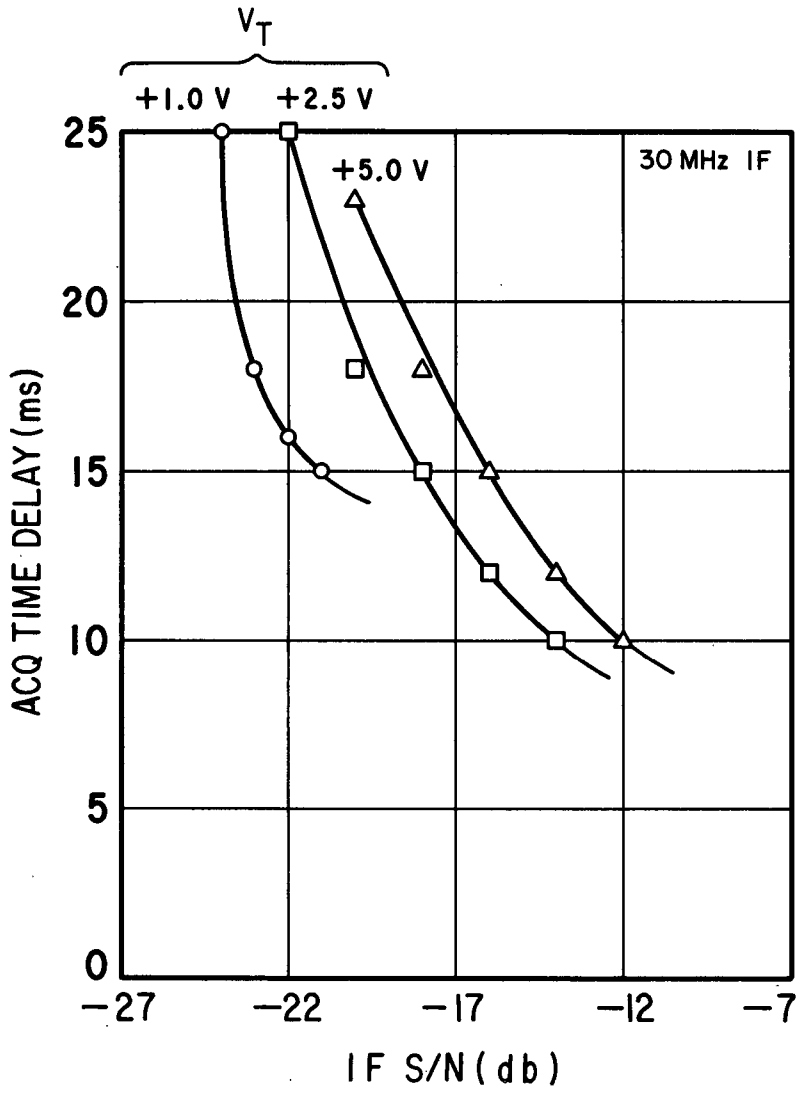

FIGURE 8. MEASURED TIME DELAY BETWEEN OPTICAL ACQUISITON AND ELECTRONIC ENCOUNTER PULSE

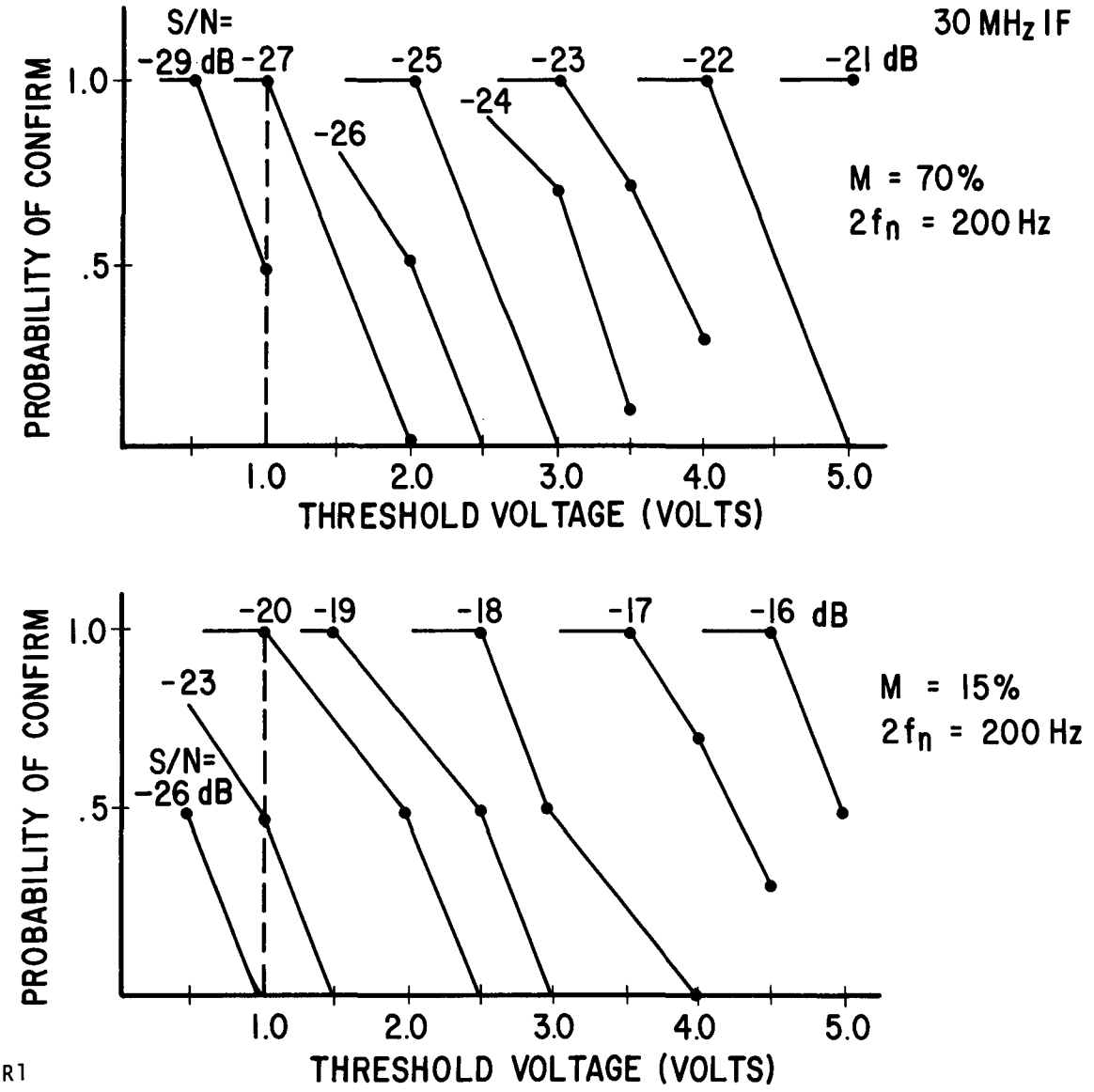

FIGURE 9. PROBABILITY OF ENCOUNTER CONFIRM PULSE AS A FUNCTION OF THRESHOLD LEVEL

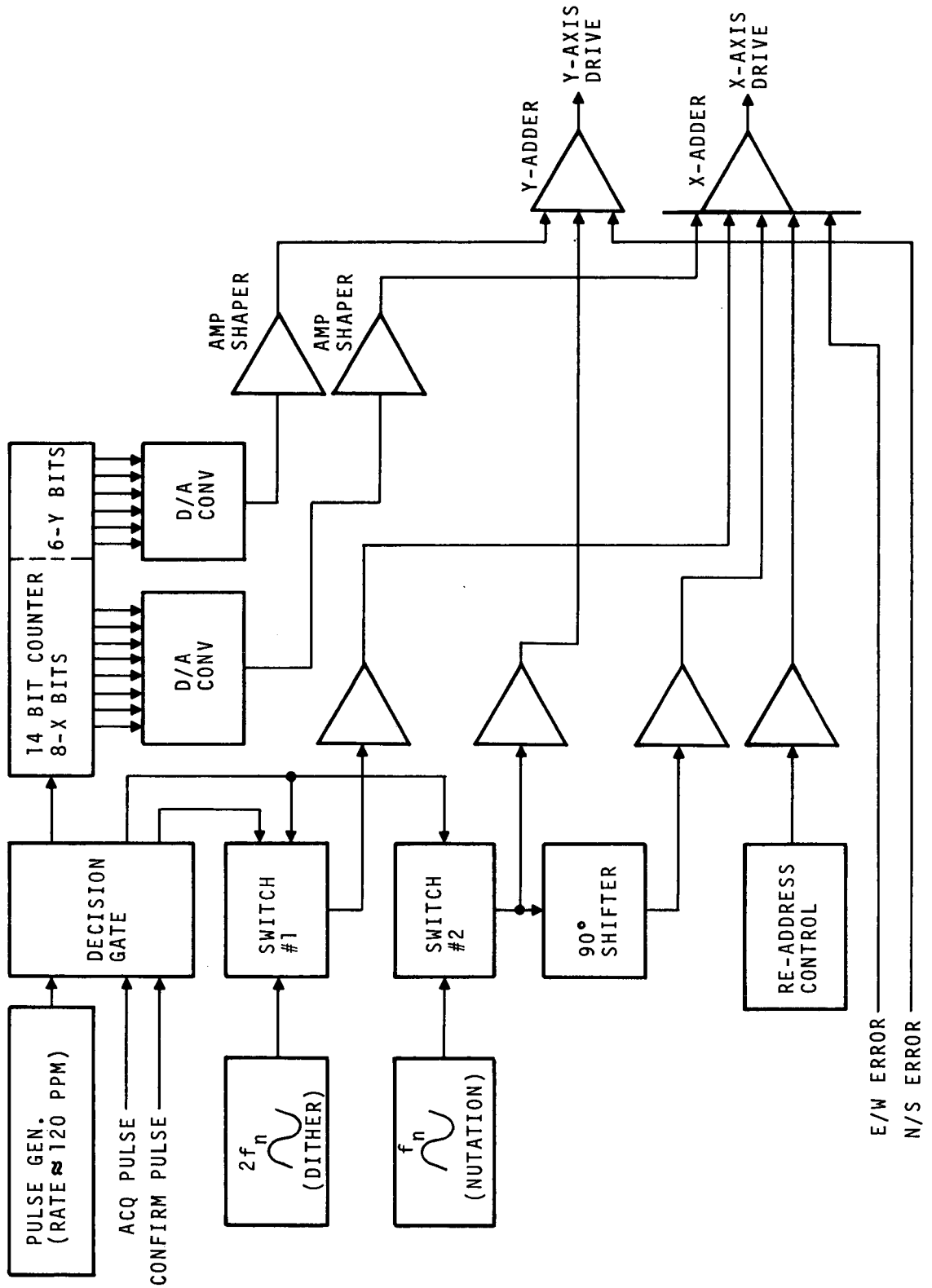

FIGURE 10. BLOCK DIAGRAM OF DIGITIZED RASTER DRIVE CIRCUITRY

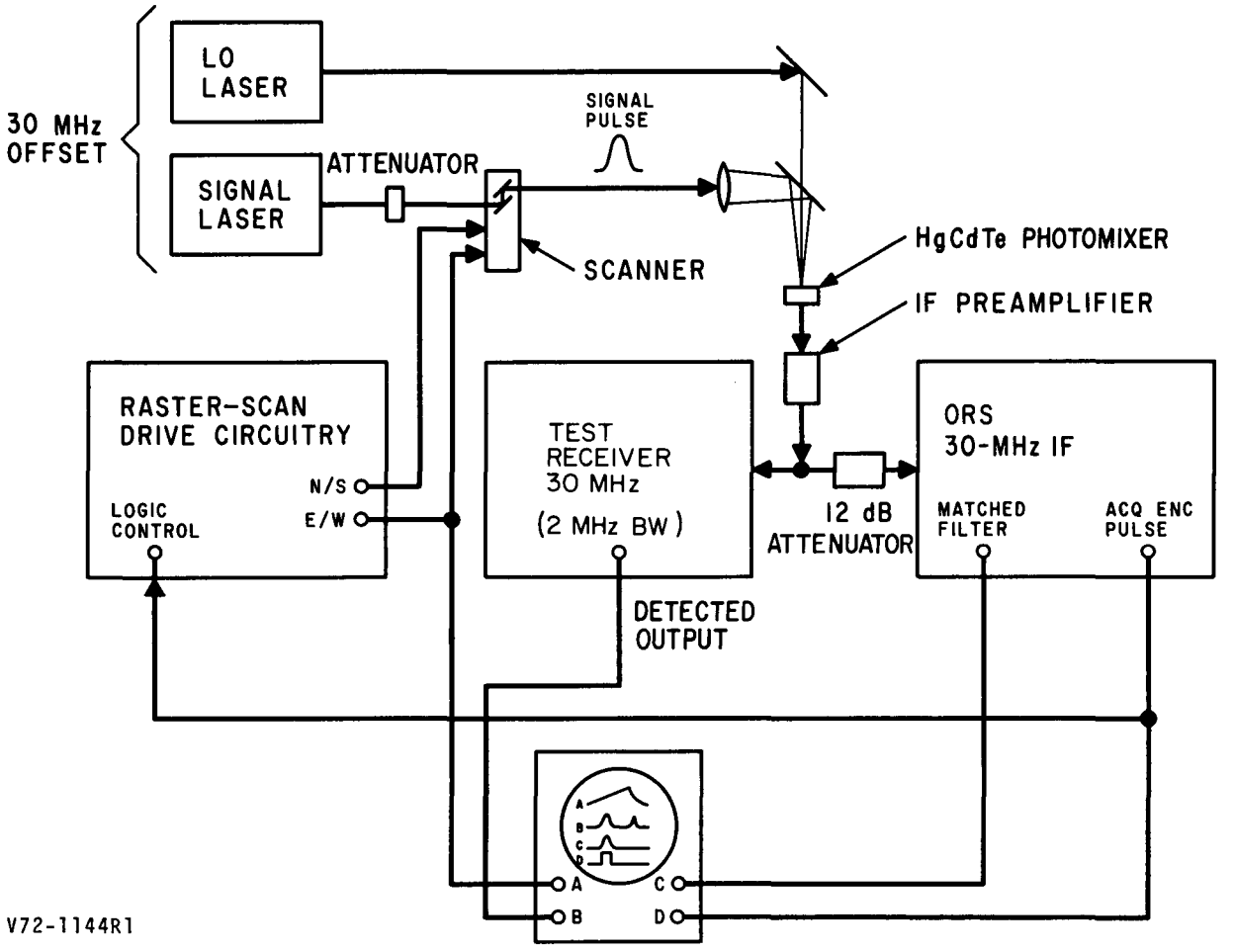

FIGURE 11. BLOCK DIAGRAM OF EXPERIMENTAL SETUP FOR ACQUISITION ENCOUNTER MEASUREMENTS

An oscilloscope display of the observed acquisition sequence of the heterodyne receiver is shown in Figure 12. Trace A shows the digitally derived ramp waveform (obtained at point A in Figure 11) which drives the E/W search scan. Trace B is the IF 30-MHz scanned signal observed at the detected output of a precision test receiver as the optical signal spot is scanned through the photomixer field of view. The duration of this swept signal is fixed to be equal to T_{max}. Trace C shows the output of the matched filter which is maximum at T_{max}, and trace D shows the acquisition encounter pulse when the matched filter output crosses the dc threshold setting of the threshold detector. For this experiment, the peak IF SNR is approximately -16 dB. As can be seen from Figure 12, there is approximately a 50-ms delay between the boresighted condition and the initiation of the acquisition encounter pulse. The 50-ms delay can be predicted based on the bandwidth of the matched filter and the threshold setting. For a threshold setting of 1 V (as used for the measurements in Figure 12) the filter output need only rise to 1/2 of its peak value.

The same acquisition sequence is shown in Figure 13. However, the acquisition encounter pulse is fed back to the digitized raster scan drive circuitry. When the acquisition pulse is received, the logic of the drive circuitry shuts down the search ramp and maintains the dc level at which the encounter pulse occurs. Since there is a delay between the actual optical acquisition and the electronic pulse out of the matched filter (due to the convolution integral), the raster scan control shutdown occurs sometime after actual optical acquisition and an overshoot of approximately one photomixer size for low SNR's is obtained. Therefore, the IF signal is not peaked after acquisition.

Since the overshoot is a direct function of T_{max}, the shape of the matched filter, and the threshold setting, an additional command to readdress the receiver field of view has been installed in the ORS which corrects for the

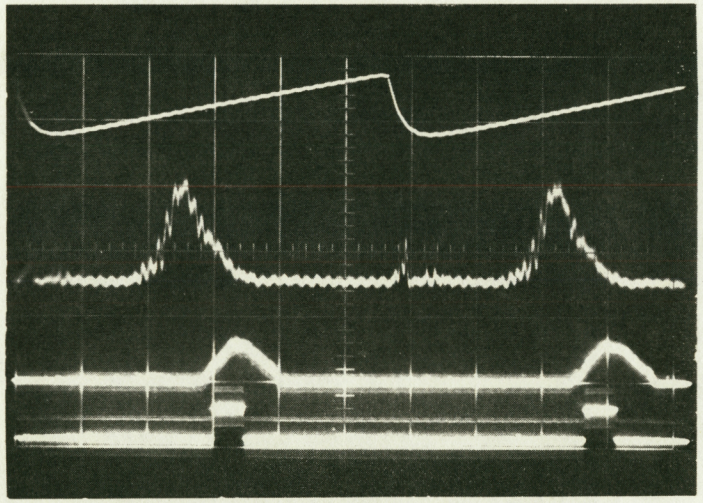

V72-1135

FIGURE 12. MEASURED ACQUISITION SEQUENCE OF ORS

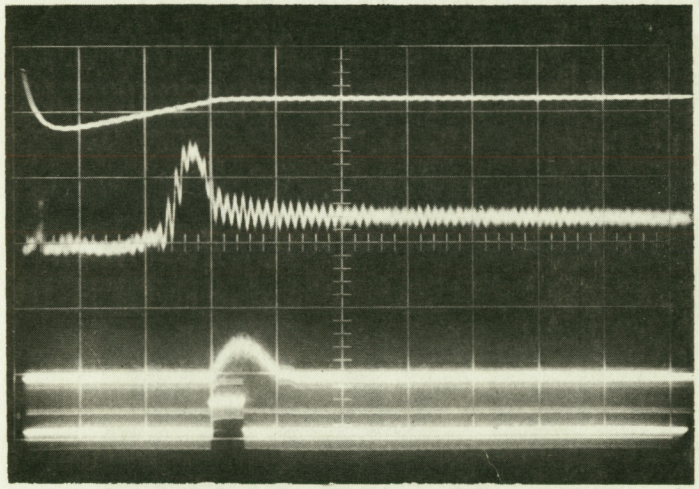

E/W SAWTOOTH (DISABLED BY CONTROL LOGIC WHEN ACQUISITION ENCOUNTER PULSE IS RECEIVED)

DETECTED OUTPUT, NOTE PRESENCE OF SOME SIGNAL AFTER ACQUISITION

MATCHED FILTER OUTPUT ACQUISITION ENCOUNTER PULSE

100 MS/CM

V72-1131R1

FIGURE 13. MEASURED ACQUISITION SEQUENCE WITH "STOP" COMMAND

slight overshoot. The resultant acquisition measurements including a readdress correction sequence is shown in Figure 14. For these measurements the search scan is begun at a position just beyond the point of acquisition encounter so that the scan must retrace before acquiring. During the retrace cycle, the receiver field of view intercepts the transmit laser beam and provides an output in the 30-MHz IF signal channel. However, the matched filter in the acquisition encounter channel is not matched for the retrace scan speed (retrace is much faster than scan). Therefore, no acquisition encounter pulse is generated. Acquisition is accomplished during the search scan and the readdressing of the scanner after acquisition produces peak IF output with some low frequency (and damped) ringing. The IF level is returned to its peak value within 200 ms of the optical acquisition.

This experimental data demonstrates that:

- Acquisition of an optical signal buried in noise at IF is possible with a raster-scan and matched filter combination
- There is a correctable overshoot of one to two photomixer widths. (Once the overshoot is even slightly corrected, the tracking error voltages of the conical scanner will correct further until boresighting is accomplished)
- The main overshoot error is constant and equal to the distance scanned in the delay time of the system. Uncertainties in actual signal-to-noise ratio during acquisition will given an additional delay (2 to 5 ms) which is small enough to be handled by the tracking error voltage

C. CONICAL-SCAN TRACKING

1. OPEN-LOOP DIRECT DETECTION TRACKING MEASUREMENTS

Direct detection measurements were carried out to obtain the conical-scan open-loop tracking error voltages (reference 10) as a function of incident signal misalignment using the experimental setup shown in Figure 15. A 100-Hz circular nutation was employed for the measurements.

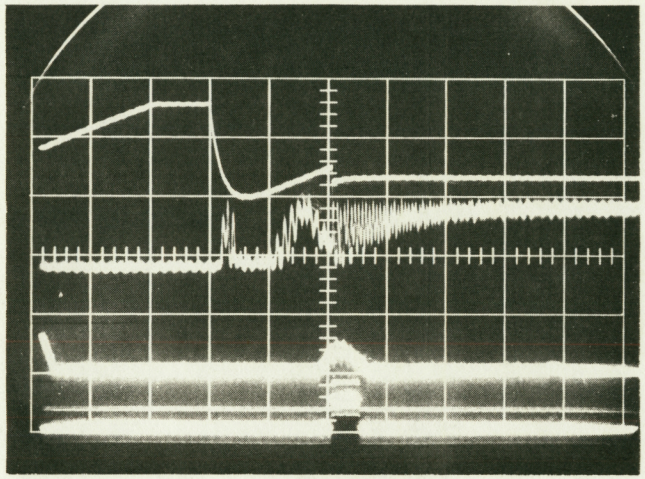

FIGURE 14. MEASURED ACQUISITION SEQUENCE WITH "STOP" AND "READDRESS" COMMANDS

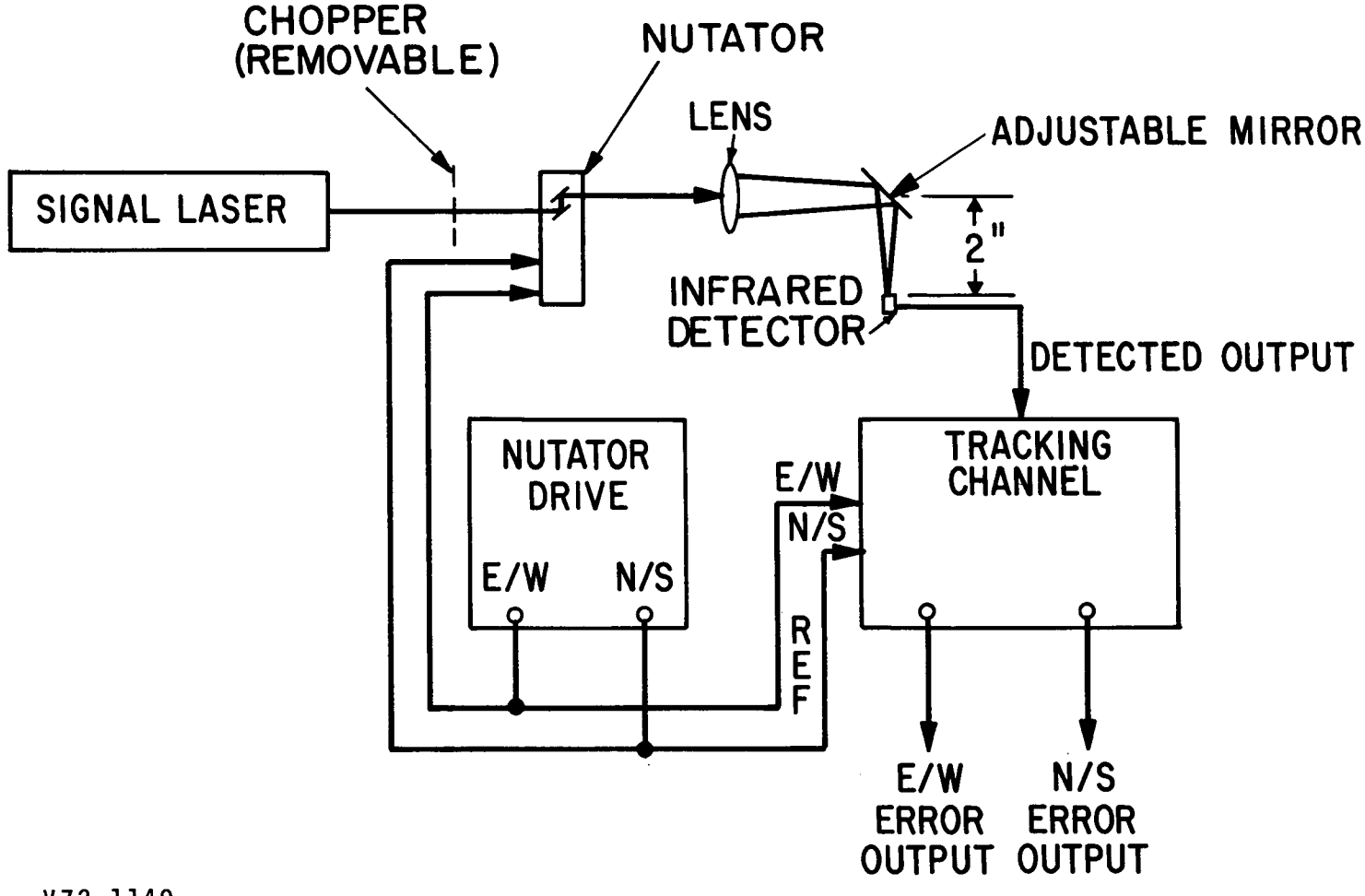

FIGURE 15. BLOCK DIAGRAM OF TEST SETUP FOR DIRECT DETECTION TRACKING MEASUREMENTS

However, an elliptical cross-section nutation can be used for non-square (or non-uniform) photomixers. A simple lens is used to focus the output signal from the nutator onto the photomixer. When the axis of nutation intersects the center of the detector, no error voltage is generated. The signal spot without nutation, with 100-Hz circular nutation and a 200-Hz dither on one axis, and with an elliptical 100-Hz nutation is shown in Figure 16.

Figure 17 shows the error voltage outputs of the E/W and N/S synchronous detectors of the ORS for the cases of the receiver on boresight and offset from boresight sufficiently to yield 1 dB decrease in IF SNR in each of the four reference directions. The nutation angle is chosen so that the boresighted signal is down 2 dB from its peak (unnutated) value (corresponding to 40 percent nutation). As the nutation axis is steered off boresight, an error voltage sensitive to the direction (east, west, north or south) and degree of misalignment is obtained. The error signal is synchronously detected so that magnitude and phase of the error correspond to the direction and amount of the offset of the receiver field of view. The waveforms shown in Figure 17 are integrated to produce the dc level used to drive the pointing optics (Figure 1).

A 1-dB change in the east direction causes an ac error voltage in both the N/S and E/W channels. The average value of the voltage in the N/S channel is zero so that no dc error voltage is obtained from the N/S integrator. The average value of the voltage in the E/W channel is positive. Therefore, a positive dc voltage is obtained from the E/W integrator and is used to drive the pointing optics thereby compensating the error.

The dc error voltage as a function of offset of the signal spot (measured in detector widths) is shown in Figure 18. Tracking error voltages are generated over at least 4 detector widths in the direct detection mode. Measurements using the heterodyne detection mode resulted in improved spatial tracking. Figure 18 shows that the E/W channel was slightly

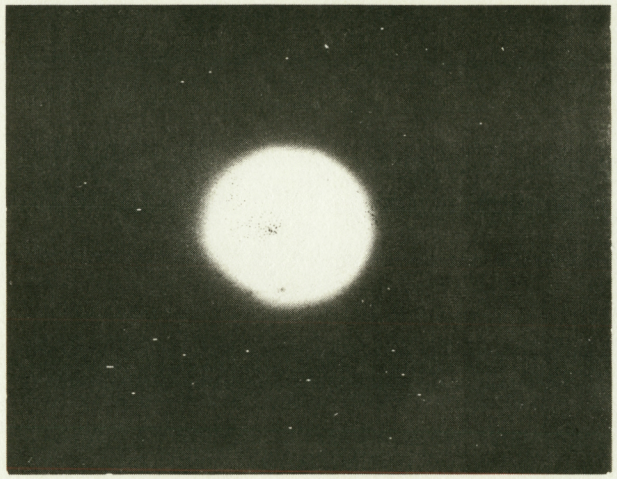

NO NUTATION

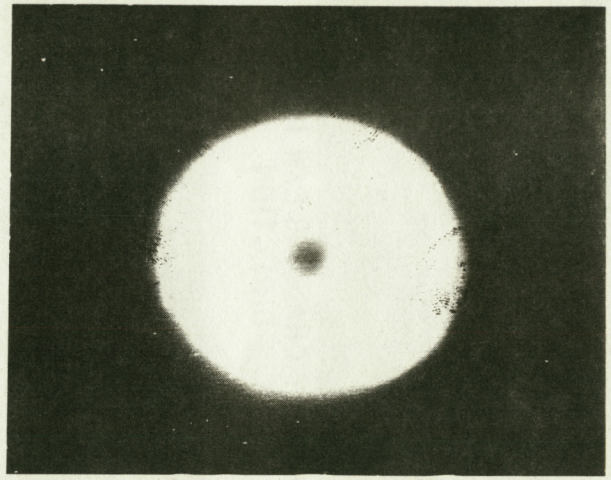

100 Hz NUTATION WITH 200 Hz DITHER

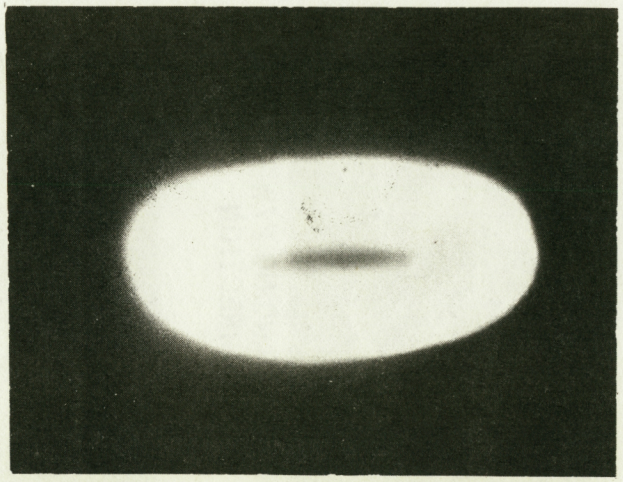

ELLIPTICAL 100 Hz NUTATION

V72-1130

FIGURE 16. OPTICAL FIELD PATTERNS WITH AND WITHOUT NUTATION

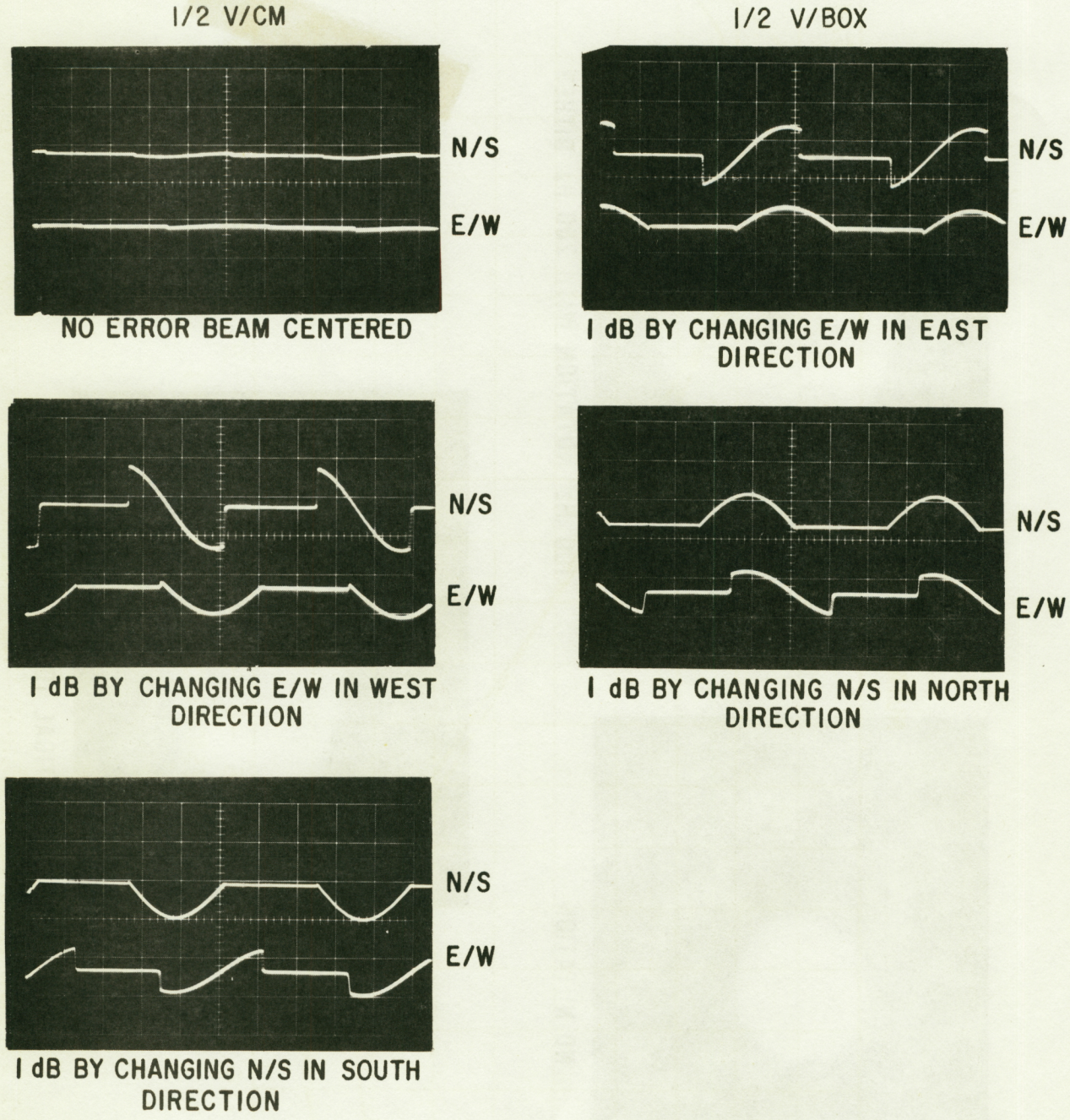

FIGURE 17. ERROR VOLTAGE OUTPUT OF E/W, N/S SYNCHRONOUS DETECTORS

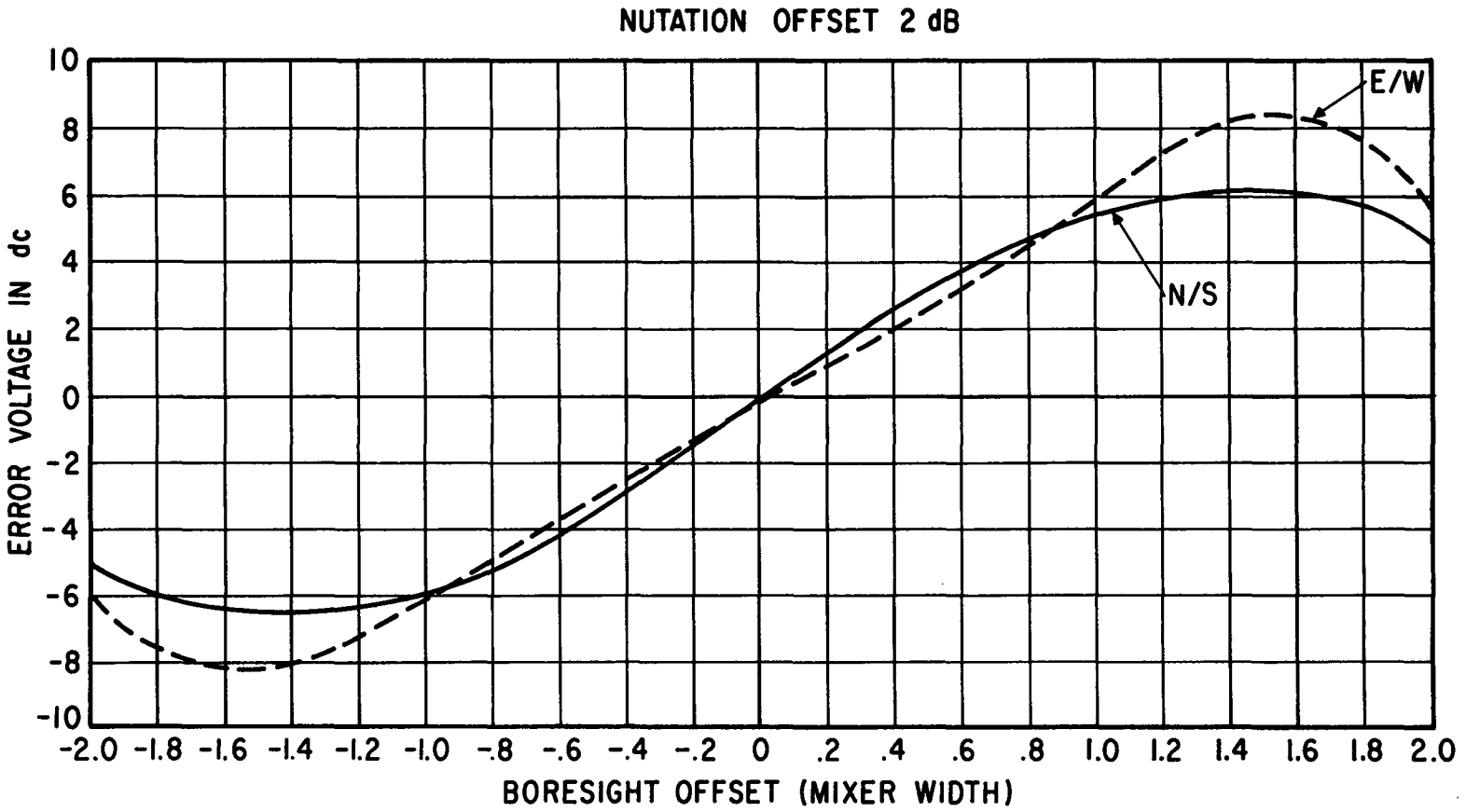

FIGURE 18. DC TRACKING ERROR VOLTAGE AS A FUNCTION OF RECEIVER BORESIGHT OFFSET

more sensitive than the N/S, due in part to the slightly rectangular photomixer used in the experiments (220 × 240 micrometers).

2. CLOSED-LOOP HETERODYNE TRACKING MEASUREMENTS

An Image Motion Compensator (IMC), which consists of two orthogonal piezoelectrically driven mirrors, was inserted between the nutator and the LO combining optics. The tracking loop between the IMC and the tracking circuitry was closed. The measured data demonstrated that acquisition tracking, and operational tracking can be realized over a spatial coverage of approximately 11 photomixers.

When the optical signal beam is steered out of the field of view of the mixer element in the E/W direction, an error voltage is developed in the E/W phase detector and the resultant dc error voltage is used to reposition the IMC.

The X-Y recorder output obtained from the closed loop heterodyne tracking measurements with an IF SNR = -1 dB and 1 dB nutation is shown in Figure 19. The X axis is proportional to the optical signal offset expressed in photomixer widths and the Y axis is the amplitude of the 30 MHz IF signal. Without spatial tracking (open-loop condition) the dependence of the signal level on optical boresighting is evident because the signal is a sharp function of position. The closed-loop tracking curve shows that as the optical signal spot approaches the photomixer, the ORS begins to track the incoming signal beam, and the IF signal increases in level sharply. (The tracking error voltages cause a "latch-on" condition where the transmit signal and the receive field of view are nearly aligned.) The ORS continues to track the optical signal as it moves away from the boresight. Once the ORS has begun to track, it continues to track beyond (to the left of) the point at which it initially latched.

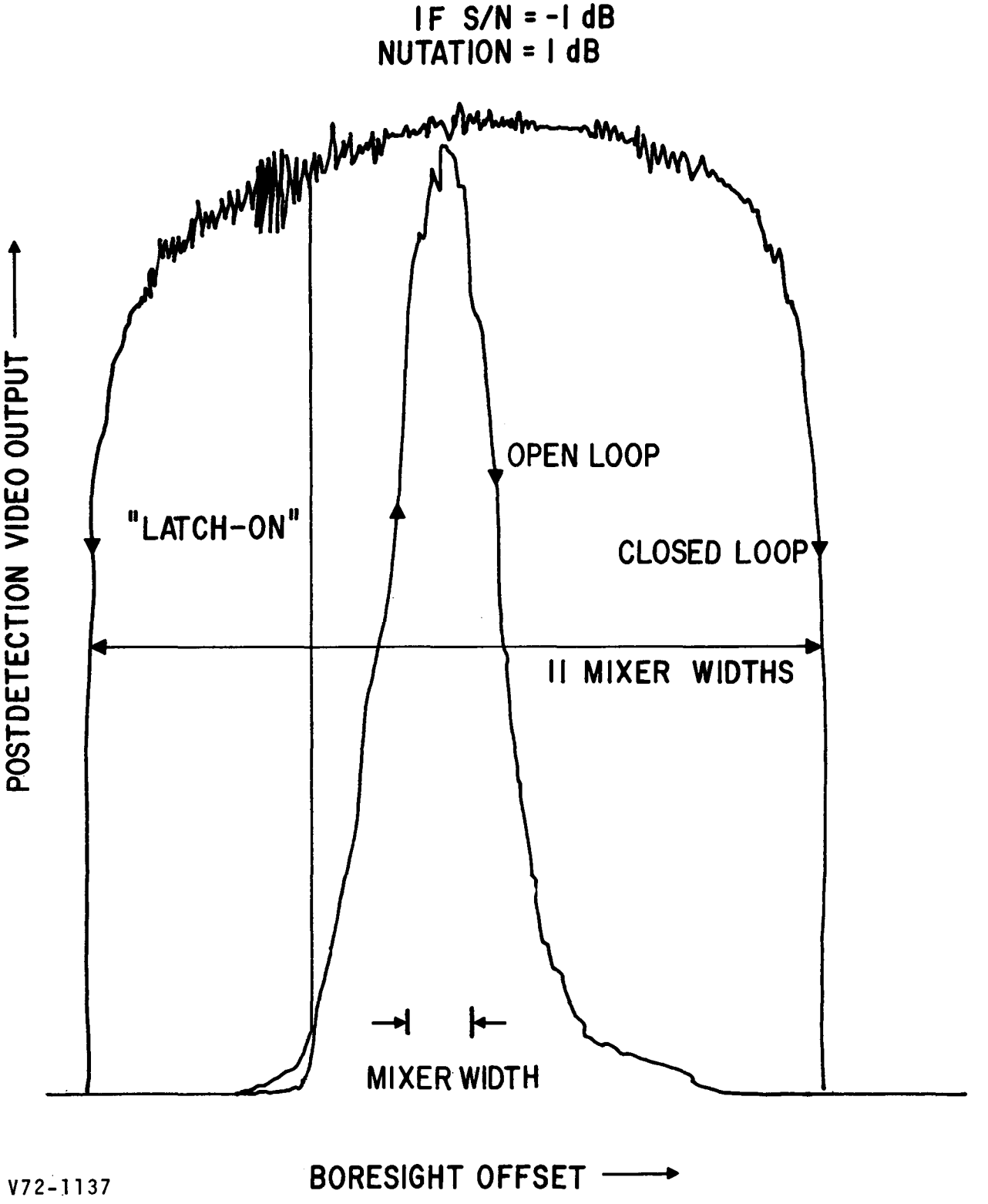

FIGURE 19. POSTDETECTION VIDEO OUTPUT LEVEL AS A FUNCTION OF RECEIVER BORESIGHT OFFSET FOR IF SNR = -1 dB

An X-Y recorder was used to produce a composite plot showing both the IF signal and the 100-Hz signal produced by the nutation for open- and closed-loop operation. Measurement results are shown in Figure 20. The curves, which are plotted with the optical beam moving from left to right, demonstrate acquisition tracking. Curve A of Figure 20 is a plot of open-loop IF signal with no nutation. Curve B shows a plot of an open-loop IF signal with nutation (approximately 1 dB below the peak of curve A). Curve C of Figure 20 is a plot of open-loop 100 Hz conical scan tracking voltage. Curve D shows a plot of closed-loop 100-Hz conical scan tracking voltage. In curve D the 100-Hz conical scan tracking voltage is reduced as the laser transmitter and ORS are boresighted. Curve E shows the closed-loop IF signal. Tracking is achieved over approximately 12 photomixer widths while maintaining a constant IF output.

The measured postdetection video output voltage as a function of boresight offset for 30-MHz IF SNR = -10 dB is shown in Figure 21. Tracking measurements are given for six nutation levels ranging between 0.7 and 19.6 dB. As expected, the output voltage level decreases with increasing nutation level. The ratio of the peak video output voltage for curves A (0.7-dB nutation) and D (3.6-dB nutation) in Figure 21 is about 0.65 compared to a calculated value of about 0.71 (for square law IF detection). The spatial tracking range is shown to increase with increasing nutation offset level until a drop in video output is observed at boresight for nutation offset levels above 8 dB. The drop in video output for large nutation offsets ($\sim$8 dB) is due to the small amount of incident energy which is intercepted by the photomixer at boresight because a donut-shaped optical field pattern is generated. In normal operation, the nutation offset would be set between 1 and 3 dB.

The measured video output voltage as a function of boresight offset for a 30-MHz IF SNR = -20 dB is shown in Figure 22. The video

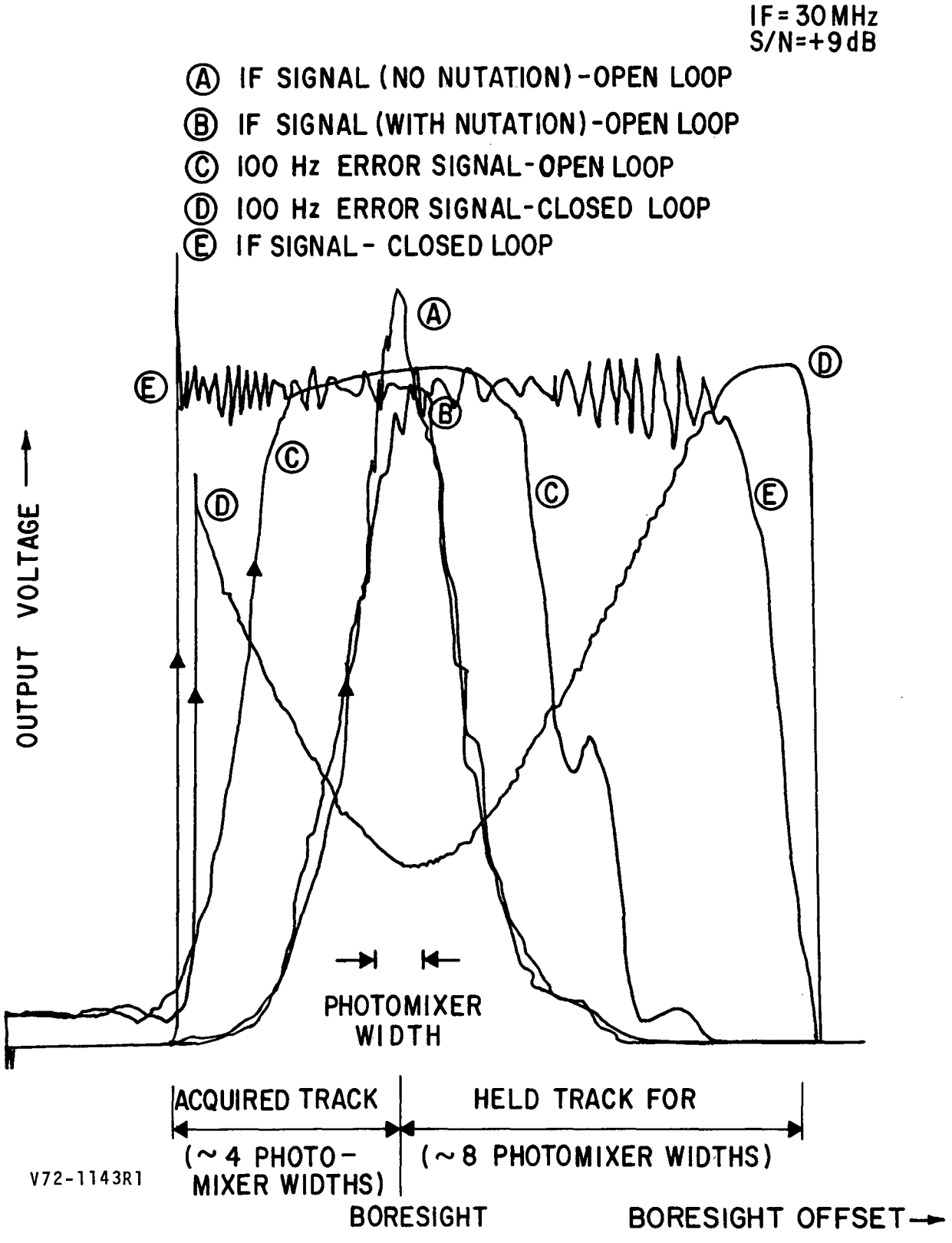

FIGURE 20. COMPOSITE PLOT OF SYSTEM VOLTAGE LEVELS FOR OPEN- AND CLOSED-LOOP OPERATION

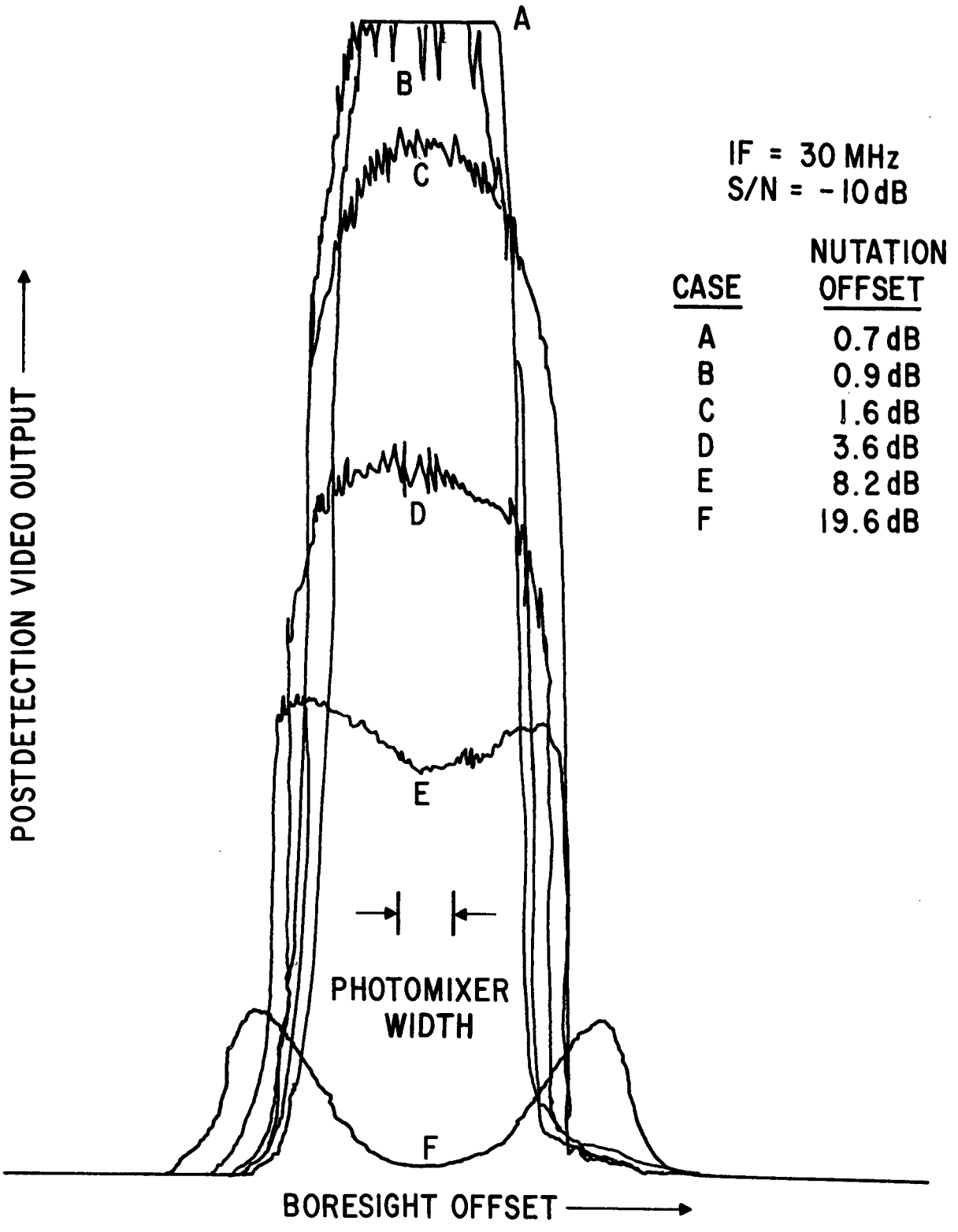

FIGURE 21. POSTDETECTION VIDEO OUTPUT LEVEL AS A FUNCTION OF BORESIGHT OFFSET FOR IF SNR = -10 dB

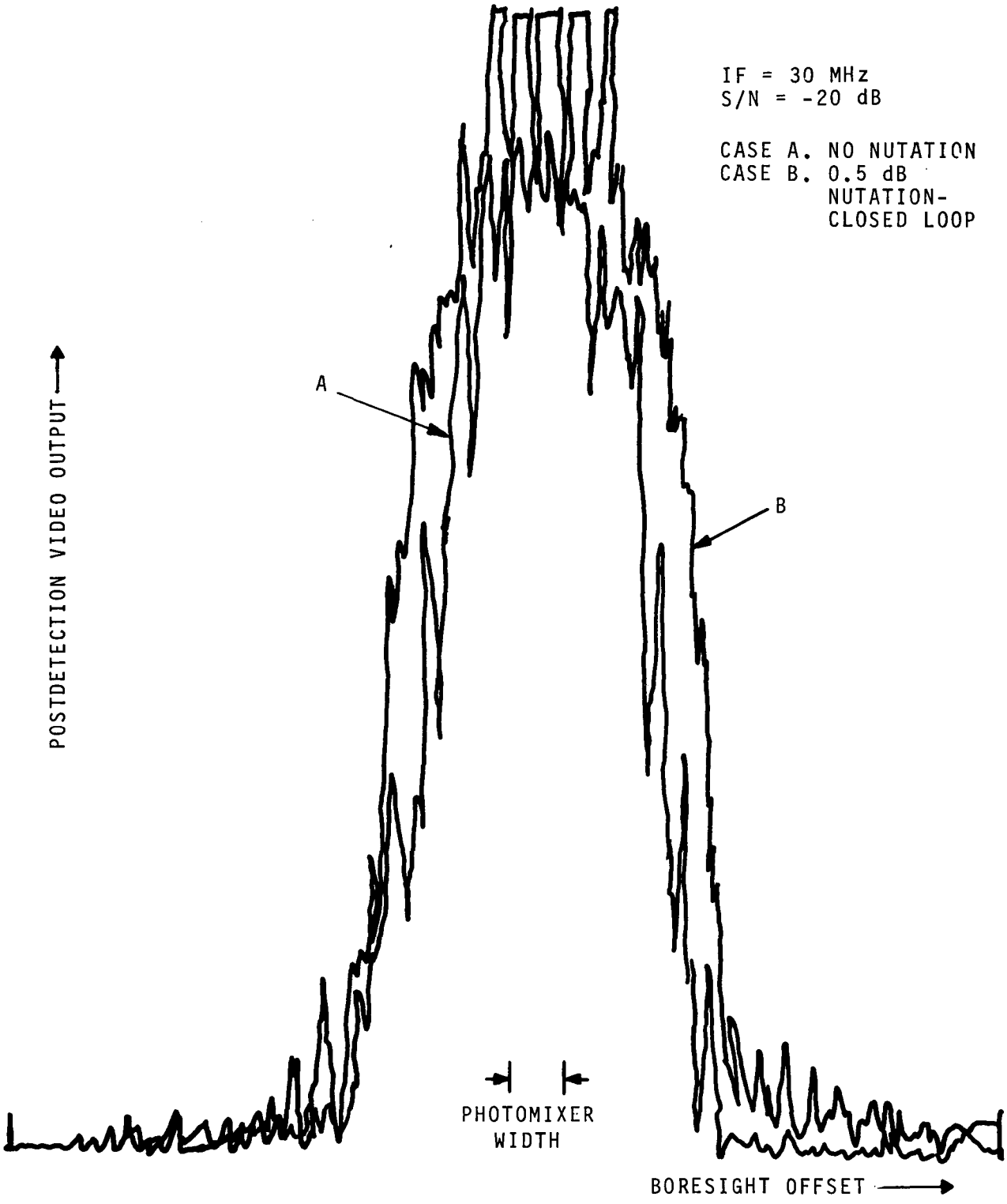

FIGURE 22. POSTDETECTION VIDEO OUTPUT LEVEL AS A FUNCTION OF BORESIGHT OFFSET FOR IF SNR = -20 dB

output for the open-loop case with no nutation is shown in curve A and curve B of Figure 22 shows the video output for a closed-loop nutation of about 0.5 dB. As can be seen, the spatial coverage of curve B is greater than that of curve A.

D. VIDEO GROUP DELAY MEASUREMENTS

The group time delay response of the receiver is strongly affected by impedance mismatches that exist between the various components that comprise the IF channel (Figure 2). Since the percentage bandwidth is large (12 MHz/30 MHz or 40 percent), it is necessary to design matching networks that will function satisfactorily over the entire band. Substantial effort was directed toward optimizing the impedance match between the limiter and channel filter, as well as between the channel filter and the discriminator. A delay equalizer was developed which compensates for slowly varying changes in delay with frequency.

The test setup used to measure time delay and amplitude response of the IF channel is shown in Figure 23. The Phase Comparator compares the phase difference between the 200-kHz modulation voltage leaving point A and the demodulated voltage arriving at point B. Time delay can be computed from this phase information. The signal is passed through the IF channel of the receiver and detected in the FM discriminator. The modulation is then amplified by the video amplifiers.

A 200-kHz filter is utilized to suppress harmonics which would otherwise disturb the measurement. The VCO is swept across the IF band by the sawtooth output of the oscilloscope. Figure 24 shows the time delay and amplitude response of the ORS. A time delay variation of ±10 ns was measured over the 24 to 36 MHz frequency band. The amplitude variation was approximately ±0.4 dB over the band.

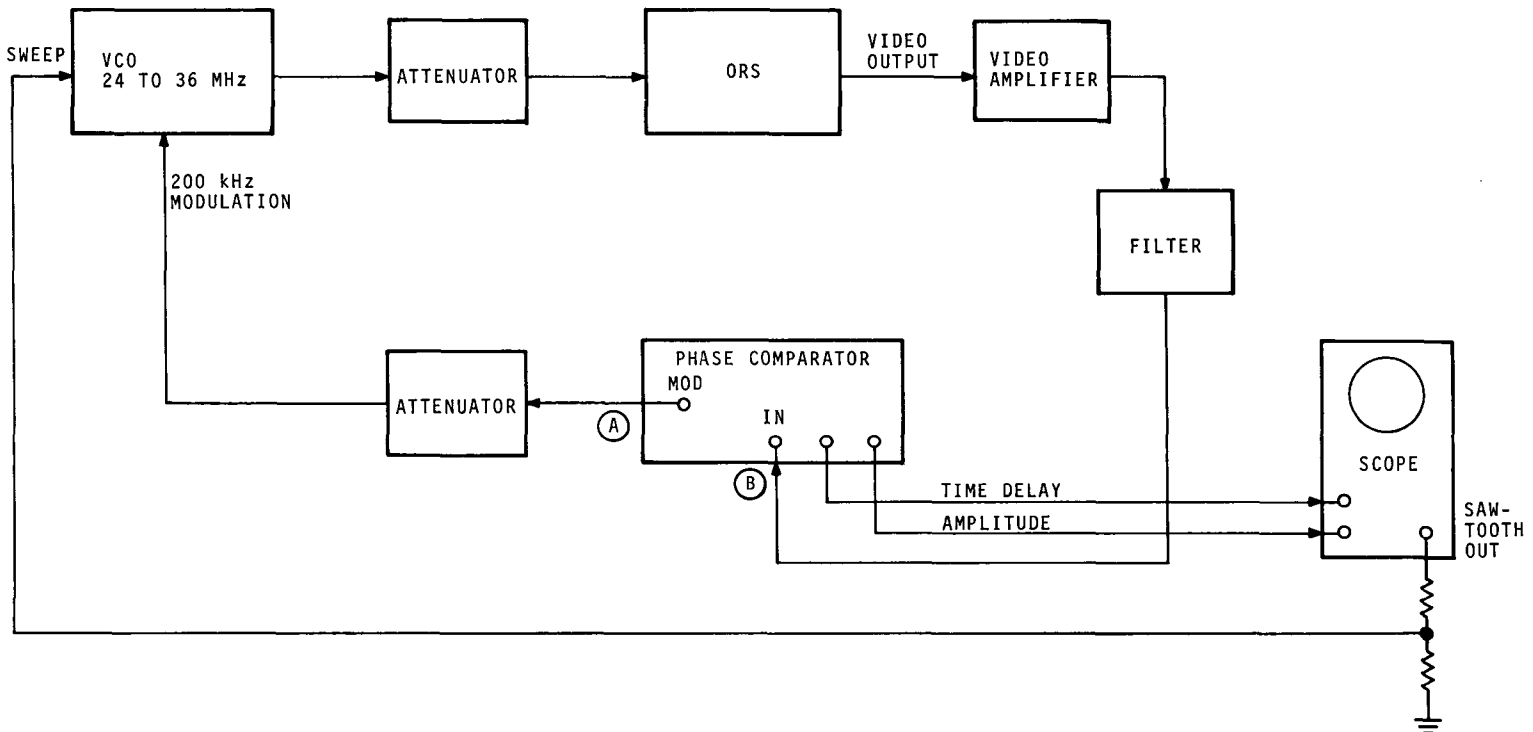

FIGURE 23. BLOCK DIAGRAM OF TEST SETUP FOR VIDEO GROUP DELAY MEASUREMENTS

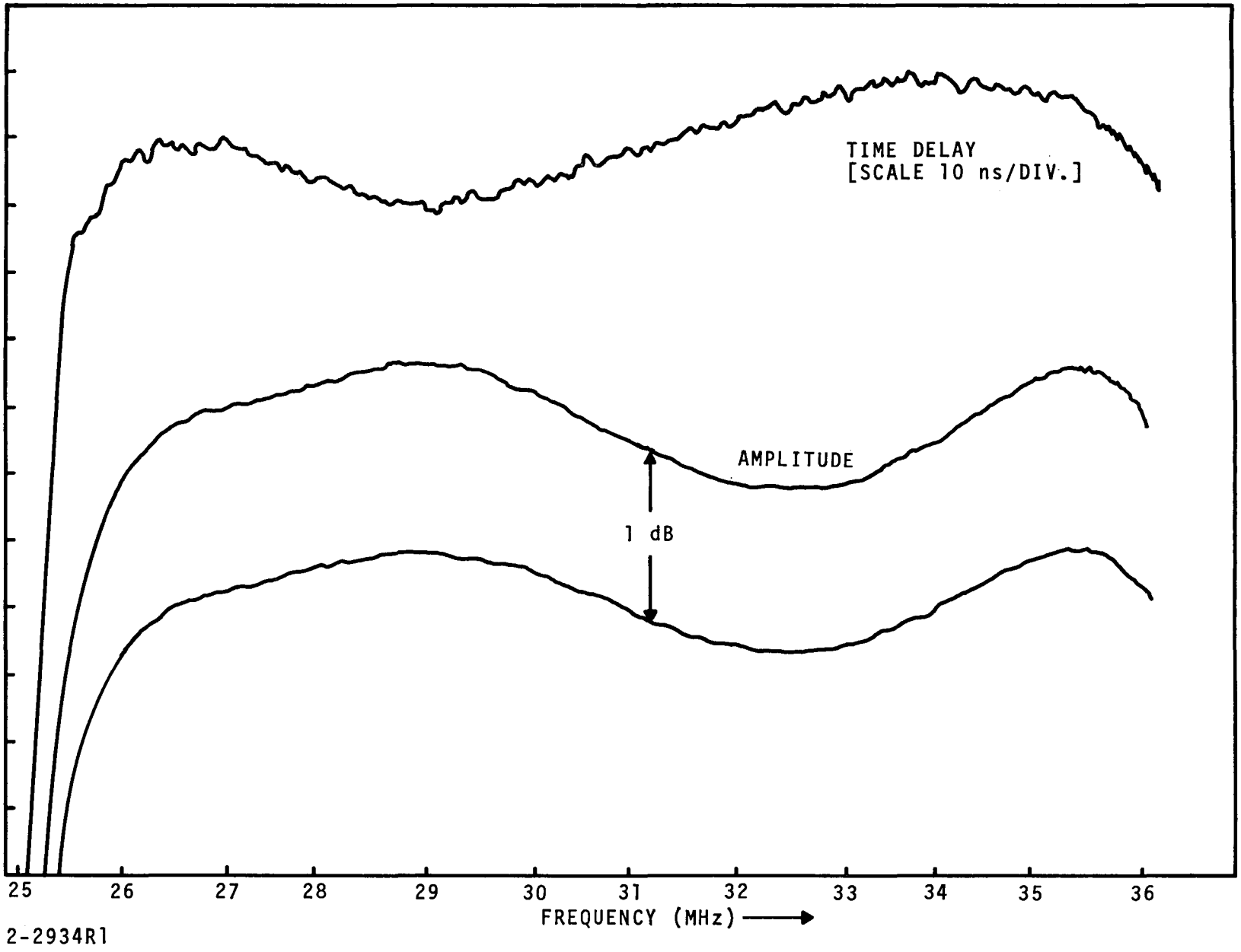

FIGURE 24. MEASURED TIME DELAY AND AMPLITUDE RESPONSE OF ORS

E. CONCLUSIONS

Laboratory measurements, made under simulated operating conditions to test the ability of a CO_2 laser communications link to acquire weak signals and establish tracking lock, have been reported. The sensitivity of the heterodyne receiver was approximately 10^{-19} W/Hz. Link analysis established that acquisition could be achieved for signal-to-noise ratios of -19 to -21 dB (referred to the IF bandwidth). The laboratory measurements show that the ORS is capable of performing the acquisition, confirm, and tracking functions at these low SNR's. The time delay during acquisition was approximately 14 ms and the spatial overshoot was 1 photomixer width. After acquiring the weak transmit signal, the transmit beam is spatially narrowed thereby increasing the IF SNR to +20 dB (or better) which is suitable for wideband communications. Spatial tracking was maintained over 11 photomixer widths during the communication mode by the same tracking circuitry as that used in the weak signal acquisition mode. AFC tracking was achieved over a ±6 MHz band and the amplitude and time delay variations in the communications channel were ±0.4 dB and ±10 ns, respectively.

III. PERFORMANCE MEASUREMENTS ON PV HgCdTe PHOTOMIXER/PREAMPLIFIER COMBINATION

Performance measurements on a selected PV HgCdTe infrared mixer have been completed. The photomixer was mounted in a specially developed detector housing (Figure 25) which was RFI shielded, hermetically sealed, suitable for mounting in a passive radiation cooler and designed for operation in a satellite-type environment (references 8 and 11). (Additional data on the detector housing is given in Appendix B.)

The photomixer exhibited the following characteristics at T_m = 77 K and zero bias (V_B = 0):

Sensitive area	2.7×10^{-4} cm^2
Peak wavelength	~ 12.7 micrometers
Series resistance, R_s	~ 15 ohms
Shunt conductance, G_D	~ 200 ohms

A. MIXER QUANTUM EFFICIENCY

Photomixer 10.6-micrometer quantum efficiency (QE) measurements were carried out over the temperature range of 77 to 152K for applied bias voltages between 0 and -400 mV. Results are shown in Figure 26. The zero bias, 10.6-micrometer quantum efficiency was 11.2 percent at 77 K, increased to 13 percent near 105 K, and then decreased to 3.2 percent near 140 K. [The spectral peak of the photomixer occurred near 12.7 micrometers at 77 K.] The increase in measured QE may be attributable to a shifting of the spectral peak toward 10.6micrometers with increasing mixer temperature.

The reverse biased, 10.6 micrometer QE at 77 K was 10.8, 6.8, and 5 percent for V_B = -100, -200, and -300 volts, respectively. The reverse

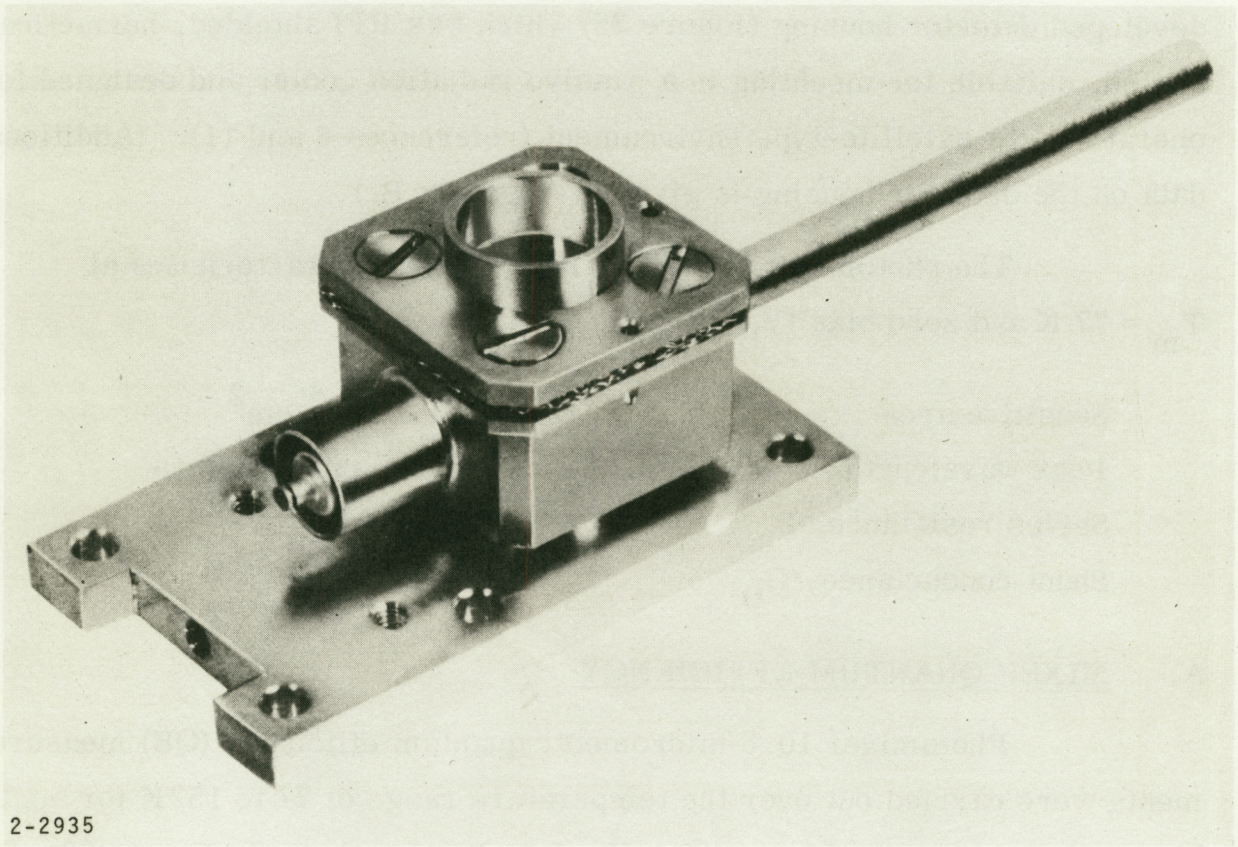

FIGURE 25. PHOTOMIXER HOUSING

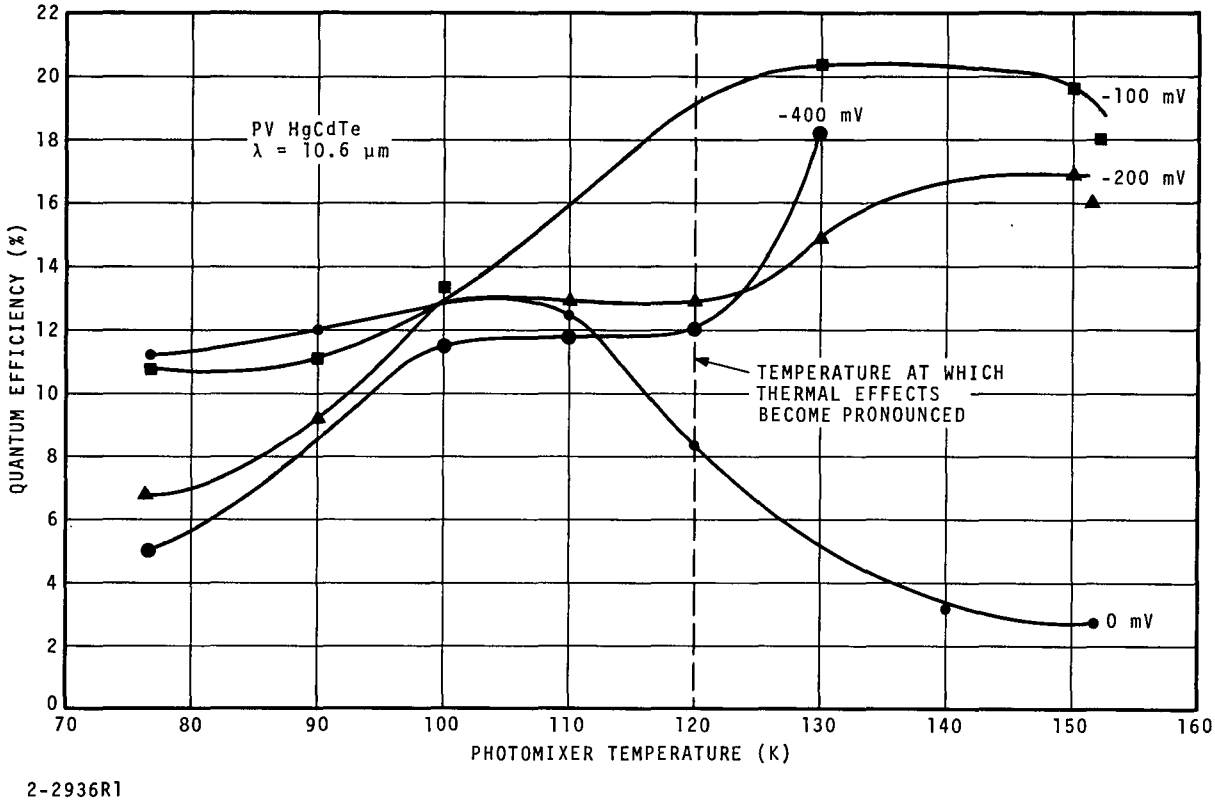

FIGURE 26. MEASURED QUANTUM EFFICIENCY OF A HgCdTe PHOTOMIXER AS A FUNCTION OF OPERATING TEMPERATURE

biased QE also increased with increasing mixer temperature up to $T_m \approx 105$ K. Above 110 K the QE continued to increase for $V_B = -100$ mV, while for $V_B = 200$ and -400 mV the QE appeared to level off until $T_m \sim 120$ K and then increased with increasing mixer temperature. The apparent effect of reverse bias is to broaden the spectral response curve in a fashion which will decrease the dependence of quantum efficiency on mixer temperature and shift the peak spectral response to higher wavelengths.

Above $T_m = 120$ degrees, it is suspected that thermal effects caused by absorbed LO power, change the photodiode characteristics and obscures the quantum efficiency measurement. These thermal effects, however, are long time-constant perturbations. Additional measurements have been carried out to verify their presence.

The CO_2 laser beam was chopped with a high-speed, short duty cycle chopper. Dynamic measurements of the relative QE which insured that no unwanted (long time-constant) thermal effects would upset the QE measurement have been completed. During these measurements, incoming laser beam power was held constant and the peak output voltage was observed on an oscilloscope as the detector temperature was raised from 77 to 150 K. Measurement results are shown in Figure 27. The zero bias 10.6 micrometer dynamic QE peaked near 90 K and then decreased with increasing temperature. For $V_B = -100$ and -200 mV the dynamically and statically measured QE followed a similar pattern for T_m between 77 and 150 K with the exception that the dynamically measured QE decreases with increasing temperature above 130 K. The static and dynamic 10.6-micrometer QE measurements at $V_B = -400$ mV exhibited a similar variation of QE with mixer temperature up to $T_m \sim 120$ K. Above this temperature the suspected thermal effects were varified since the dynamically measured QE degraded sharply at $V_B = -400$ mV while the static measurement QE was seen to increase.

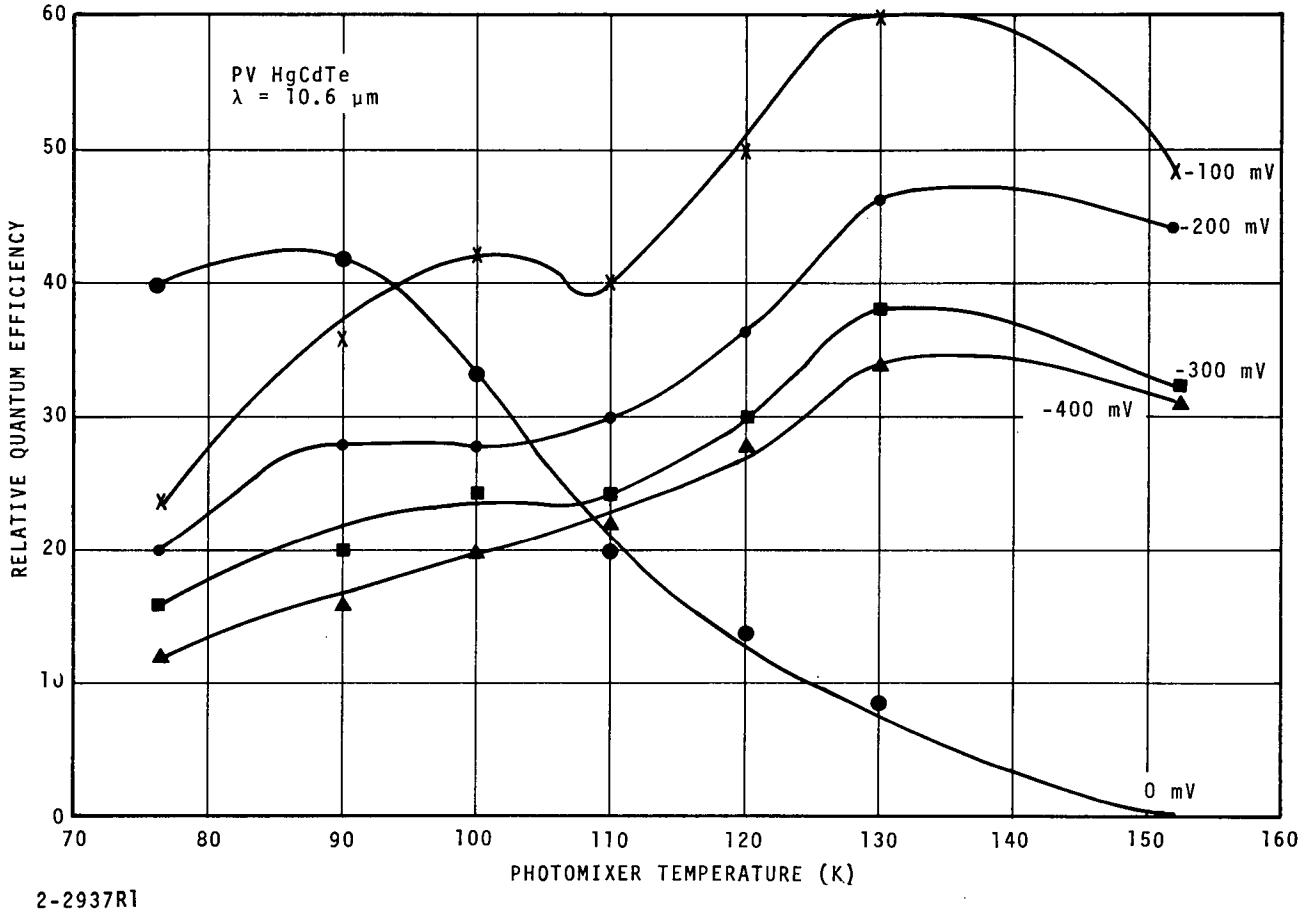

FIGURE 27. DYNAMICALLY MEASURED QUANTUM EFFICIENCY OF A HgCdTe PHOTOMIXER AS A FUNCTION OF OPERATING TEMPERATURE

Based on the 10.6-micrometer QE measurements, it appears that this photomixer may be useful for mixer temperatures up to 130 K and mixer bias voltages between -100 and -200 mV, without exhibiting any degradation due to thermal effects.

B. CURRENT/VOLTAGE CHARACTERISTICS

The current/voltage (I/V) characteristics of a PV HgCdTe photomixer have been measured with and without incident laser LO illumination at mixer temperatures between 77 and 152 K. Results of these measurements are shown in Figure 28. At bias levels beyond the "knee" in the I/V curves, the slope resistance was unchanged with the application of LO power. In general, the photomixer operating point is selected to be beyond the "knee" in the I/V characteristic.

The slope resistance of the photomixer was measured as a function of temperature for reverse bias levels of -100, -200, and -400 mV (Figure 29). Photomixer slope resistance is an important parameter used in determining the input impedance requirements of the IF preamplifier. For photomixer operation over a wide temperature range, it is desirable to have a preamplifier which will operate over a large range of input impedance levels without serious degradation in amplifier noise factor or gain. Increasing the mixer temperature generally increases the reverse slope resistance, and for the photomixer under test, this effect was more pronounced at V_B = -100 mV bias than for V_B = -200 mV. Therefore, operation at the higher bias is more desirable for this photomixer even though the maximum quantum efficiency is obtained for the -100 mV case (Section III-A). The selection of optimum photomixer bias level depends on factors such as QE, mixer slope resistance, and the photomixer 3-dB cutoff frequency. Other conditions such as the variation of the induced shot-noise with photomixer temperature and bias may also have to be taken into account to a lesser degree.

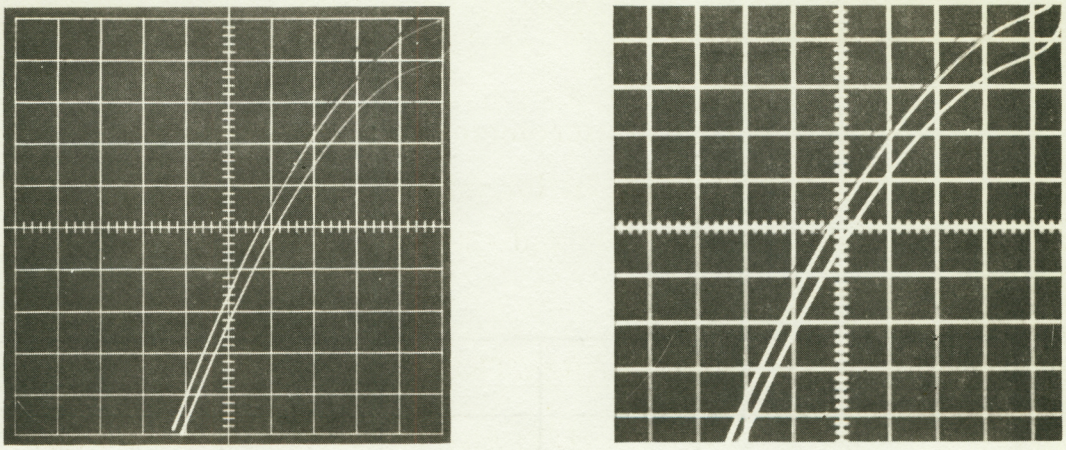

A = 77 K

B = 90 K

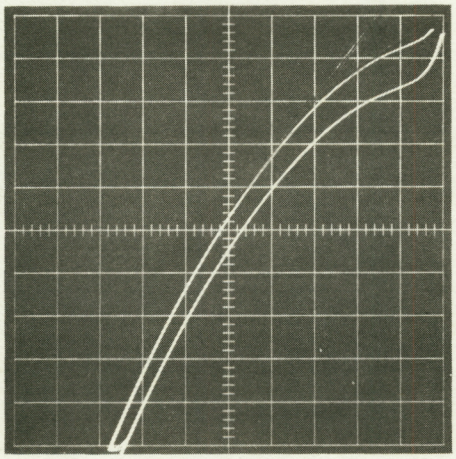

C = 102 K

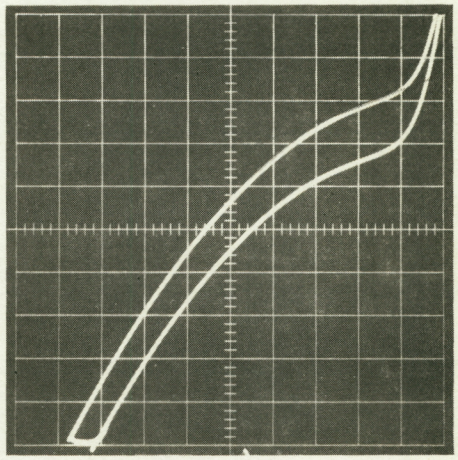

D = 130 K

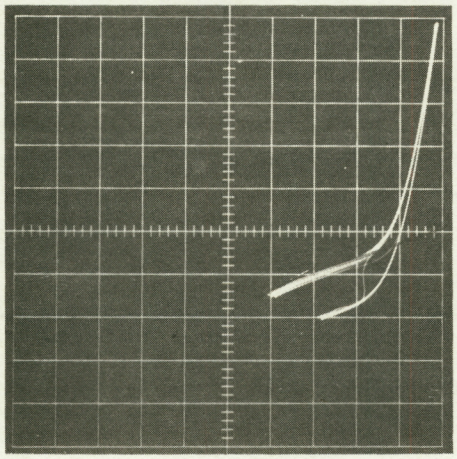

E = 152 K

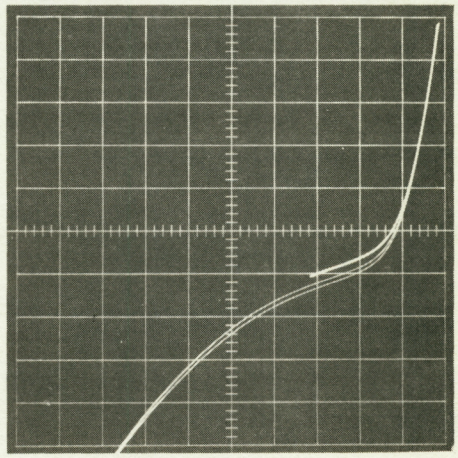

F = 152 K

VERT = 0.2 mA/DIV

HORIZ = 50 mV/DIV

2-2938

FIGURE 28. I-V CURVES FOR VARIOUS TEMPERATURES WITH/ WITHOUT LO ILLUMINATION

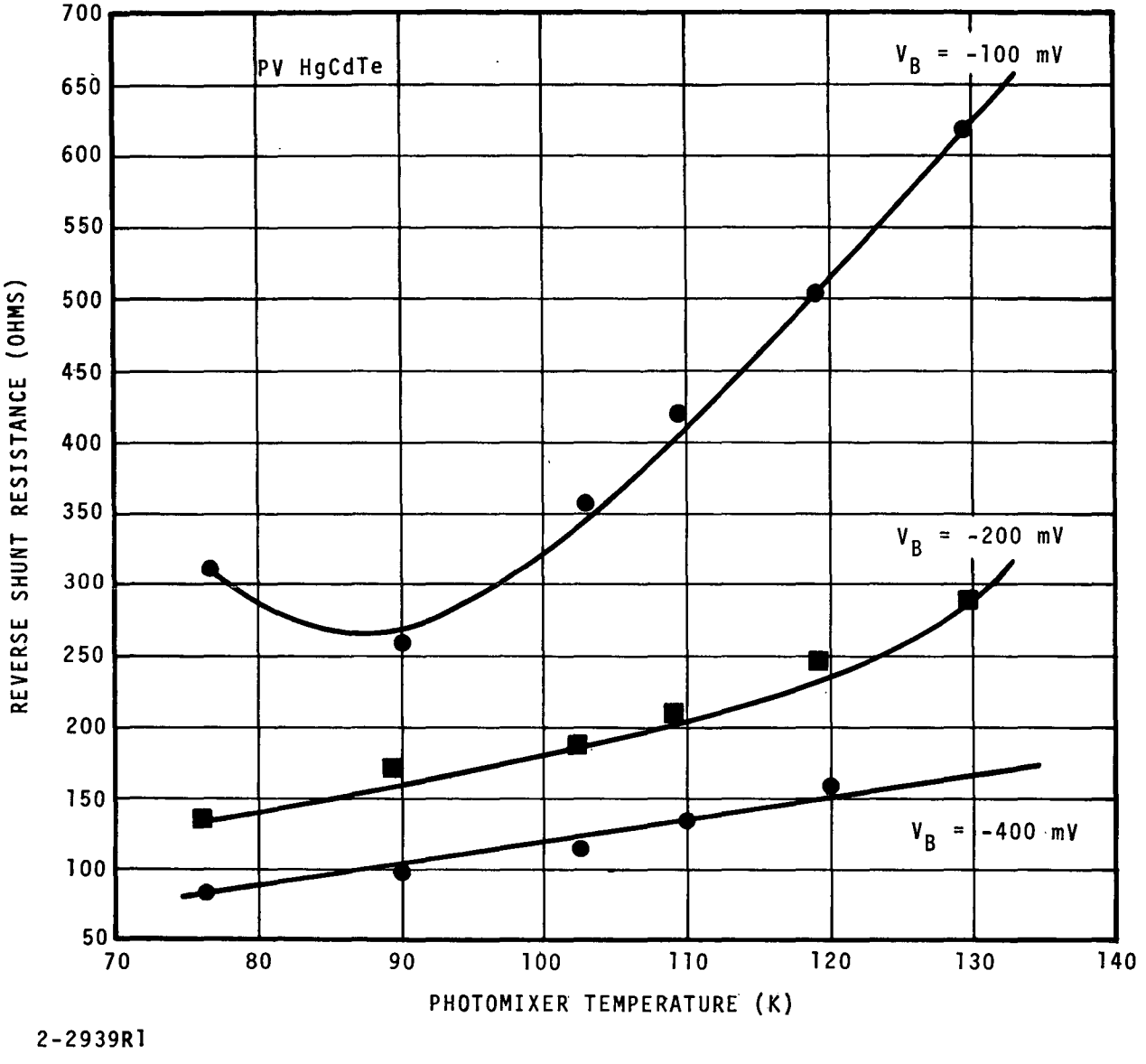

FIGURE 29. REVERSE SLOPE RESISTANCE OF A PV HgCdTe PHOTOMIXER AS A FUNCTION OF OPERATING TEMPERATURE

The measured I/V characteristic of the selected mixer exhibited a retrace offset for T_m = 152 K (Figure 28) which is attributed to thermally generated effects in the photomixer. These thermal effects are also observed when statically measuring the quantum efficiency. The applied bias on the detector alters the I/V curve at these higher temperatures causing an instability which should be avoided in system use. Therefore, the maximum operating mixer temperature for the measured photomixer is estimated to be approximately 130 K.

Photomixer operation at these higher temperatures (T_m > 130 K) may cause nonreversible changes in the photomixer and a reduction in overall receiver sensitivity. In addition it should be noted that:

- The particular photomixer under test was developed for 77 K operation; no special provision was made for operation at higher temperatures
- Other selected photomixers may exhibit degraded operations at mixer temperatures below 130 K.

C. PHOTOMIXER FREQUENCY RESPONSE

Under this program, the 3-dB cutoff frequency of a photovoltaic photomixer has been shown (reference 12 and Appendix A) to be

$$f_c = \frac{\left(1 + R_S G_D\right)^{1/2}}{2\pi C_D \left(R_S/G_D\right)^{1/2}} \approx \frac{1}{2\pi C_D \left(R_S/G_D\right)^{1/2}}, \quad R_S G_D << 1 \qquad (3)$$

where

G_D = small-signal shunt conductance (slope of I/V curve in reverse direction) of the photomixer

R_S = series resistance of the photomixer

C_D = junction capacitance of the photomixer

The frequency response of the photovoltaic HgCdTe photomixer was measured as a function of bias voltage and mixer temperature using the previously developed shot noise measurement technique (references 2 and 3). The variation of the 3 dB cutoff frequency with dc bias at T_m = 77, 100 and 125 K is shown in Figure 30. The cutoff frequency varied from 85 MHz at V_B = -100 mV to 420 MHz at an applied bias voltage of -600 mV.

The measurements were in general agreement with previously reported measurements (reference 13) in that:

- The cutoff frequency varied with bias voltage as $(V_b)^n$ where n= constant
- The cutoff frequency variation with reverse bias voltage is independent of temperature over the range from 77 K to 125 K
- The frequency response appears to be limited by the RC time constant of the junction

The shot noise power versus IF frequency for the photomixer preamplifier combination is plotted in Figure 31 for T_m = 125 K, V_B = -600 mV, I_o = 1.7 mA and an IF amplifier with a 4 dB noise figure. The measured 3 dB cutoff frequency was 420 MHz.

D. NOISE EQUIVALENT POWER

The noise equivalent power (NEP) for a reverse-biased PV heterodyne receiver (reference 12 and Appendix I) is the value of signal power which gives an IF signal-to-noise ratio of unity and is given by:

$$NEP = \frac{h\nu B}{\eta} \left\{ 1 + \frac{2k\left(T_M + T'_{IF}\right)}{qI_o} \left[G_D \left(1 + R_S G_D \right) + \omega^2 R_S C_D^2 \right] \right\} \quad (4)$$

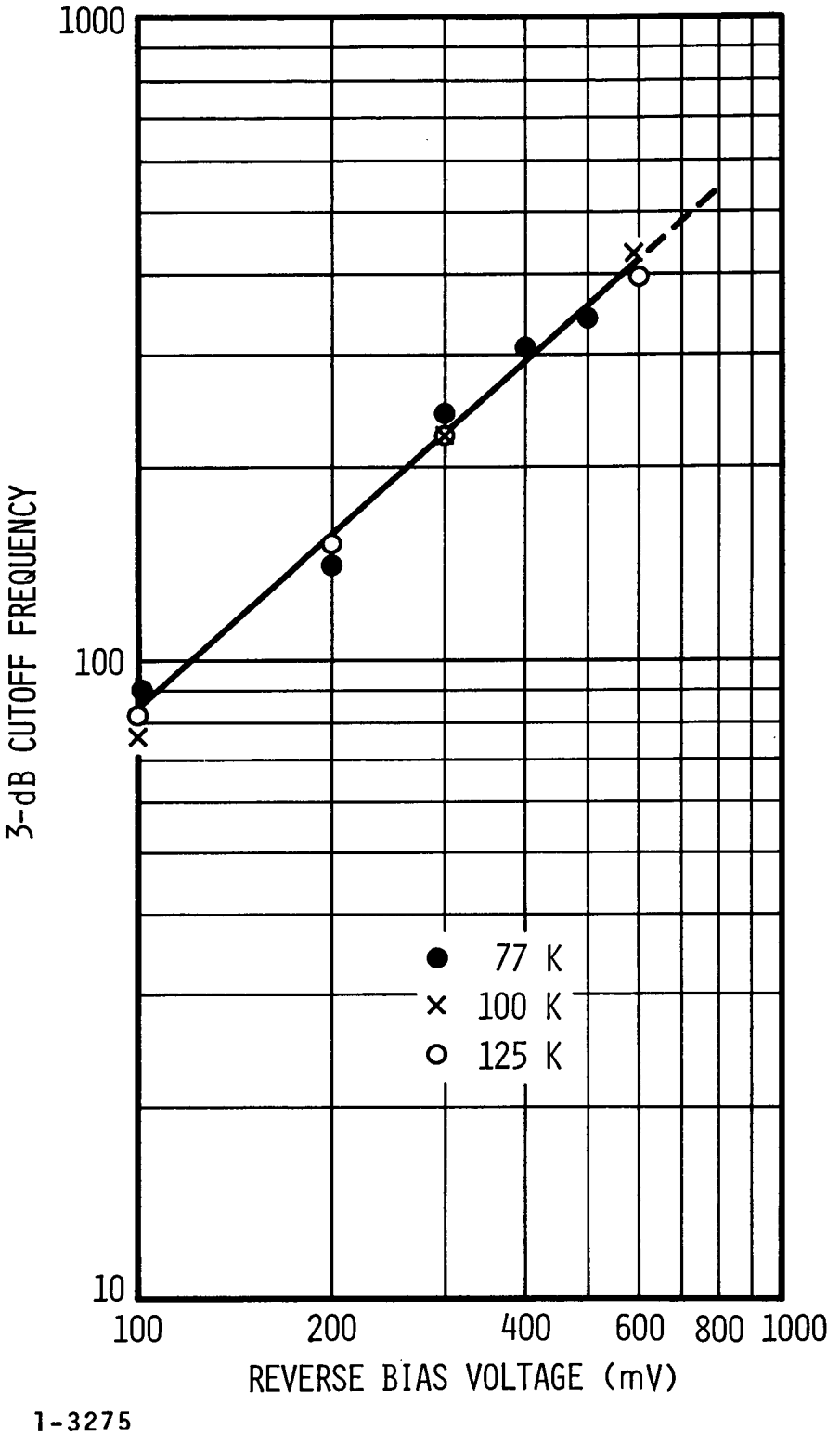

FIGURE 30. CUTOFF FREQUENCY VERSUS BIAS VOLTAGE FOR HgCdTe PHOTODIODE

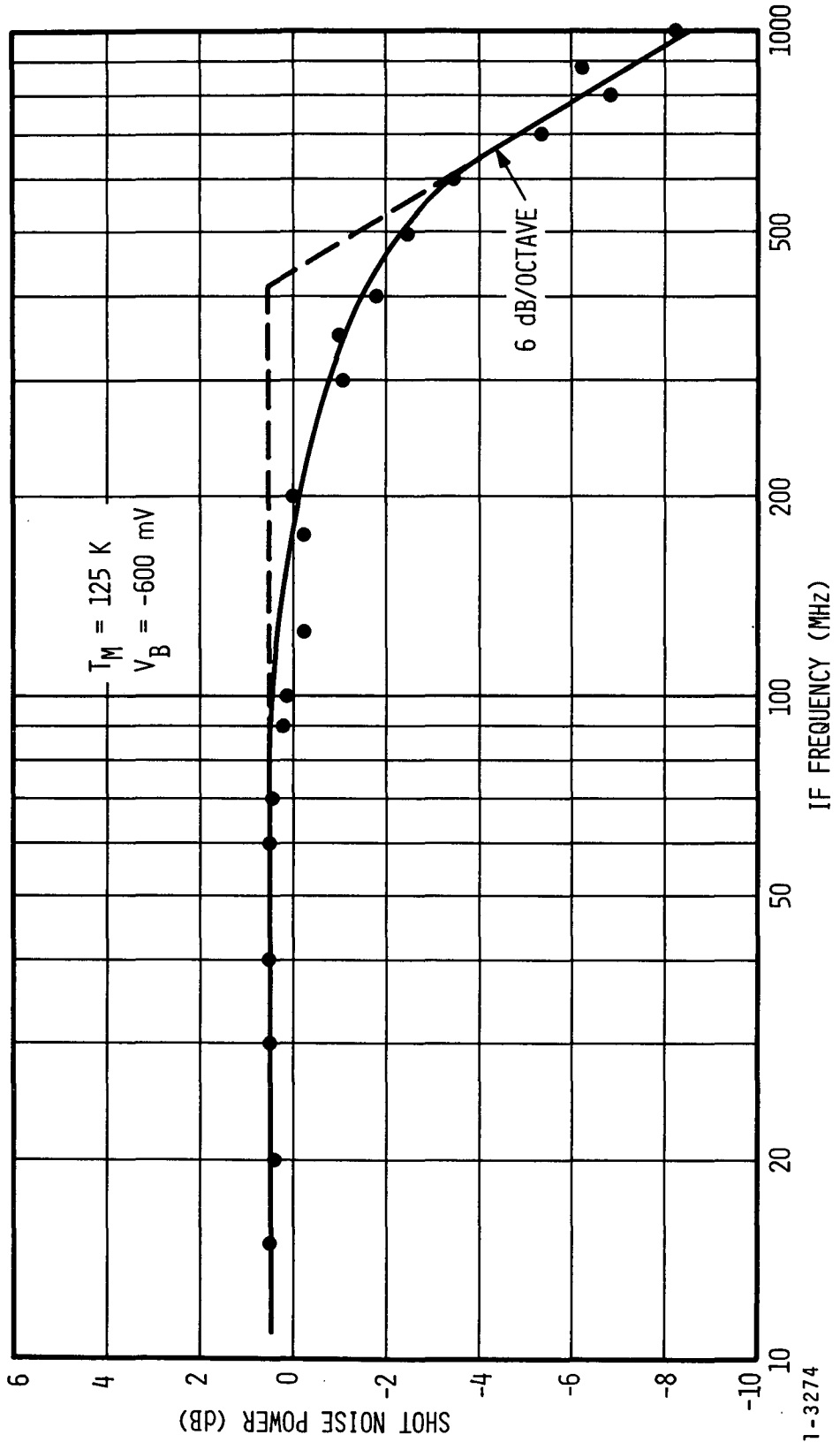

FIGURE 31. SHOT NOISE SPECTRUM OF HgCdTe PHOTODIODE

This is reducible to

$$NEP = \frac{h\nu B}{\eta} + \frac{k\left(T_M + T'_{IF}\right)B}{G} \qquad (5)$$

where

h = Planck's constant

ν = infrared frequency

B = IF bandwidth

η = photomixer quantum efficiency

k = Boltzmann's constant

T_m = physical temperature of the photomixer

T'_{IF} = effective input noise temperature of the IF preamplifier

G = available conversion gain of the photomixer

ω = IF radian frequency

q = electronic charge

I_o = DC photocurrent induced by the laser LO

Equation 5 is the same expression as the one derived for the photoconductive mixing case (reference 2) with the exception of the elimination of a factor of two in the first term. The first term in equation 5 represents the quantum noise contribution and can be expressed as $P_{MIN} \equiv h\nu B/\eta$, where P_{MIN} = minimum achievable NEP.

E. RECEIVER SENSITIVITY

Mixer sensitivity measurements as a function of LO power and temperature have been completed on the photovoltaic HgCdTe photomixer mounted in a specially designed housing. The entrance window of the mixer

housing was an antireflection coated germanium (95 percent minimum transmission at 10.6 micrometers). (The reported NEP measurements have not been corrected for the window transmission loss.) The mixer sensitivity measurements were carried out with uniform-field, plane-wave optical spots for both LO and signal beams in order to ensure uniform optical energy distribution over the sensitive area of the mixer.

Figure 32 shows a plot of receiver sensitivity measured at an IF of 30 MHz as a function of mixer temperature. The measured NEP was below 10^{-19} watt/Hz for mixer temperatures between 82 and 104 K, and below 2×10^{-19} watt/Hz for mixer temperatures between 77 and 140 K. Above 110 K, the measured NEP was slightly degraded by what is believed to be excess thermal noise in the mixer (Section III A and B). A thermally induced current has been observed in the photodiode above $T_m > 120$ K which appears similar in behavior to photocurrent but exhibits a long time constant. The thermally induced current produces greater noise than expected at these higher temperatures, thereby, reducing the overall receiver signal-to-noise ratio.

The NEP measurements were made with -400 mV of reverse bias on the mixer. This results in a mixer cutoff frequency in excess of 300 MHz. Since the NEP measurements were carried out at an IF of 30 MHz, which is much less than the mixer cutoff frequency, the dynamic impedance of the mixer should be close to the reverse slope resistance (G_D^{-1}). The measured G_D^{-1} at -400 mV bias as a function of temperature is shown in Figure 29. At 77 K, the resistance is 85 ohms and varies linearly to 174 ohms at 140° K. Since minimum noise figure of the preamplifiers used for these measurements is obtained near 100 ohms source impedance, the effect of impedance match between the photomixer and preamplifier as a function of temperature is an important design parameter. A set of matched amplifiers with variable input impedance were constructed to investigate the effects of impedance mismatch between the photomixer and the preamplifier (Section V-D). Since photo-induced shot noise must overcome the thermal noise of the photomixer and

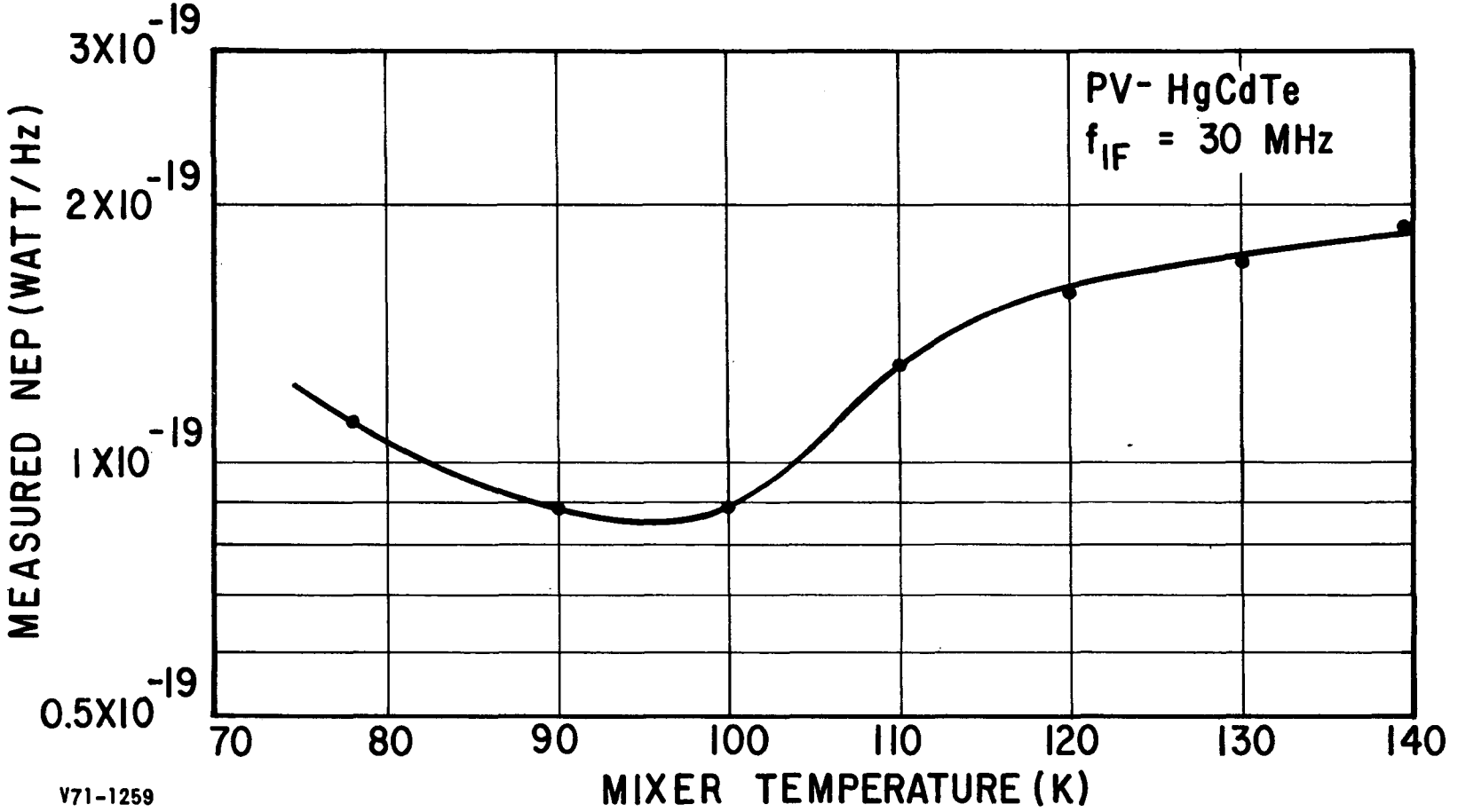

FIGURE 32. RECEIVER SENSITIVITY VERSUS MIXER TEMPERATURE

IF preamplifier, it is important to select a preamplifier which allows maximum transfer of shot noise so that the ratio of shot to thermal noise is maximized.

The measured receiver NEP as a function of incident LO power at an IF of 30 MHz is shown in Figure 33. In order to achieve quantum noise limited operation it is necessary to operate with approximately 1.5 mW of local oscillator power intercepted by the mixer. Photo-induced shot-noise exceeds the thermal noise for these values of LO power ensuring quantum noise limited operation and optimum receiver sensitivity.

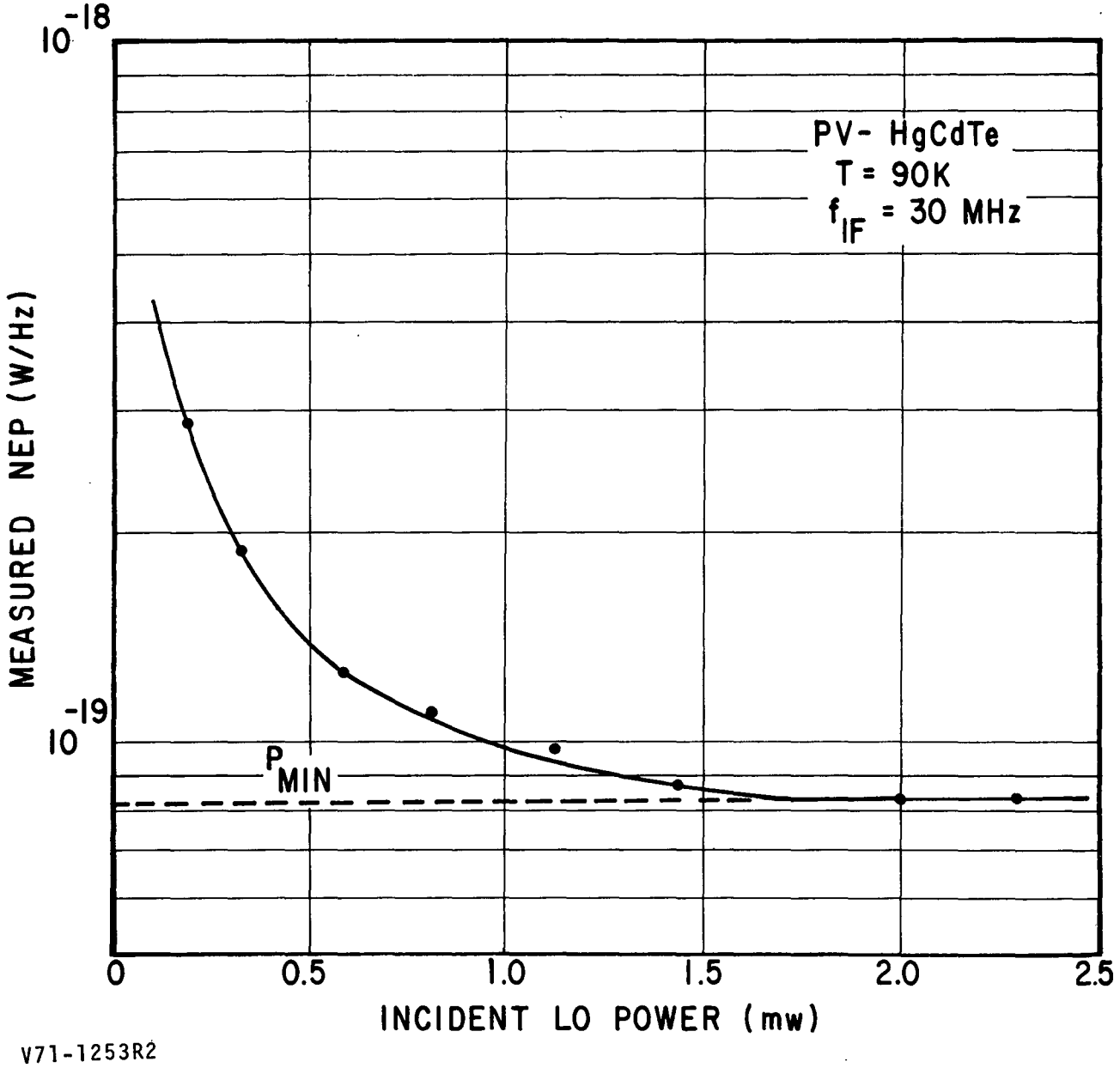

FIGURE 33. MEASURED RECEIVER NEP AS A FUNCTION OF OSCILLATOR POWER

IV. TEMPERATURE AND DC BIAS CYCLING OF PV HgCdTe PHOTOMIXERS

Two randomly selected HgCdTe photomixers which had been fabricated and specified (by the manufacturer[1]) for 77 K temperature operation were extensively tested over a 9 month period in an attempt to establish some environmental and operational limits on these devices. Photomixer 1 was operated between 77 and 152 K with applied laser LO and dc bias which exceeded the manufacturer's specified values. Photomixer 2 was temperature cycled between 77 and 86 K and operated within the manufacturer's specified laser LO and dc bias limits. In addition, it was also operated up to 150 K with dc bias applied.

A. PHOTOMIXER 1

Photomixer 1 was temperature cycled and biased stressed beyond normal operational limits in an attempt to establish some upper limits of photomixer performance and to determine if a catastrophic failure would occur.

Heterodyne operation was achieved at photomixer temperatures up to 152 K. After:

- Over 200 cycles of mixer temperature between 77 and 152 K.
- The application of up to 10 mW of laser LO power (manufacturer's maximum recommended value at 77 K was 3.5 mW).
- The application of the maximum rated dc bias voltage and current (established for 77 K operation) at photomixer temperatures as high as 152 K.

Some changes in the photomixer quantum efficiency were observed.

---

[1] The photomixers were manufactured by Societe Anonyme de Telecommunications, Paris, France.

Although there were some changes in photomixer quantum efficiency characteristics, no catastrophic failures occurred and stable heterodyne operation could be achieved over the 77 to 152 K temperature range throughout the entire 9 month test period.

The photomixer exhibited extremely stable characteristics between 77 and 110 K over the entire test period. When the photomixer was operated above 120 K, excess thermal noise effects which degraded the heterodyne receiver sensitivity were observed. Slight changes in photomixer characteristics occurred when the mixer temperature was increased above 120 K under heterodyne operational conditions. However, even though the photomixer characteristics were altered somewhat due to operation above all reasonable limits, stable operation was achievable.

Table 1 summarizes the measured QE at $V_B = 0$, -200 and -400 mV for $T_M = 77$, 100, 120, and 140 K at the start, midpoint and end of the 9 month test period. As can be seen, the QE of photomixer 1 varied throughout the test cycle. On the average, the QE exhibited a peak near the midpoint of the cycle. In addition, it should be noted that the QE measurements at photomixer temperatures above 130 K were obscured by excessive thermally induced dc current.

A change in the photodiode spectral response can be postulated as a reason for the measured change in the QE of the widely temperature cycled photomixer. For example, a change in the mercury concentration of the upper (p-type) absorption layer due to the application of large laser LO and dc bias power levels at elevated temperature might be sufficient to cause such a shift. Based on the measured data, it appears that the spectral peak shifted from its initial value of 12.7 micrometers towards 10.6 micrometers, during the 9-month test period. It should be noted that the 12.7 micrometer spectral peak, measured at 77 K, also shifts toward 10.6 micrometers with increasing photomixer temperature. The

TABLE I. VARIATIONS OF HgCdTe PHOTOMIXER QUANTUM EFFICIENCY OVER A 9-MONTH TEST PERIOD

V_B (mV)	Temp (K)	Quantum Efficiency Initial (%)	Intermediate (%)	Final (%)
0	77*	11	-	9
	100	13	-	9
	120	8	-	6
	140**	3	-	5
200	77	7	12	6
	100	13	15	7
	120	13	20	8
	140**	16	39	15
400	77	5	10	3
	100	12	13.5	6
	120	12	20	7
	140**	-	25	13

* Photomixer 1 was developed for 77 K temperature operation.
** Excess thermal noise was induced at photomixer temperatures of 130^{o}K, and above.

spectral response of the photomixer at 77 K was measured at AIL at the conclusion of the test period and compared to the manufacturer's measurement data (Figures 34 and 35). The spectral peak apparently changed 1.2 micrometers during the test period. Thus, the hypothesis of a chemical change appears to be confirmed. However, the accuracy of the spectral response measurements and the fact that they were made at different laboratories introduces uncertainties in the conclusion. The difference in the measured spectral shapes (Figures 34 and 35) also adds additional uncertainties.

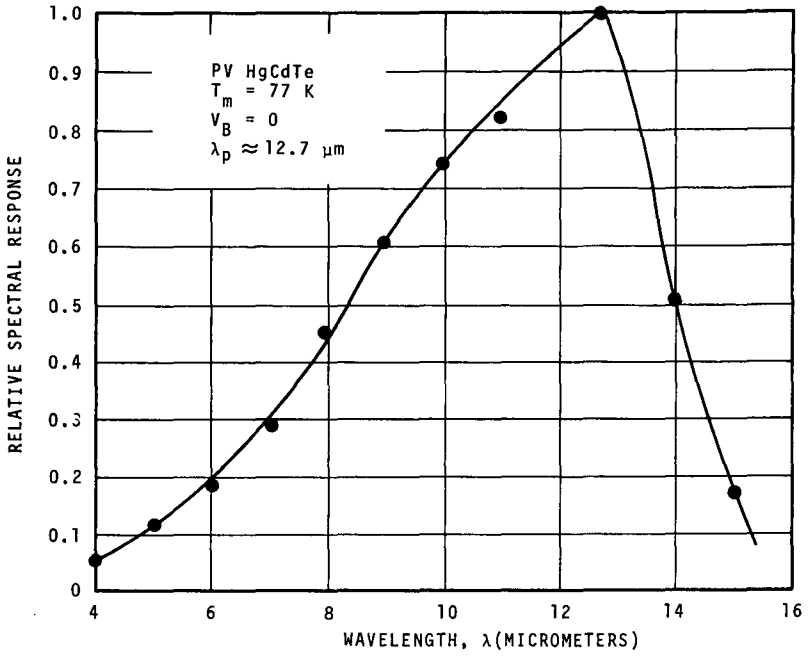

FIGURE 34. MEASURED SPECTRAL RESPONSE OF PV HgCdTe PHOTOMIXER 1 AT THE BEGINNING OF TEST PERIOD

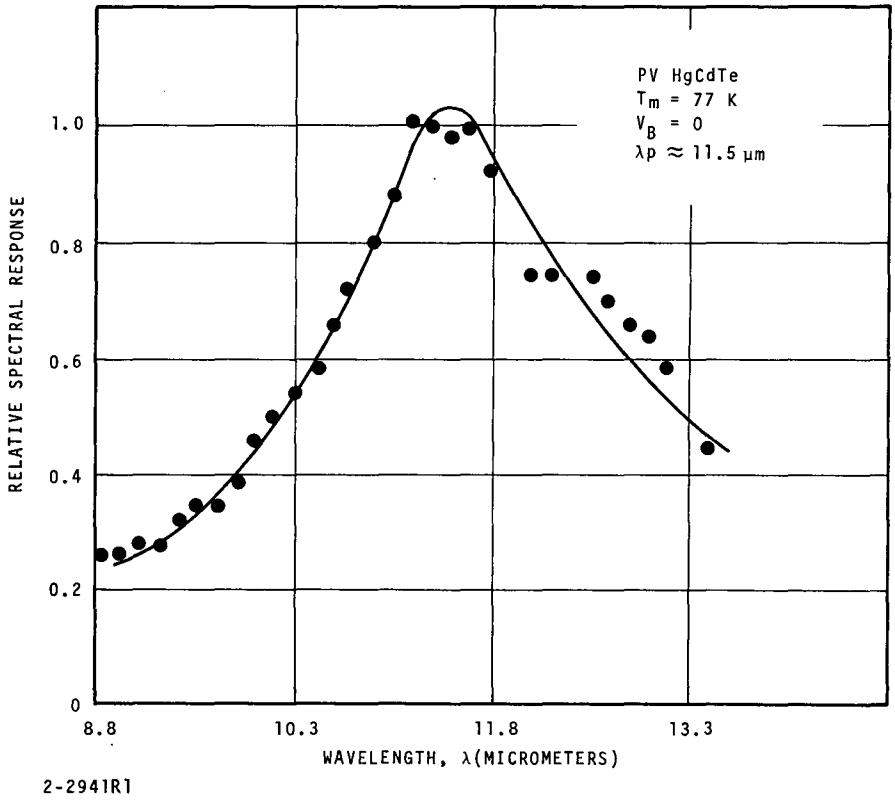

FIGURE 35. MEASURED SPECTRAL RESPONSE OF PV HgCdTe PHOTOMIXER 1 AT THE CONCLUSION OF TEST PERIOD

It should also be noted that:

- The accuracy of the QE measurement setup is estimated to be ±5 percent
- A thermistor type balometer which is calibrated to an NBS traceable standard was used to measure the incident CO_2 laser radiation
- The transmittance of the window* on the cryogenic dewar was checked regularly

The current/voltage (I/V) characteristics of photomixer 1 were also monitored over the 9-month test period. The I/V characteristics measured at the beginning and end of the 9-month test period are shown in Figure 36. Although the zero bias points are offset by about 0.4 mA, it can be seen that almost no change in the I/V characteristic occurred due to the extensive temperature and bias cycling.

B. PHOTOMIXER 2

Photomixer 2 was operated in the heterodyne mode at a maximum temperature of 86 K under conditions where the applied laser LO and dc bias levels did not exceed the manufacturer's maximum recommended value. Over the 9-month test period, no change in the detector characteristics of photomixer 2 were observed.

In addition, photomixer 2 underwent 10 temperature cycles between 77 and 150 K with dc bias applied, but without any incident laser LO power. The photomixer exhibited no change in detector characteristics during these cycles.

A 77 K life test was carried out on a PV HgCdTe photomixer with an applied bias voltage of -200 mV and a laser induced photocurrent of 0.5 mA. After 30 cycles between 77 K (with bias and laser LO applied) and

---

* During one experimental run the NaCl window in the cryogenic dewar was sprayed with water and allowed to dry. Visible clouding was observed due to moisture absorption but no change in 10.6-micrometer transmittance was observed.

T_M = 77 K
PV HgCdTe

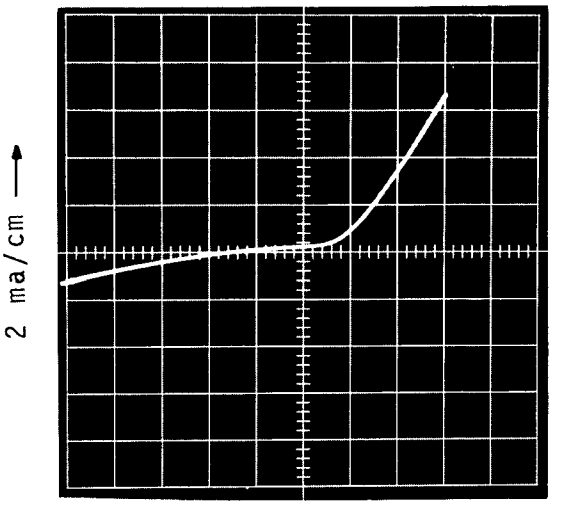

A. INITIAL MEASUREMENT DATA

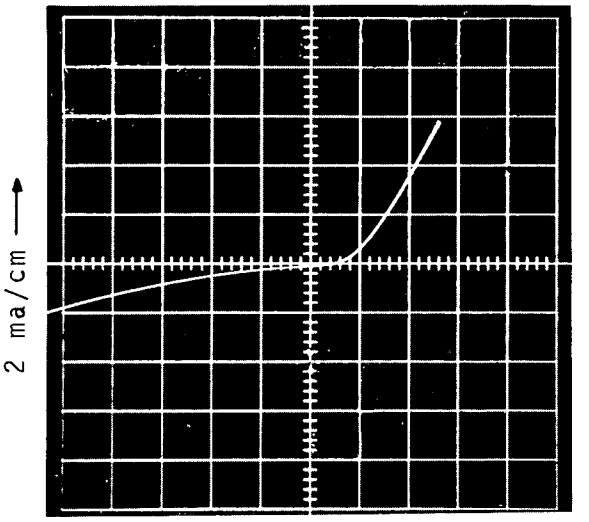

B. MEASURED DATA AFTER
NINE MONTH TEST PERIOD.

2-2942

FIGURE 36. CURRENT-VOLTAGE CHARACTERISTICS OF PHOTOMIXER 1 OVER A 9-MONTH TEST PERIOD

290 K (without bias or laser LO applied), the CO_2 laser failed, ending the life test. The total life test period covered 130 hours of photomixer operation in the heterodyne mode. The photomixer quantum efficiency, current/voltage characteristic, applied bias voltage, and LO-induced photocurrent were monitored throughout the life test program. No changes in photomixer characteristics were observed.

C. CONCLUSIONS

Based on the testing of two photomixers, stable heterodyne operation is achievable at mixer temperatures of 120 K, and above. However, some temporary and permanent changes in photomixer characteristics were observed. The temporary changes occurred when the photomixer was operated under test conditions which exceeded the manufacturer's recommended operation limits; that is, operating temperature, dc bias, and applied laser LO power. It is suspected that the permanent changes (the measured change in quantum efficiency and the apparent shift in the spectral peak) may be a result of operating the photomixer in an overstressed test condition. Excess thermal noise effects which degrade heterodyne sensitivity were also observed at photomixer temperatures above 130 K.

Photomixers, which have not been cycled above 100 K and have been operated within the specified LO and dc bias limits, have not exhibited changes in detector characteristics. These results should be considered preliminary since more extensive measurements are needed to pinpoint the causes for the changes in photomixer characteristics.

---

* Neither AIL nor NASA can guarantee the performance of photomixers when they are operated above those operating conditions set by the manufacturer. The conclusions reached in this report are based strictly on the laboratory testing of randomly selected detectors which were fabricated and specified for 77 K temperature operation.

V. DESIGN CONSIDERATIONS FOR AN OPERATIONAL 10.6-MICROMETER HETERODYNE RECEIVER

Infrared 10.6-micrometer heterodyne receivers have been developed for communications, radar and radiometric applications. This section considers the heterodyne receiver design considerations of:

- Laser LO illumination
- Heat load requirements for photomixer cooler
- Photomixer uniformity
- Effects of the photomixer/preamplifier impedance match on the heterodyne receiver sensitivity

A. LASER LOCAL OSCILLATOR POWER REQUIREMENTS

It has been shown that for a PV HgCdTe photomixer operating in the flat portion of its frequency response ($f/f_c << 1$), quantum-noise-limited heterodyne operation is obtained when

$$I_o >> \frac{2k\,(T_m + T'_{IF})\,G_D}{q} \tag{6}$$

or

$$P_{LO} >> \frac{2k\,(T_m + T'_{IF})\,G_D\,h\nu}{q^2\eta} \tag{7}$$

where

I_o = dc photocurrent induced by the laser LO

k = Boltzmann's constant

T_m = physical temperature of the photomixer

T'_{IF} = effective input noise temperature of the IF preamplifier

G_D = small-signal shunt conductance of the photomixer

q = electronic charge

h = Planck's constant

ν = infrared frequency

η = photomixer quantum efficiency

When the terms on the left and right side of equations 6 or 7 are equal, the thermal noise of infrared mixer and IF amplifier degrades the receiver sensitivity by 3 dB.

Calculated and measured data on 10.6-micrometer heterodyne receivers at AIL (Appendix A) indicate that a properly designed heterodyne receiver can exhibit quantum-noise-limited operation for approximately 2 mW of incident laser LO power illuminating the PV HgCdTe photomixer. In general the laser LO beam diameter is fixed so that it is larger than the photomixer cross section in the focal plane in order to minimize effects due to any uncertainty in the photomixer position.

A study of the local oscillator power requirements and the corresponding heat loading due to laser illumination of a 10 micrometer PV HgCdTe photomixer have been completed. The expected heterodyne receiver signal-to-noise ratio (SNR) has been calculated as a function of off-axis misalignment of the LO for a 200 micrometer square photovoltaic HgCdTe mixer having a 15 percent quantum efficiency which is illuminated by an f/10 signal laser beam, and a variable f number laser local oscillator beam. The study was

aimed at examining the case where the mixer position has a lateral uncertainty of about ±100 micrometers (due to operational support instabilities of the photomixer cooler). The Airy disc of the received beam matches the diameter of the photomixer sensitive area and is held fixed on the mixer independent of its uncertain position (by means of a conical scan nutator and image motion compensator) while the local oscillator is deliberately misaligned by a controllable amount. For this calculation, the displacement from boresight is assumed to take place in the x axis (or y axis) only in the image plane (random misalignment along an x-y diagonal reduces the S/N by a factor of $\sqrt{2}$).

Figure 37 gives the calculated receiver SNR as a function of LO offset (x axis) with local oscillator f number as a parameter. Such a computation is important in minimizing the heat load on the photomixer cooler due to LO power spillover. For f/∞ (the case of a uniform laser LO field) the physical tolerances on the LO beam are minimized, however, this case results in maximum power requirements and heat load. However, for a uniform LO illumination and 2 mW of laser LO power incident on the photomixer, the total flux impinging on the input aperture (3 mm diameter) of the cooler is approximately 350 mW.

For an f/20 system (a realistic case), the boresighted SNR is actually 1/2 dB better than the uniform LO illumination case. The f/20 optical spot size is about 2.4 λ (f-number) = 510 micrometers. Assuming a Gaussian energy distribution for the LO beam, the total input power flux is approximately 8 mW for the case of 2 mW of laser LO power incident on the photomixer. With this LO distribution the offset in x-axis causes a decrease in S/N as shown in Figure 37. The SNR is 3 dB down from the peak value at 160 micrometers offset which is a very large proporation of the mixer size.

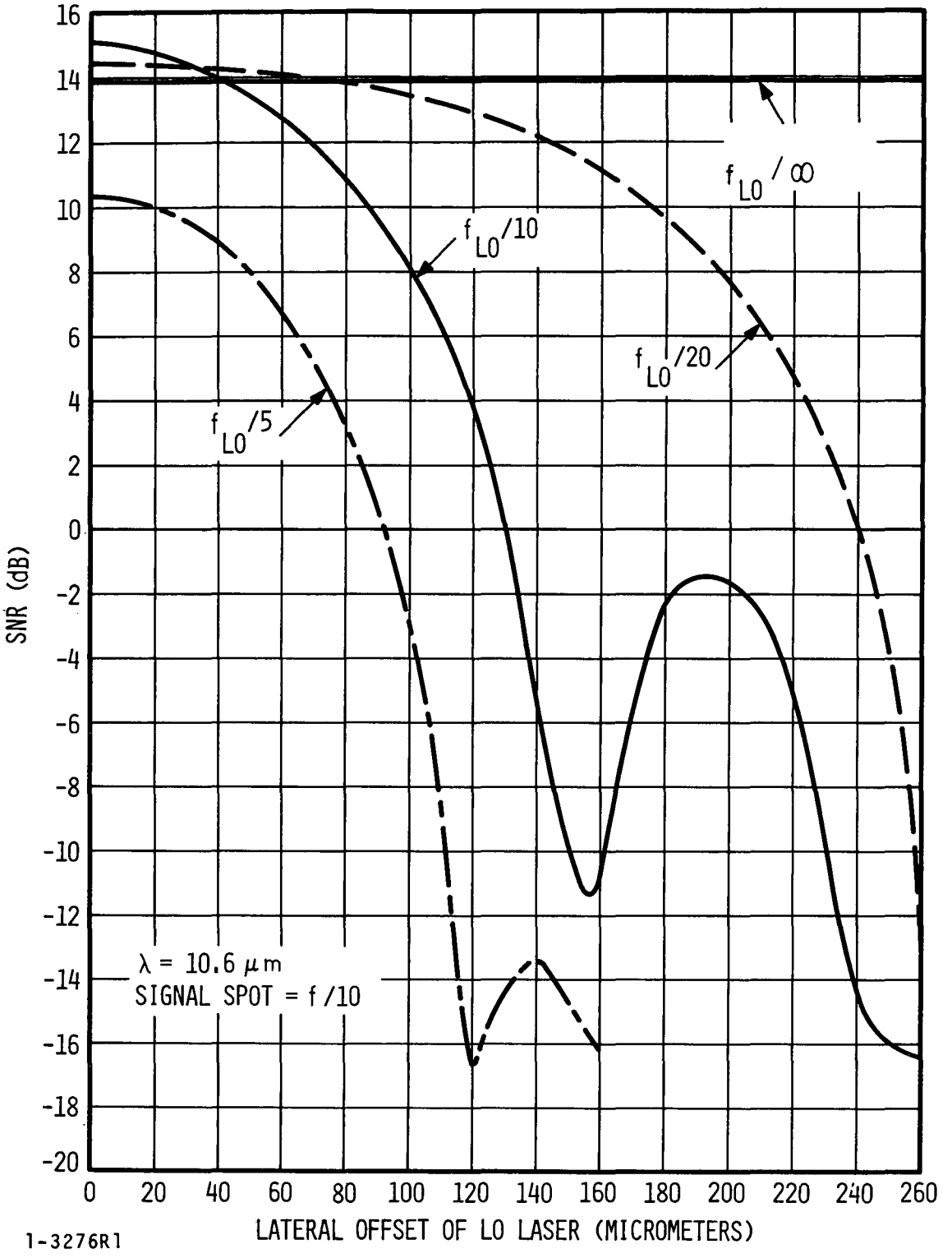

FIGURE 37. HETERODYNE SIGNAL-TO-NOISE RATIO AS A FUNCTION OF LATERAL DISPLACEMENT OF LO LASER BEAM IN FOCAL PLANE WITH f-NUMBER OF LOCAL OSCILLATOR BEAM AS A PARAMETER

For the f/10 case, the optical f-numbers of the signal and local oscillator are identical. On boresight an improved S/N of 15 dB is obtained and the total incident energy is approximately 3 mW for 2 mW illuminating the mixer. However, the system is much more sensitive to LO offset. The SNR is 3 dB down from the peak value at 68 micrometer offset (approximately 1/3 the mixer linear dimension).

The f/5 case is included for completeness but it is not a realistic choice because of the stringent tolerances which must be placed on the LO offset to maintain a good receiver SNR. The results of the SNR calculations are summarized in Table II.

TABLE II. RESULTS OF LASER LOCAL OSCILLATOR POWER STUDY

(Conditions: 200-micrometer square mixer, 15 percent quantum efficiency, f/10 signal beam)

Local Oscillator f-Number	Boresighted S/N (dB)	Mixer Position for -3 dB S/N (Micrometers)	Total Local Oscillator Power for 3 mm Diameter Entrance Aperture (mW)
∞	14	--	350
20	14.5	160	8
10	15	68	3
5	10.5	60	8

A heterodyne receiver having a LO beam which is 1.5 to 2 times the diameter of the signal beam appears to be a good engineering compromise ($f_{LO}/20$ in this case) in order to realize a good receiver SNR, low heat load, and reasonable design tolerances.

B. HEAT LOADS OF PHOTOMIXER COOLER

Measurements have been carried out to determine the amount of incident laser local oscillator power absorbed by the photomixer cooler (terminal temperature $\approx$ 90 K) when the heterodyne receiver is operated near its quantum-noise-limited sensitivity limit. The photomixer used was mounted in a variable temperature liquid nitrogen dewar having a temperature sensor and heater for accurate temperature control. An uncoated NaCl window was used on the entrance window of the dewar and the operating conditions were as follows:

Photomixer Cooler Temperature	90 K
Photomixer Bias Voltage	-300 mV
Photomixer Dark Current	1.8 mA
Incident Flux on Photomixer	2 mW

The incident flux on the mixer element, P_{LO}, was calculated by measuring the amount of induced photocurrent and using the equation:

$$P_{LO} = \frac{h\nu}{\eta q} I_o \tag{8}$$

where

I_o = induced photocurrent

η = mixer quantum efficiency

h = Planck's constant

ν = optical frequency

q = electronic change

The area of the circular photomixer element was 2.7×10^{-4} cm^2, (4.2×10^{-5} $inch^2$), and the mixer radius was approximately 3.6×10^{-3} inch.

The Gaussian local oscillator laser beam cross section was measured and the beam diameter at the $\pm 3\ \sigma$ points was 0.20 inch. Therefore, $\sigma = \frac{0.20}{3} = 0.033$ inch.

Since

$$\frac{P_{LO}}{P_{Total}} = 1 - e^{-\left(\frac{R^2}{2\sigma^2}\right)}$$

$$\approx \frac{R^2}{2\sigma^2} \approx 5.9 \times 10^{-3} \qquad (9)$$

where R = photomixer radius, P_{LO} is the incident LO power on the photomixer and P_{Total} is the total incident LO power.

Therefore

$$P_{Total} = \frac{P_{LO}}{5.9} \times 10^{+3} \approx 340 \text{ mW}$$

The total incident power was also measured with a Coherent Radiation power meter and found to be 370 mW, in excellent agreement with the calculated value.

A block diagram of the setup used to measure the laser LO heat load is shown in Figure 38. The dewar terminal temperature was held constant by means of a small heater mounted on the cold plate. The heater voltage was continuously monitored on a chart recorder.

When the laser LO was turned on, the heater power necessary to maintain a given terminal temperature was found to decrease due to absorption of laser power; the drop in heater power being approximately equal to the absorbed laser power.

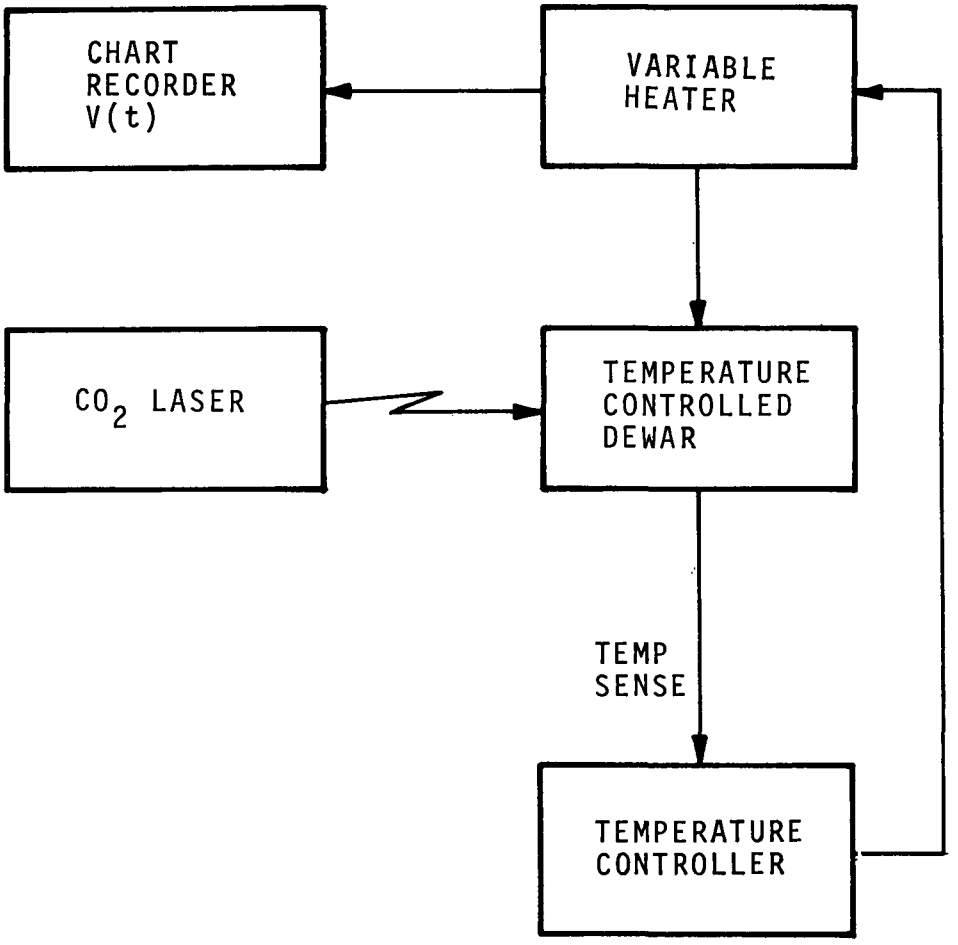

FIGURE 38. EXPERIMENTAL SETUP FOR MEASUREMENT OF LASER LO HEAD LOAD

The change in heater power with the application of LO power was measured and the average of the five measurements calculated. The five readings were:

120 mW
110 mW
80 mW
125 mW
140 mW

115 mW average

Therefore, approximately 115/340 or 34 percent of the power incident on the detector window was absorbed. Based on this measurement, the amount of power absorbed has been calculated for various diameter Gaussian laser beams with 2 mW illuminating the photomixer. Table III summarizes these results.

TABLE III. ABSORBED AND REFLECTED LASER LO POWER FOR VARIOUS LO f/NUMBERS UNDER THE CONDITION OF 2 mW OF INCIDENT POWER ON THE PHOTOMIXER

LO f/Number	LO Spot Size (Diameter) (inches)	Total Incident LO Power (mW)	LO Power Absorbed By Cooler (mW)	Reflected LO Power (mW)
200	0.20	340	115	225
90	0.090	77	26	51
60	0.060	57	19	38
43	0.043[1]	17	(6 to 11)	(11 to 6)

[1] The extrapolation for f/43 may be somewhat optimistic since a significant percentage of the laser LO beam falls on nonreflecting surfaces near the photomixer element.

The measurement results shown in Table III indicate that for an f/60 laser LO beam and 2 mW of LO power incident on the photomixer, only 19 mW of laser LO power is absorbed by the cooler. Consequently, an f/60 LO beam is a reasonable choice for an operational system which employs a 200 × 200 micrometer detector element because the spot size is large enough to allow relatively large photomixer position uncertainties without decreasing the heterodyne receiver signal-to-noise ratio (Section V-A). The results of the laser LO power requirements indicate that an f/20 LO beam is suitable from the point of view of mechanical stability of the cooler and receiver SNR. The use of an f/20 LO beam will result in less than 10 mW of LO power loading on the photomixer cooler.

Further, the photomixer used for these measurements was mounted in a preliminary detector housing with no provision for reflecting unused LO power. A recently developed detector housing has provision for rejection of some of the unneeded LO power. Therefore, it is expected that the measurements made here may represent slightly higher heat loading than would be expended when using the improved housing configuration.

It should be noted that the laser LO power and the thermal loss of the coaxial cable between the photomixer and the IF preamplifier provide the principal thermal loads on the photomixer cooler. The dc bias power, for the typical operational case of V_B = -300 mV and I_T = 4 mA, is only 1.2 mW.

C. PHOTOMIXER UNIFORMITY

Uniformity of responsivity measurements on a HgCdTe photodiode have been carried out to determine its usefulness in a heterodyne receiver system which utilizes a conical scanner and image motion compensator for spatial tracking of the incoming signal laser beam. A block diagram of the measurement setup is shown in Figure 39. A finely focused CO_2 laser beam

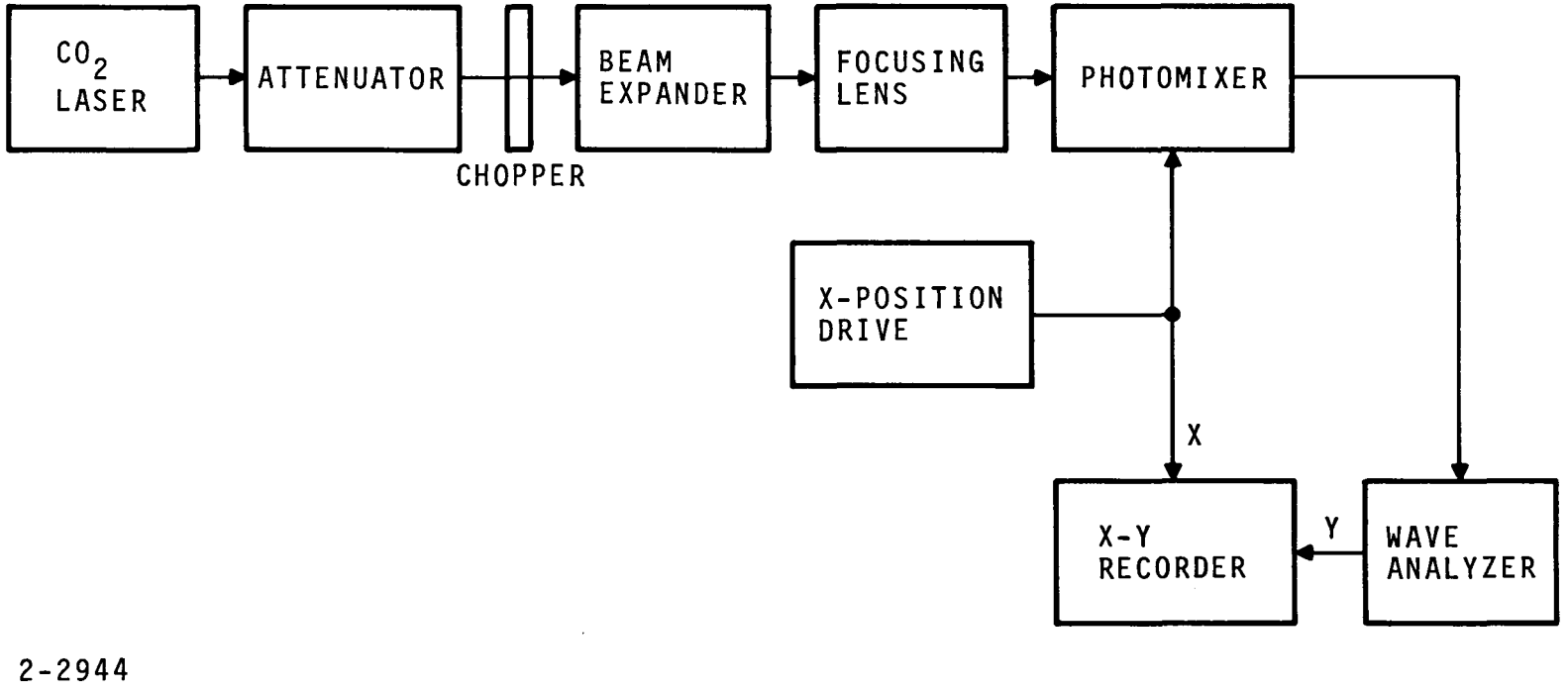

FIGURE 39. BLOCK DIAGRAM OF MEASUREMENT SETUP USED TO DETERMINE PHOTOMIXER UNIFORMITY

was used as a probe by using a beam expander and diffraction limited focusing lens.

The 10.6 micrometer CO_2 laser beam was attenuated to a suitable power level so that it would not damage the photomixer. The attenuation is accomplished by using IRTRAN-1 windows which absorb at 10.6 micrometers but do not affect the beamwidth or divergence of the incident laser beam. The beam was chopped by a mechanical chopper at a 20 Hz rate and the output signal was measured with a wave analyzer tuned to the chopping frequency. The lens system used a collimator to expand the beam to 2 inches in diameter, which increased the relative aperture of the focusing lens of f/4 in order to produce a diffraction limited 100 micrometer focused spot.

Before the mixer uniformity measurement was performed, a test measurement was made to experimentallly measure the spot size. The 100 micrometer diameter spot size was measured by replacing the photomixer with a small (110 × 100 micrometer) uniform response bolometer. The bolometer was swept across the focused spot producing an output voltage proportional to the spatial convolution of the optical spot and the bolometer sensitive area. These results are plotted in Figure 40. Using a computer program to extract the optical spot size from the convolution, the focused laser spot was found to be 100 micrometers in diameter, thus confirming an f/4 system and indicating that the focusing system is performing at the theoretical limit for diffraction limited operation.

The bolometer was then replaced by the photomixer and the responsivity uniformity measurements were carried out. For a series of measurements taken in vertical (Y) increments of 50 micrometers, the mixer was swept across the optical spot in the horizontal (X) direction. The chopped signal from the output of the photomixer was fed to the wave analyzer and the analog output of the wave analyzer was fed to the Y input on an X-Y recorder. The motorized micrometer stage which moved the mixer was also fitted with

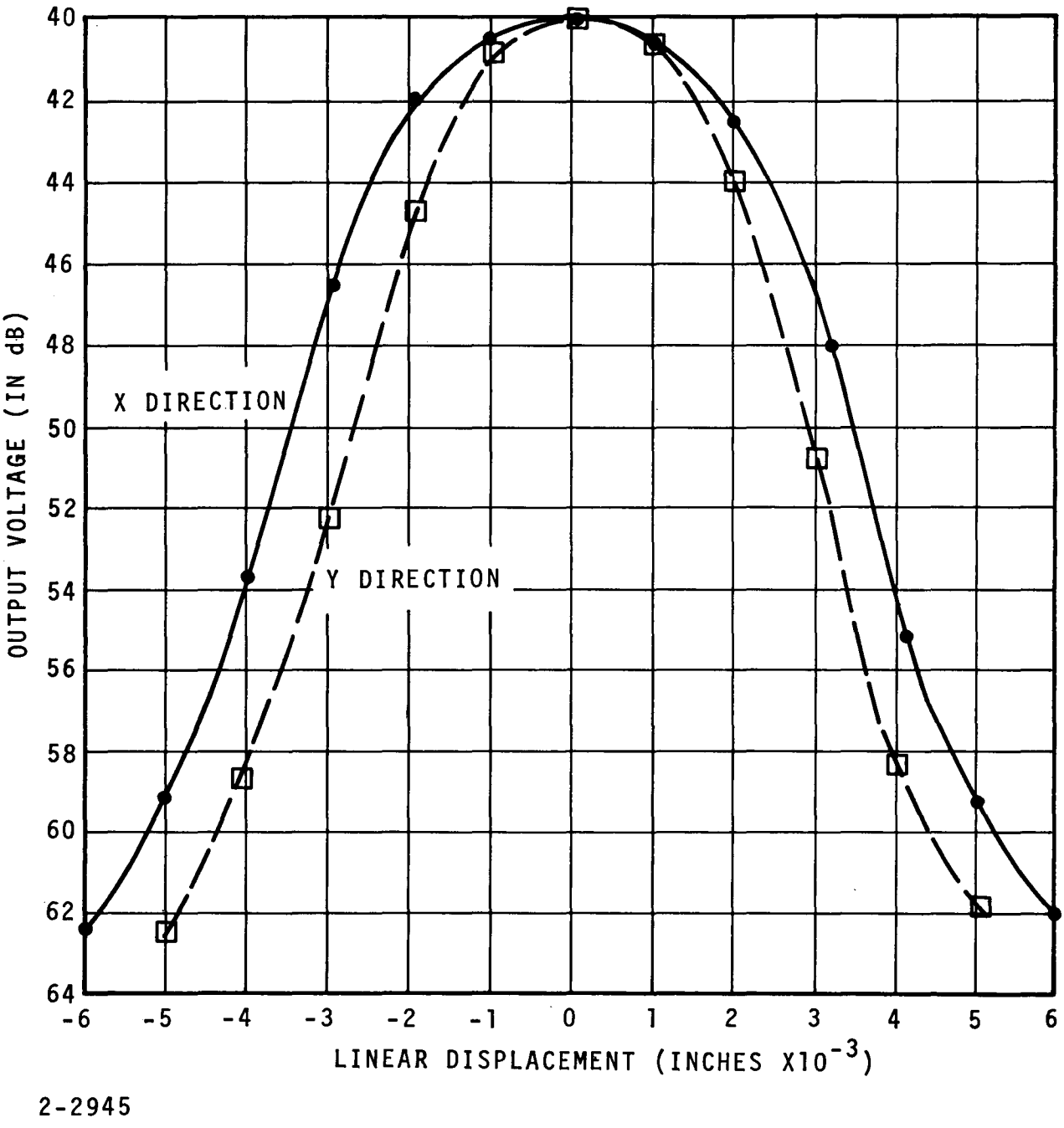

FIGURE 40. SPATIAL PATTERN OF FOCUSED CO_2 LASER BEAM

an analog output to provide a reference voltage to the X-Y recorder. The recorder trace was calibrated in thousandths of an inch (25 micrometers) in the X direction and decibels in the Y direction. (In this measurement setup, the photomixer acts as a square law device.) The wave analyzer scale used was calibrated for a linear device so that 20 dB corresponds to a change of one decade of input laser power.

Examples of typical X-Y recorder plots are shown in Figures 41 and 42. From a complete set of these recorder plots, a contour plot of regions of uniform photomixer response was obtained (Figure 43). The departure of these contours from a series of concentric shaped rings resembling the photomixer profile establishes the departure of the sensitive surface from one of uniform response. The only strikingly irregular region of the photomixer under test was found in the upper left region of the detector.

An attempt was made to correlate the shape of the response contours with a photomicrograph (Figure 44) and an engineering sketch (Figure 45) of the photomixer. Except for the irregularity in the upper left of the contour, there is strong similarity among the contour shape, the drawing, and the photomicrograph.

Some possible reasons for the irregularity in the upper left hand corner of the photomixer are:

- A defect in the photomixer which reduces the localized quantum efficiency. (This defect could be an irregularity in the junction or some contaminant in the bulk material.)
- Some bonding cement may have seeped onto the photomixer causing a locally opaque response.
- A variation in the thickness in the upper (p-type) layer due to variation in etch rate across the surface during the final stages of manufacture of the photomixer. Some rounding of the photomixer can be observed when it is examined under a microscope, reinforcing the hypothesis of variation in etch rate.

- Reflections off the large irregular solder contact on the right side of the photomixer may cause the "apparent" detector size to be larger than the measured geometry.
- A quantum efficiency peak in the lower left hand corner of the photomixer due to (1) etching irregularities which caused a more optimum p layer, or (2) an exposed junction. This hypothesis is further conformed by the fact that the measured response contour falls in the lower left hand portion of the photomixer.

This photomixer has been tested in the ORS (Section II) and has exhibited a quantum-noise-limited sensitivity while performing all the acquisition and conical scan tracking functions of the receiver. It has been concluded that the nonideal detector uniformity of this photomixer did not degrade the spatial tracking functions or the receiver sensitivity of the ORS. The exact reason for the nonideal responsivity profile has not been established.

D. PHOTOMIXER/PREAMPLIFIER IMPEDANCE MATCH

An analysis of the effects of the photomixer/preamplifier impedance match on infrared heterodyne receiver performance has been carried out. The coupling of the shot noise energy generated in the photomixer to the IF preamplifier can be analyzed in terms of the Norton Equivalent Circuit shown in Figure 46 where only the real component of the admittance is considered since we are dealing with noise properties of the photomixer.

G'_{out} is given (equation 10 of Appendix A) by

$$G'_{out} = \frac{G_D + R_S (G_D^2 + \omega^2 C_D^2)}{(1 + R_S G_D)^2 + (\omega C_D R_S)^2} \tag{10}$$

$$= \frac{G_D \left[(1 + R_S G_D) + R_S \omega^2 C_D^2 / G_D \right]}{(1 + R_S G_D)^2 + (\omega C_D R_S)^2} \tag{11}$$

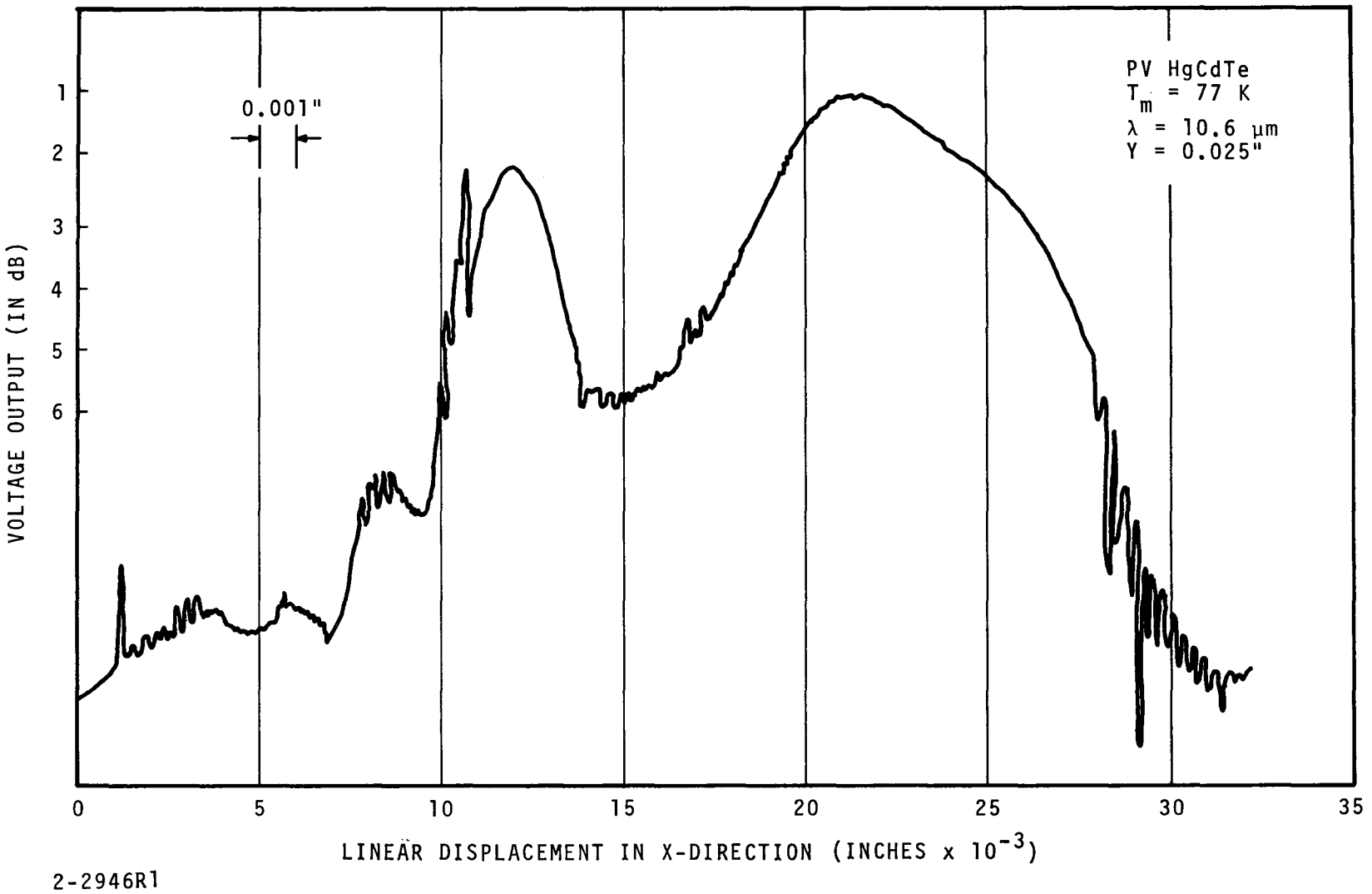

FIGURE 41. RESPONSIVITY PROFILE OF PV HgCdTe PHOTOMIXER AT Y = 0.025 POSITION

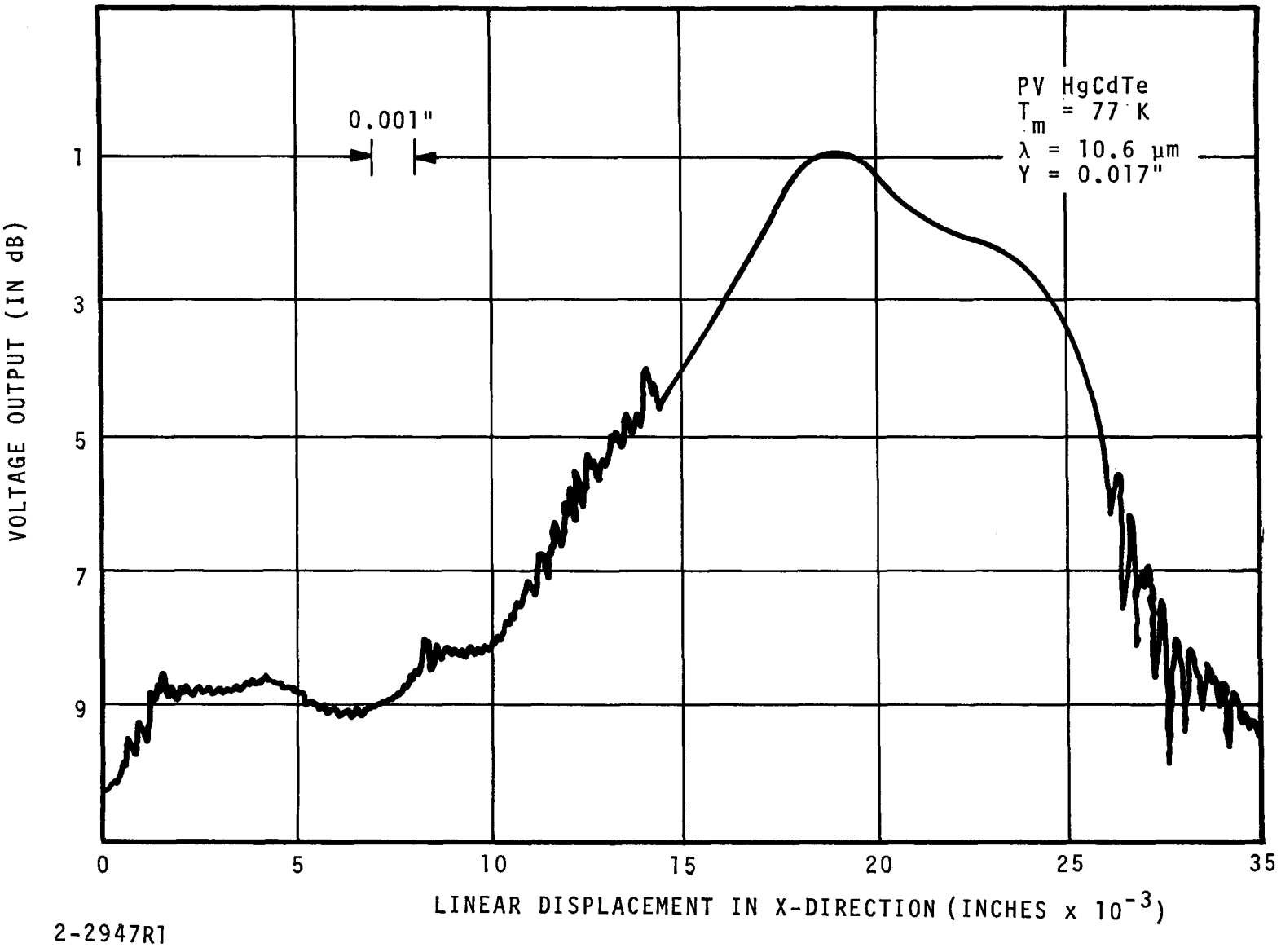

FIGURE 42. RESPONSIVITY PROFILE OF HgCdTe PHOTOMIXER AT Y = 0.017 POSITION

FOLDOUT FRAME 1

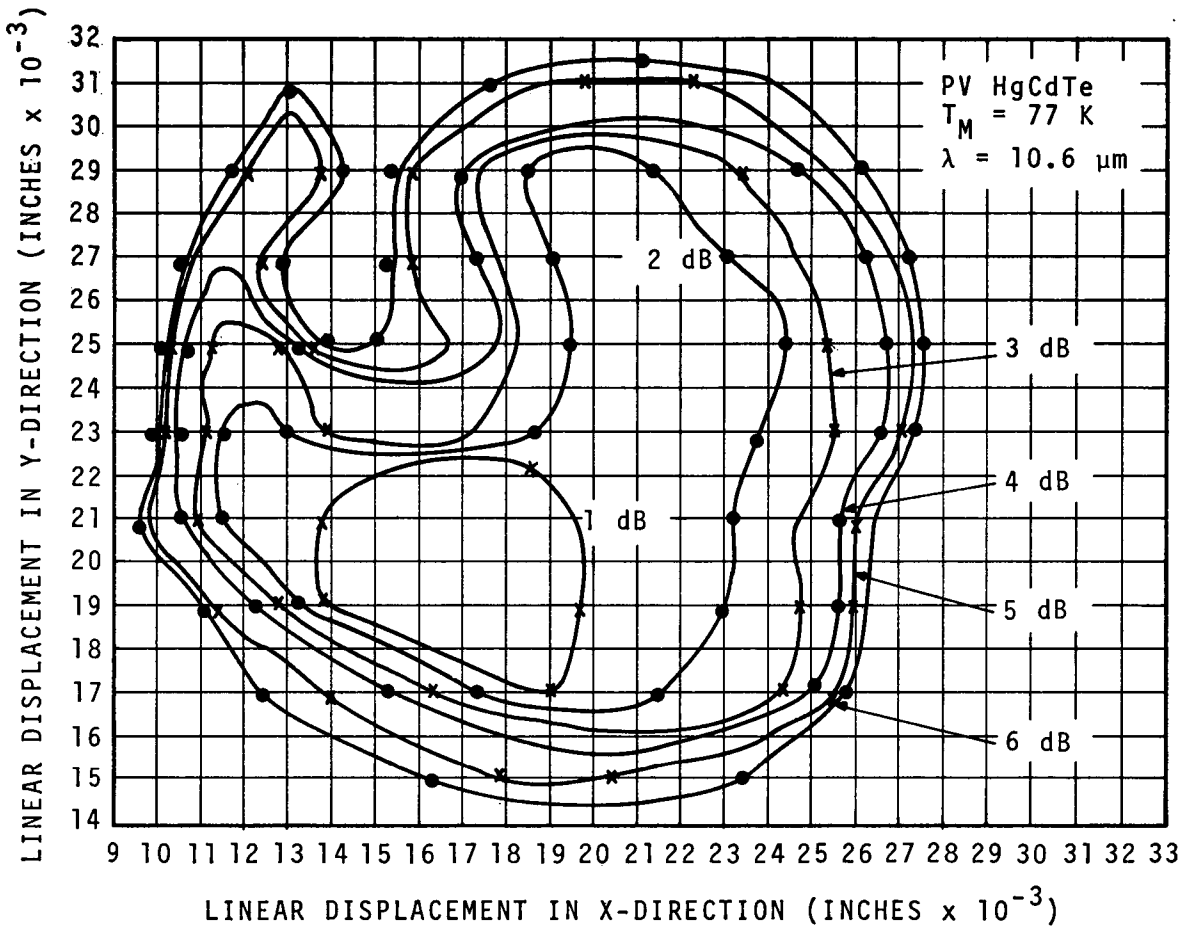

2-2948R1

FIGURE 43. MEASURED RESPONSIVITY CONTOURS FOR HgCdTe PHOTOMIXER

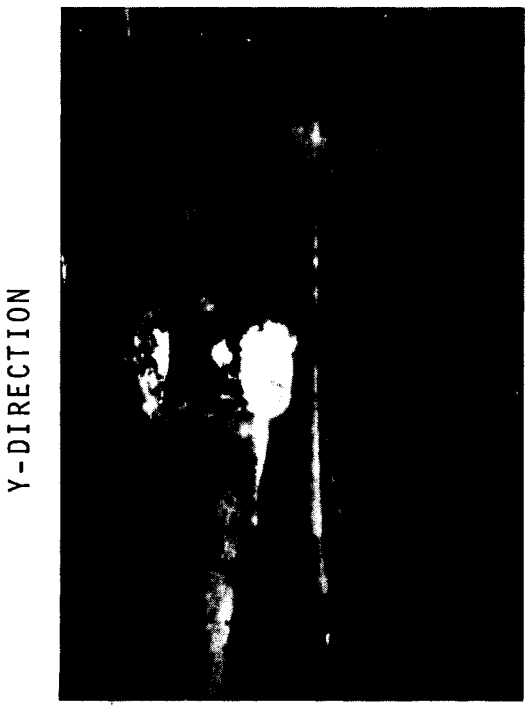

2-2966R1

FIGURE 44. PHOTOMICROGRAPH OF PV HgCdTe MIXER

FOLDOUT FRAME 2

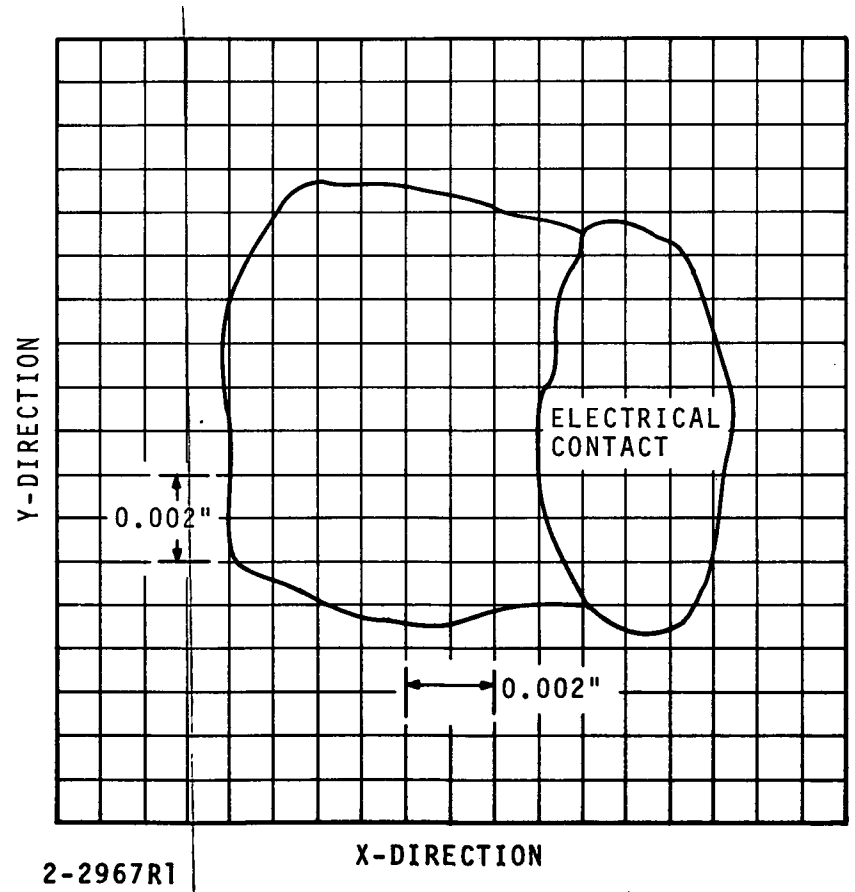

2-2967R1

FIGURE 45. ENGINEERING SKETCH OF PV HgCdTe PHOTOMIXER

85/86

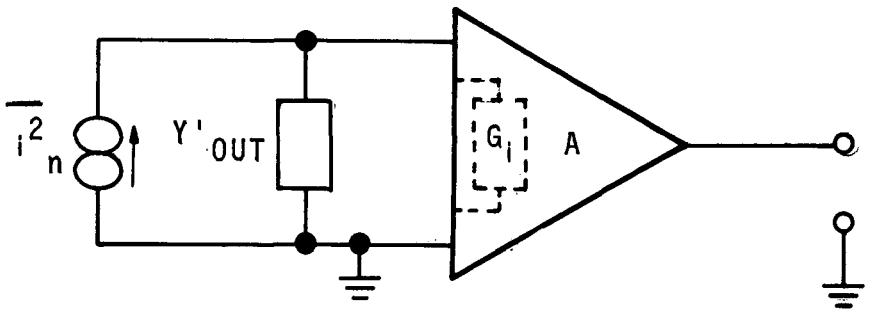

2-2949

FIGURE 46. NORTON EQUIVALENT FOR PV HgCdTe MIXER/PREAMPLIFIER

for the case $1 + R_S G_D \approx 1$

$$G'_{out} = \frac{G_D \left(1 + R_S \omega^2 C_D^2 / G_D\right)}{1 + (\omega C_D R_S)^2} \tag{12}$$

The 3-dB cutoff frequency (Appendix A) is

$$\omega_C^2 = \frac{G_D}{R_S C_D^2} \tag{13}$$

Substituting, we obtain

$$G'_{out} = \frac{G_D \left[1 + \left(\frac{f}{f_c}\right)^2\right]}{1 + \left(\frac{f}{f_c}\right)^2 \left[R_S G_D\right]} \tag{14}$$

In the absence of LO induced photocurrent I_o, the overall system thermal noise, P_T, can be measured. The overall thermal noise depends on the physical temperature of the photomixer and the equivalent input noise temperature of the IF preamplifier. When LO power is applied to the photomixer, hole-electron pairs are generated which rise to photoinduced dc current, I_o. This photoinduced current contributes to the photomixer shot noise. The thermal noise power and shot noise power are

$$P_T = \frac{G_i}{(G_i + G'_{out})^2} \; 4\,k\,(T_M + T'_{IF})\,G'_{out}\,B \tag{15}$$

$$P_S = \frac{G_i}{(G_i + G'_{out})^2} \; \frac{2\,q\,I_o\,B}{1 + \left(\frac{f}{f_c}\right)^2 \left[R_S G_D\right]} \tag{16}$$

The measured noise power ratio $(P_S + P_T)/P_T$ can be obtained by combining equations 14, 15, and 16.

$$\frac{P_S + P_T}{P_T} = 1 + \frac{2\,q\,I_o}{4k\,(T_M + T'_{IF})\,G_D \left[1 + \left(\frac{f}{f_c}\right)^2\right]} \tag{17}$$

where

G_i = input conductance of IF amplifier

T_M = mixer temperature

T'_{IF} = equivalent input noise temperature of amplifier

B = IF bandwidth

q = electron charge

k = Boltzmann's constant

The total (shot-plus-thermal) noise generated in the photomixer-preamplifier combination has been measured as a function of LO induced photocurrent using three specially designed IF preamplifiers. The IF preamplifiers were designed to have input impedances of approximately 75, 150, and 260 MHz. Table IV summarizes the measured noise factor of each IF preamplifier for photomixer source impedances of 85, 125, and 200 ohms.

Noise measurements of the various photomixer-preamplifier combinations were carried out at applied bias voltages of -200, -300, and -400 mV where the photomixer source resistance was 200, 125, and 85 ohms, respectively. The measured and calculated values of heterodyne receiver noise are given in Figure 47, sheets 1 through 8. The measured values of receiver noise were in good agreement with the calculated values and the experimental error is estimated to be ± 0.5 dB. For an applied bias voltage below -200 mV the shunt conductance of the photomixer varied with applied LO power and careful attention had to be given to the selection of the IF preamplifier and applied laser LO power (Figure 47, sheets 1 through 8). For bias voltages above -200 mV, the shunt conductance of the photomixer remains nearly constant with applied LO, affording more stable receiver operation.

The results of the receiver noise measurements indicate that the IF preamplifier should be designed primarily for lowest noise figure with the impedance match between the photomixer and IF amplifier being a secondary consideration. As long as the reverse shunt conductance and amplifier input impedance are constant with local oscillator power, sufficient gain will be available in the photomixer to overcome the effects of reasonably low IF noise figures and provide nearly quantum-noise-limited receiver operation.

It should be noted that T'_{IF} is a function of source impedance (reference 12) and the heterodyne receiver sensitivity (equation 5) may be degraded when a large impedance mismatch exists between the photomixer and the IF preamplifier.

TABLE IV. MEASURED NOISE FACTORS OF TEST PREAMPLIFIERS

Preamplifier Input Impedance (ohms)	Photomixer Source Impedance (ohms)	Preamplifier Noise Factor (dB)
75	85	~1.8
75	125	~2.0
148	85	~3.8
150	125	~3.5
150	200	~3.5
260	85	~5.8
260	125	~4.8
264	200	~3.7

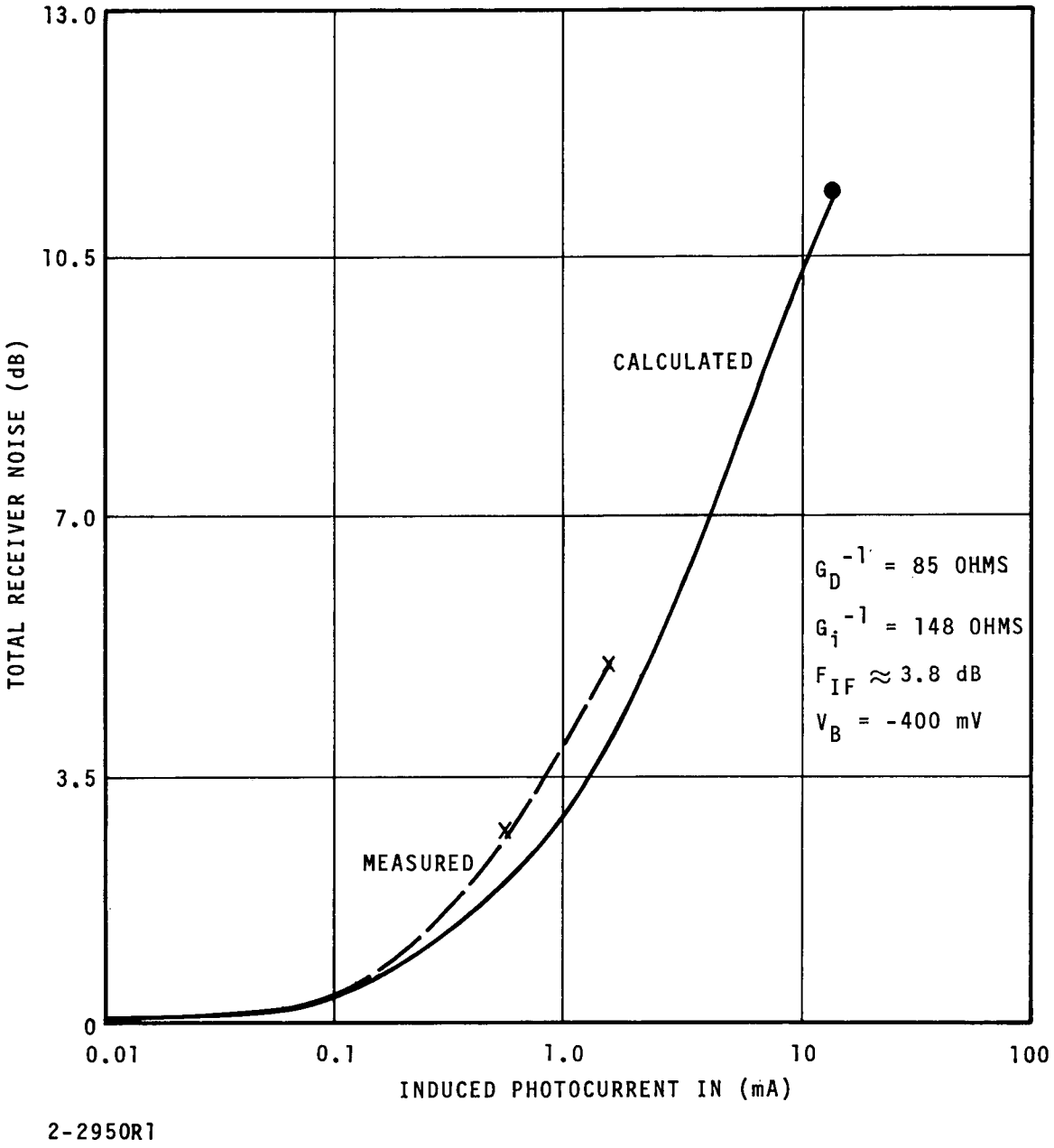

FIGURE 47. TOTAL RECEIVER NOISE VERSUS LO INDUCED PHOTOCURRENT FOR PV HgCdTe PHOTOMIXER (SHEET 1 OF 8)

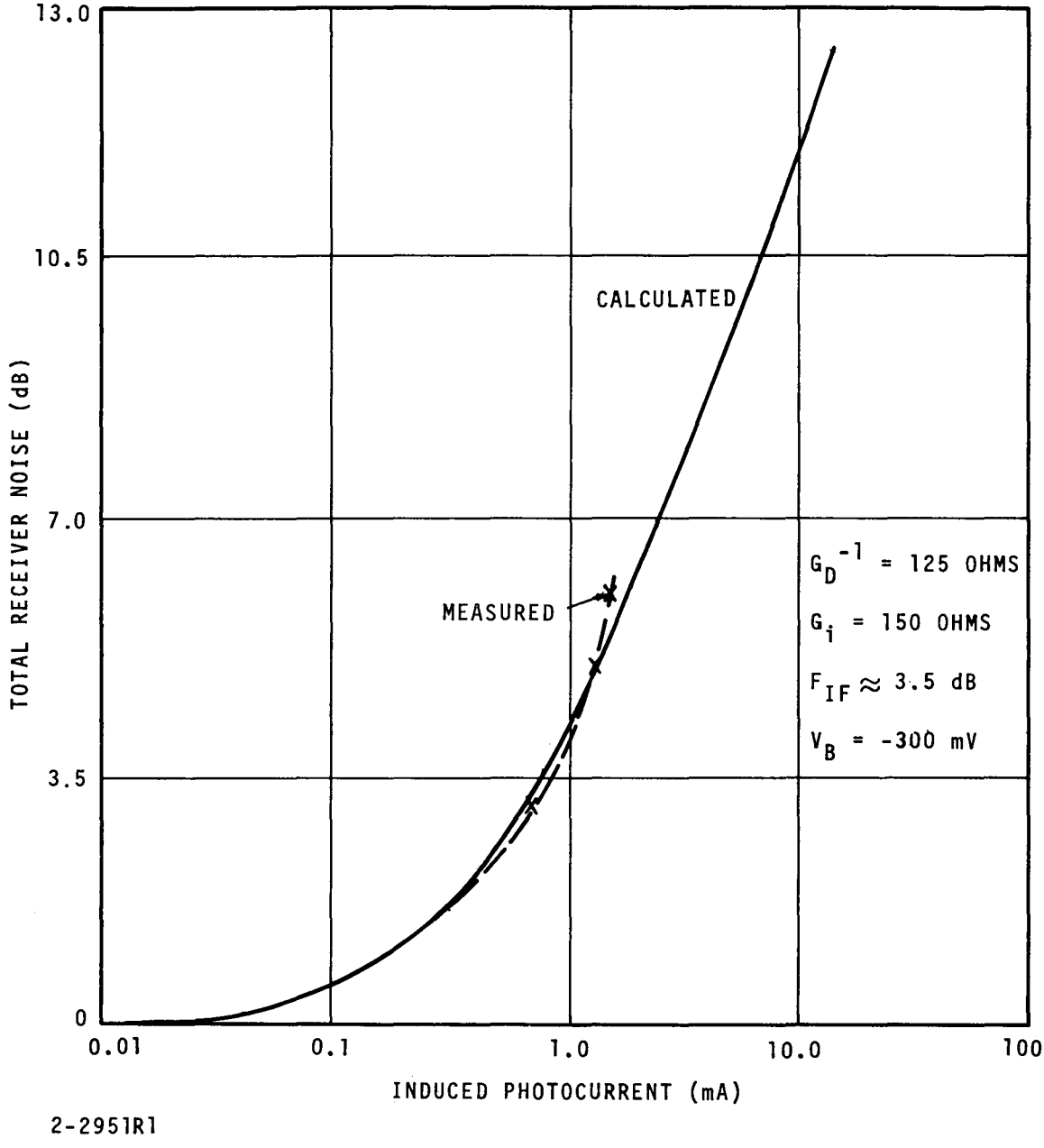

FIGURE 47. TOTAL RECEIVER NOISE VERSUS LO INDUCED PHOTOCURRENT FOR PV HgCdTe PHOTOMIXER (SHEET 2 OF 8)

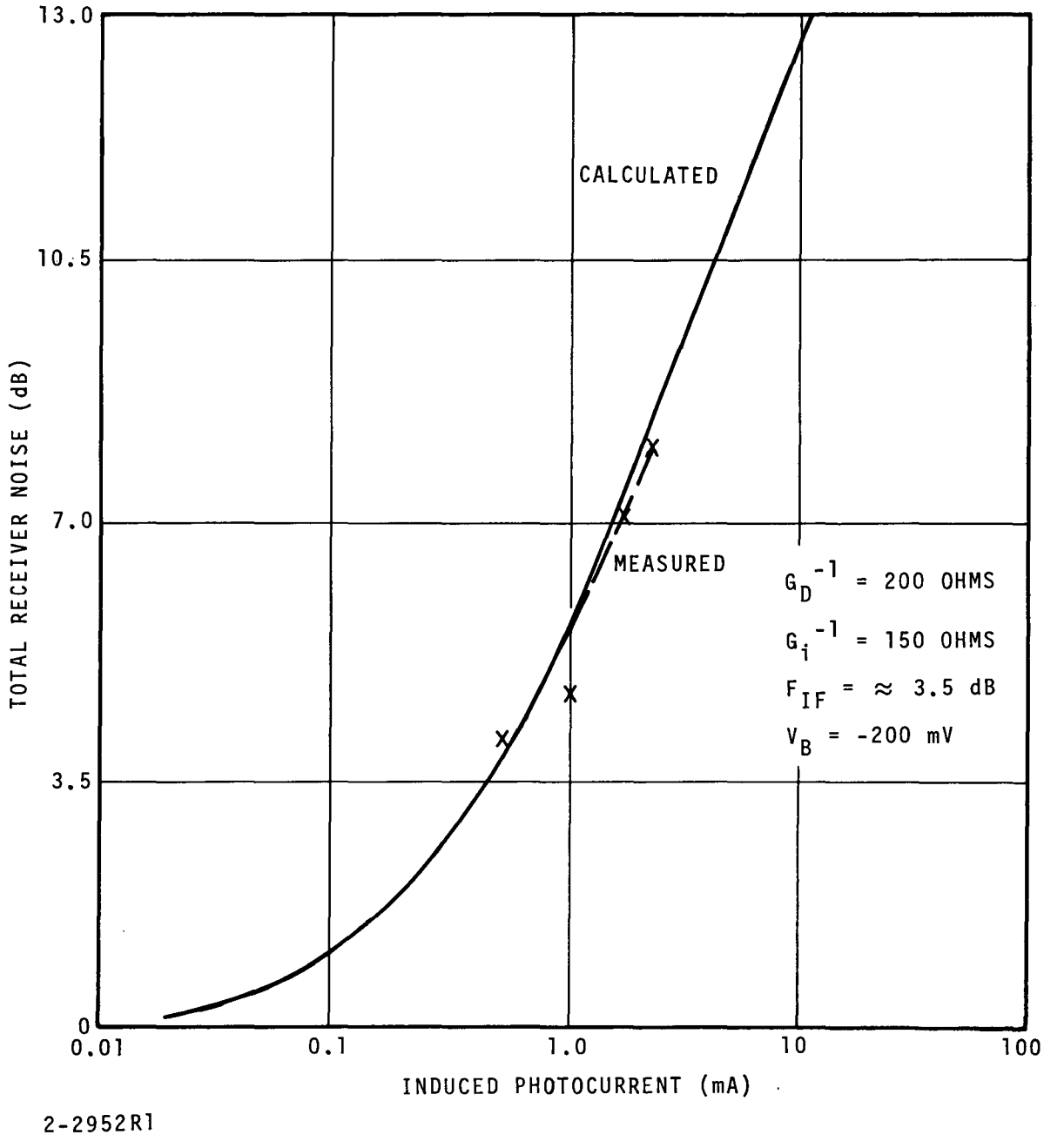

FIGURE 47. TOTAL RECEIVER NOISE VERSUS LO INDUCED PHOTOCURRENT FOR PV HgCdTe PHOTOMIXER (SHEET 3 OF 8)

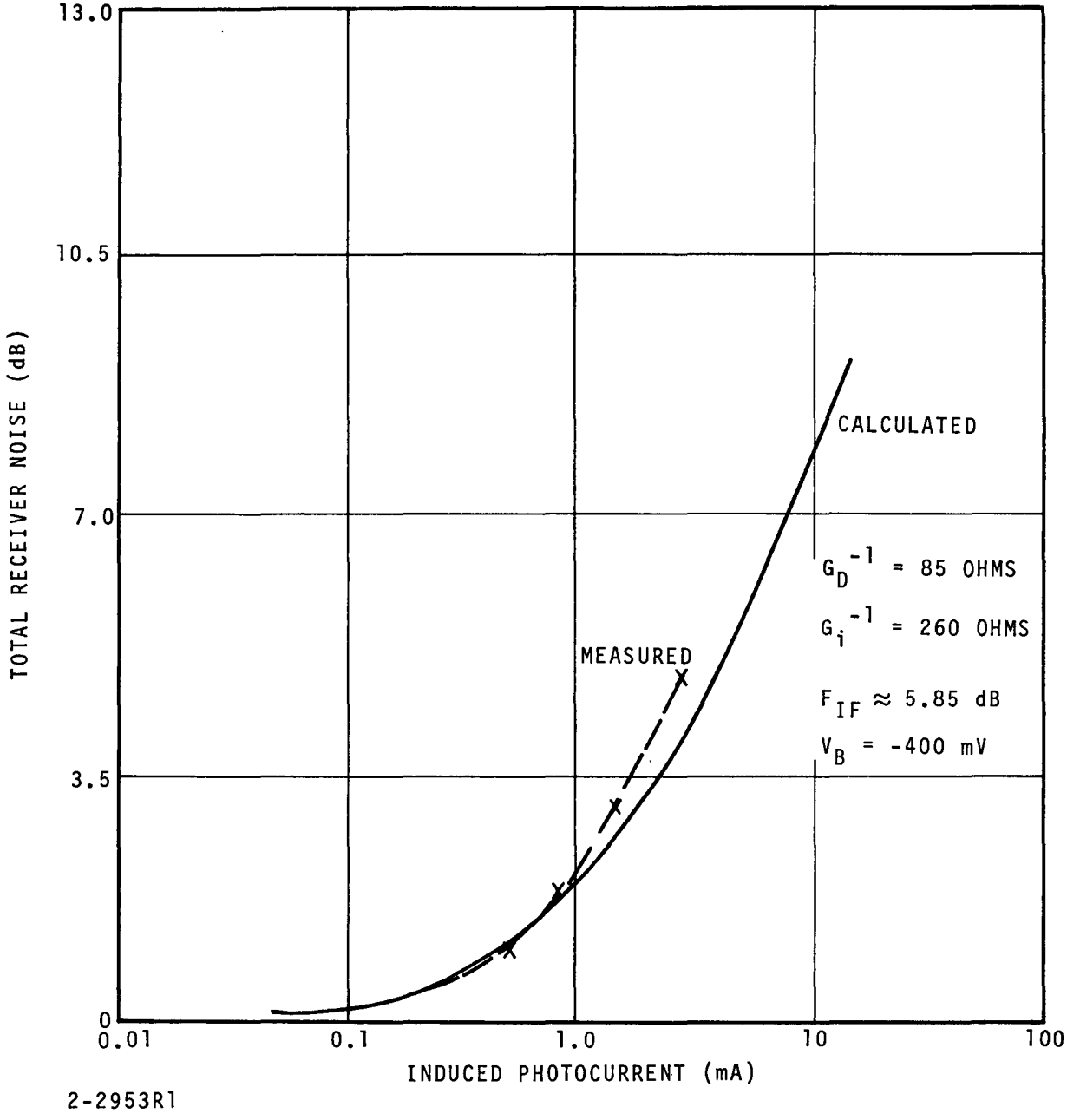

FIGURE 47. TOTAL RECEIVER NOISE VERSUS LO INDUCED PHOTOCURRENT FOR PV HgCdTe PHOTOMIXER (SHEET 4 OF 8)

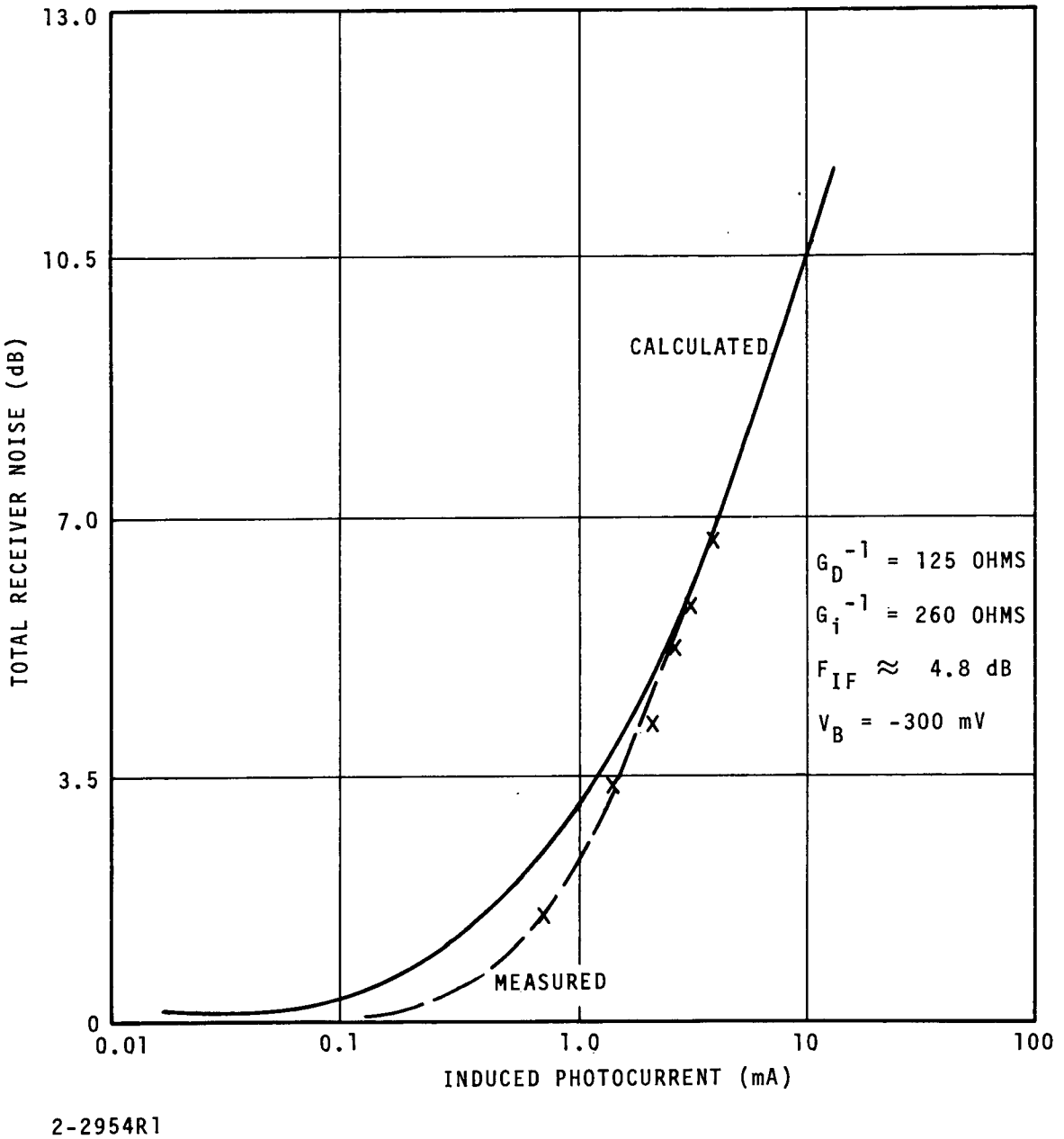

FIGURE 47. TOTAL RECEIVER NOISE VERSUS LO INDUCED PHOTOCURRENT FOR PV HgCdTe PHOTOMIXER (SHEET 5 OF 8)

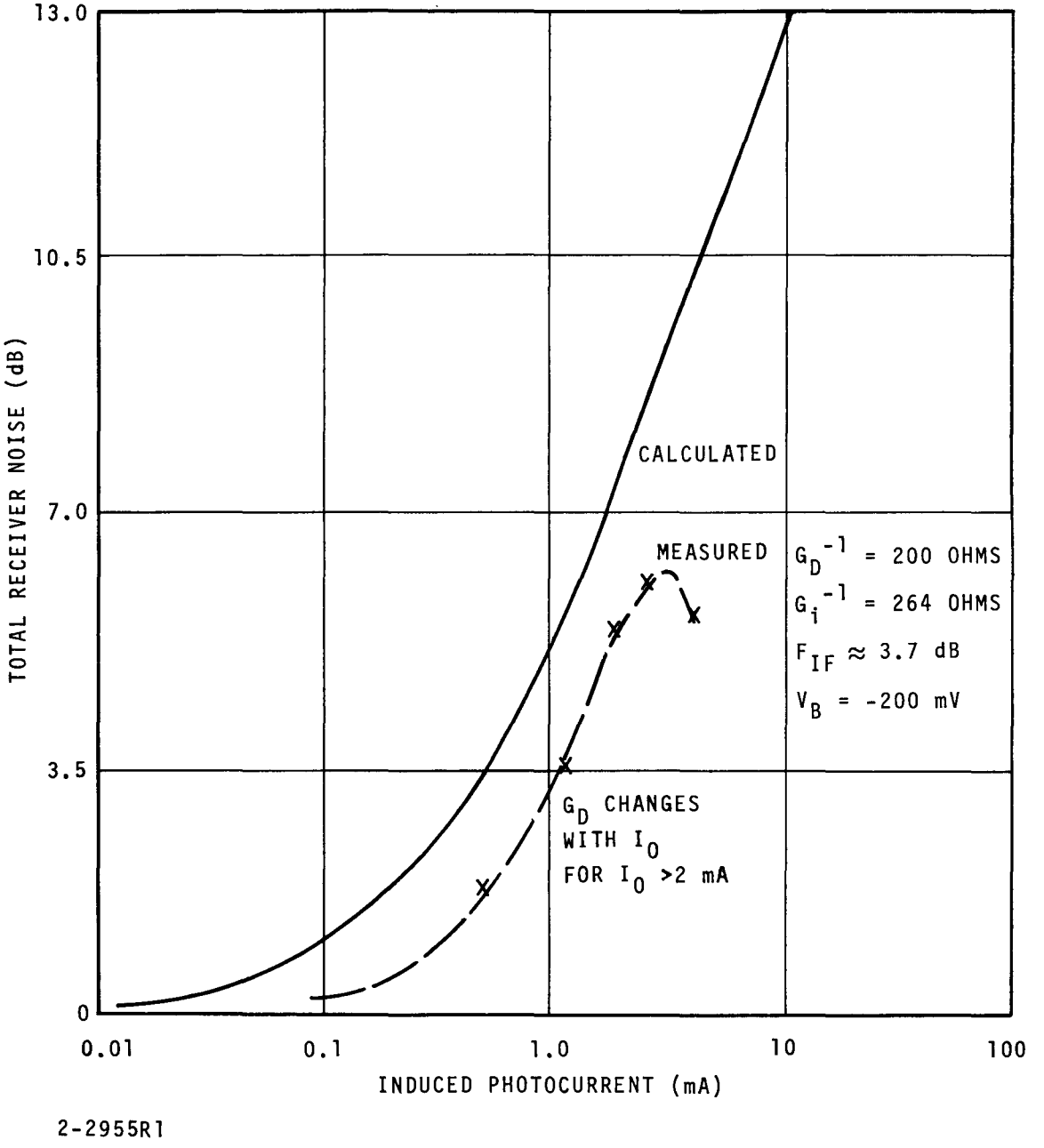

FIGURE 47. TOTAL RECEIVER NOISE VERSUS LO INDUCED PHOTOCURRENT FOR PV HgCdTe PHOTOMIXER (SHEET 6 OF 8)

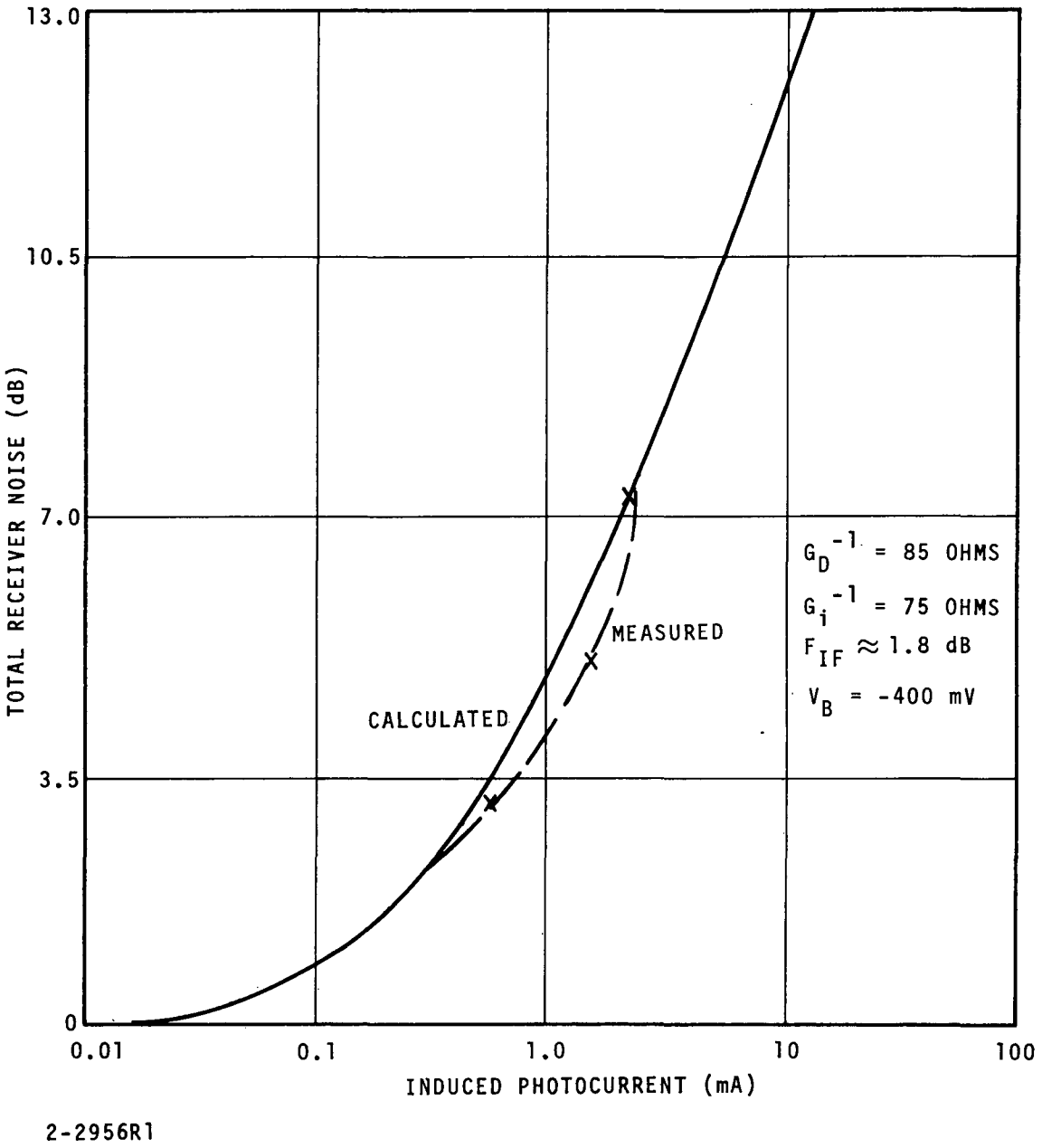

FIGURE 47. TOTAL RECEIVER NOISE VERSUS LO INDUCED PHOTOCURRENT FOR PV HgCdTe PHOTOMIXER (SHEET 7 OF 8)

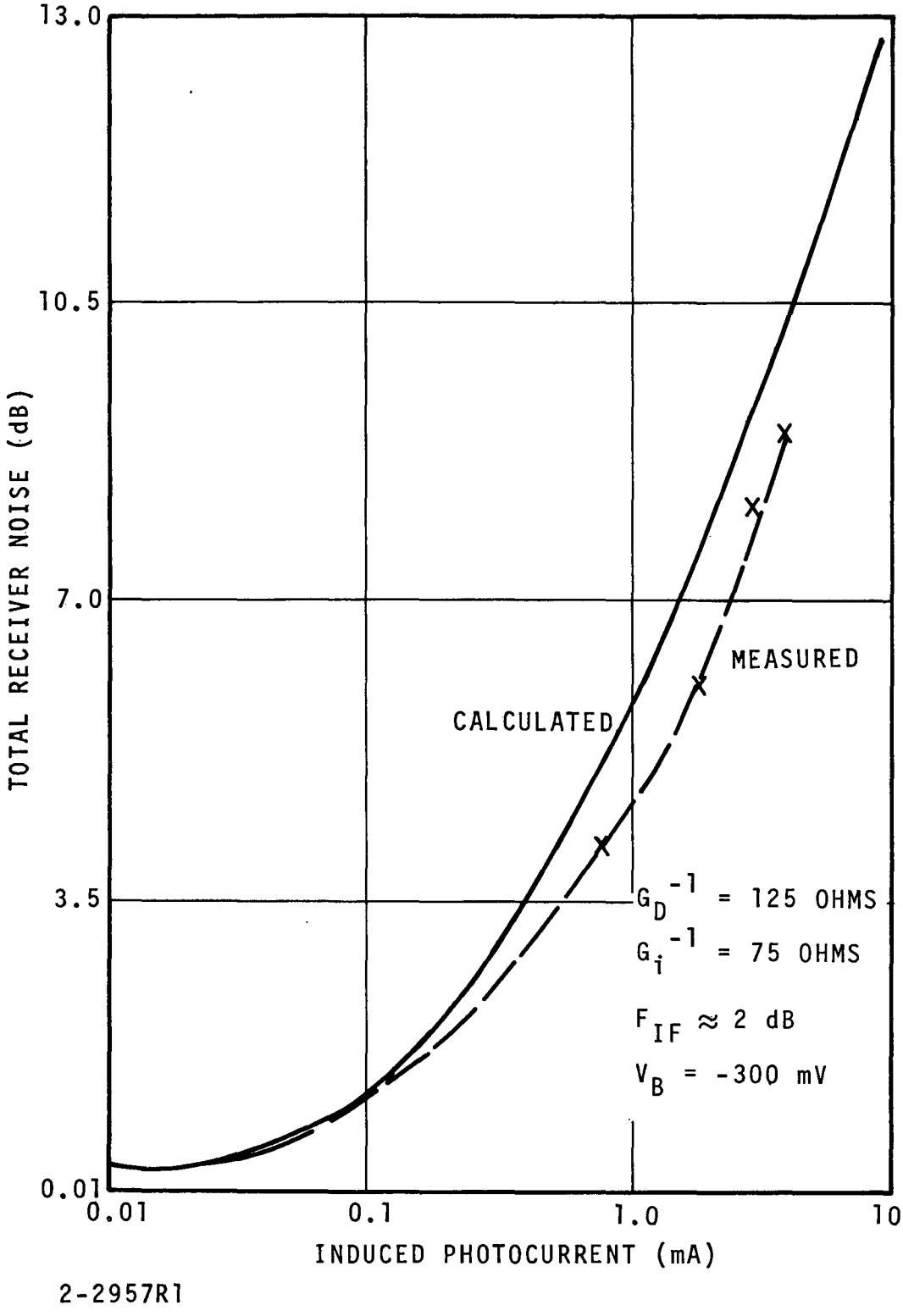

FIGURE 47. TOTAL RECEIVER NOISE VERSUS LO INDUCED PHOTOCURRENT FOR PV HgCdTe PHOTOMIXER (SHEET 8 OF 8)

VI. 10.6 MICROMETER HETERODYNE DETECTION USING p-TYPE HgCdTe PHOTOMIXERS

Analysis and measurements of 10.6-micrometer heterodyne detection in p-type HgCdTe photomixers were carried out using concepts of heterodyne (small-signal) lifetime and LO (large-signal) lifetime for the case of finite mixer dark conductance ($g_D/g_o \neq 0$). For these intrinsic photoconductive photomixers, the total mixer conductance (under laser LO illumination) is dependent on the photomixer dark conductance g_D. The equivalent circuit for the photomixers is shown in Figure 48.

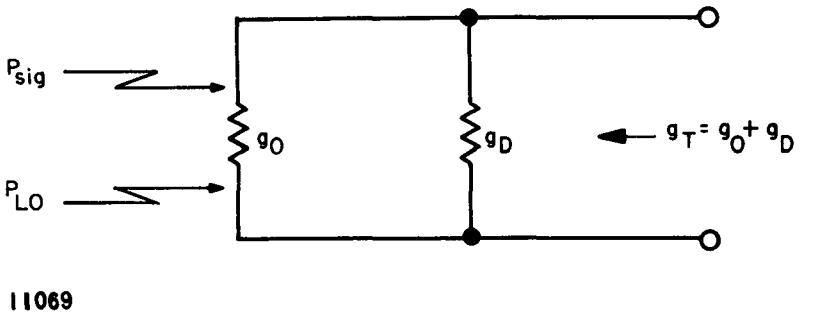

FIGURE 48. EQUIVALENT CIRCUIT FOR MIXER WITH FINITE DARK CONDUCTANCE

A. ANALYSIS OF MIXING IN p-TYPE HgCdTe

An analysis of infrared heterodyne detection in intrinsic photoconductors with finite dark conductances has been developed (reference 12). This section extends the analysis for the case of p-type HgCdTe photoconductive mixers having an Auger recombination process.

1. PHOTOMIXER LIFETIME

The photoconductance-to-dark conductance ratio is

$$\frac{g_o}{g_D} = \frac{\sigma - \sigma_D}{\sigma_D} = \frac{n_e (\mu_e + \mu_h)}{n_o \mu_e + p_o \mu_h} \approx \frac{\frac{n_e}{p_o}}{\frac{1}{b} + \frac{n_o}{p_o}} \tag{18}$$

where

$b = \frac{\mu_e}{\mu_h} \gg 1$

σ_D = dark conductivity

σ = photoexcited conductivity

n_o = dark electron concentration

p_o = dark hole concentration ($\gg n_o$ for p-type material)

n_e = excess hole-electron pair concentration due to photo-excitation

μ_e = electron mobility

μ_h = hole mobility ($\ll \mu_e$)

The excess hole-electron pair concentration is related to the applied LO power by

$$n_e = \frac{\eta P_{LO} \tau_{LO}}{\text{Vol } h\nu_{LO}} \tag{19}$$

where

η = mixer quantum efficiency

P_{LO} = applied laser LO power

τ_{LO} = large signal lifetime of the principal carriers

Vol = volume of photomixer

h = Planck's constant

ν_{LO} = laser local oscillator frequency

The small signal, large signal, and dark carrier lifetimes (references 12, 16, and 17) are given by:

$$\tau_{het} \approx \frac{n_i^2}{K_{ee}\, n_e\, (3n_e + 2p_o) + p_o\, (K_{ee}\, n_o + K_{hh}\, p_o)} \tag{20}$$

$$\tau_{LO} \approx \frac{n_i^2}{K_{ee}\, n_e\, (n_e + p_o) + p_o\, (K_{ee}\, n_o + K_{hh}\, p_o)} \tag{21}$$

$$\tau_D = \frac{n_i^2}{p_o\, (K_{ee}\, n_o + K_{hh}\, p_o)}, \quad n_e = 0 \tag{22}$$

where

K_{ee} = normalized electron-electron generation rate

K_{hh} = normalized hole-hole generation rate ($< K_{ee}$)

n_i = intrinsic carrier concentration ($= \sqrt{p_o\, n_o}$)

The variation of the photoconductive-to-dark conductance ratio with applied laser local oscillator power (reference 12) is given by

$$P_{LO}\frac{\mathcal{R}}{V} = \frac{g_o}{g_D}\left\{1 + \frac{\frac{g_o}{g_D}\left[1 + \frac{g_o}{g_D}\left(\frac{1}{b} + \frac{n_o}{p_o}\right)\right]}{\left[\frac{\frac{K_{hh}}{K_{ee}} + \frac{n_o}{p_o}}{\frac{1}{b} + \frac{n_o}{p_o}}\right]}\right\} \tag{23}$$

$$a_1 P_{LO} = \frac{g_o}{g_D} + a_2\left(\frac{g_o}{g_D}\right)^2 + a_3\left(\frac{g_o}{g_D}\right)^3 \tag{24}$$

where

$\mathcal{R}$ = open circuit responsivity

V = applied bias voltage

$a_1 = \mathcal{R}/V$

a_2 and a_3 are defined in Figure 56 ($a_2 >> a_3$).

Figure 49 shows a calculated curve (plotted on full logarithmic paper), describing the general behavior (based on equation 23) of the photoconductance-to-dark conductance ratio as a function of local oscillator power. As Figure 49 shows, the conductance varies directly as P_{LO} for low LO power, changing to a $P_{LO}^{1/2}$ dependence and, then, to a $P_{LO}^{1/3}$ dependence with increasing LO power. The measured breakpoints between the linear and quadratic region, and the quadratic and cubic region, can be used to determine mixer parameters a_2 and a_3. Parameters a_2 and a_3 can be used to calculate the ratio of the normalized electron-electron generation rate (K_{ee})

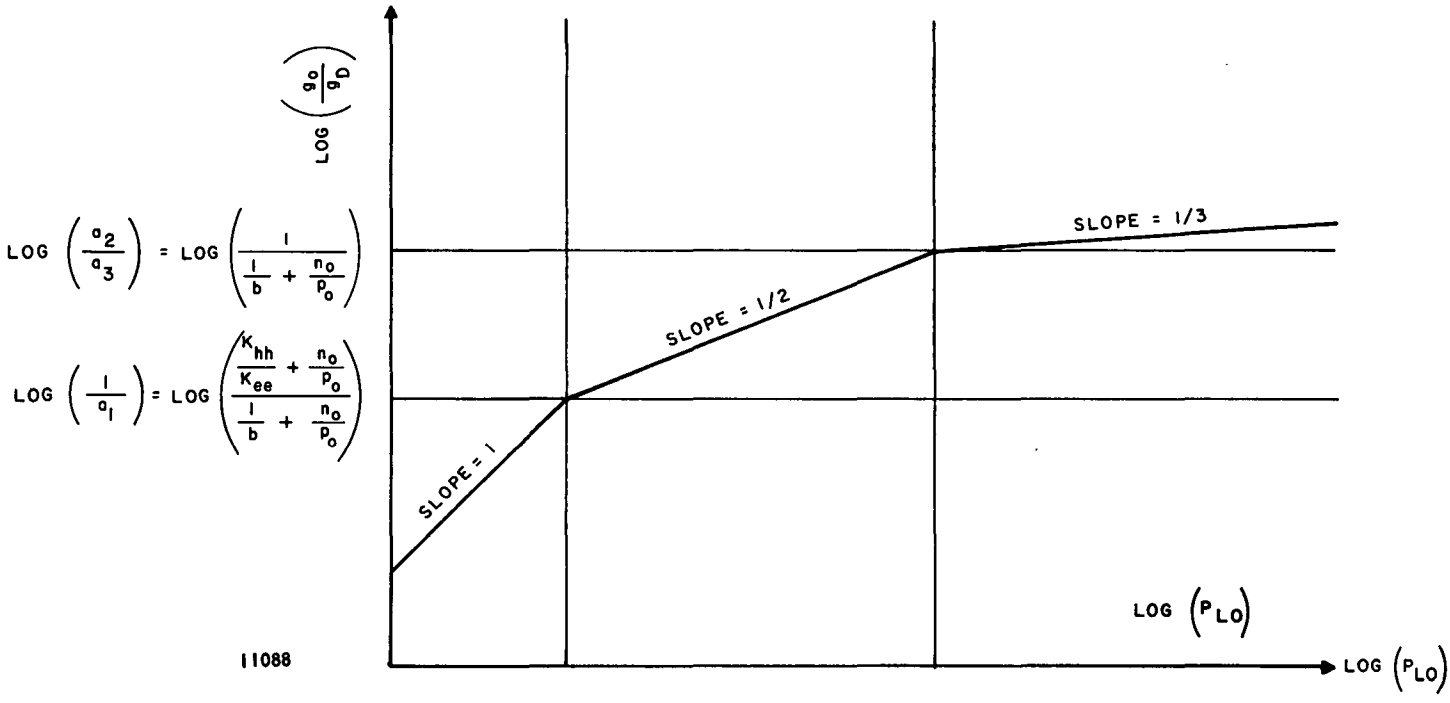

FIGURE 49. THEORETICAL CONDUCTANCE RATIO VERSUS LO POWER FOR p-TYPE HgCdTe (AUGER RECOMBINATION)

and the normalized hole-hole generation rate (K_{hh}). It should be noted that only p-type Auger lifetime limited photoconductors exhibit the relationship shown in Figure 48 since:

- n-type Auger lifetime limited photoconductors exhibit a linear and cubic region
- The radiative lifetime limited photoconductors and photoconductors with free carrier capture by flaws exhibit a linear and quadratic region
- The Shockley-Read lifetime limited photoconductors exhibit a linear, a greater than linear and a linear region

when the conductance ratio (g_o/g_D) is plotted as a function of applied LO power (reference 18).

Therefore, this identifying characteristic of photoconductive detectors is a useful technique in determining the dominant recombination mechanism in an infrared detector or photomixer.

Using the parameters a_2 and a_3 which are defined in Figure 48, the ratio of the small signal heterodyne lifetime to the large signal lifetime can be expressed as

$$\frac{\tau_{het}}{\tau_{LO}} = \frac{1 + \frac{g_o}{g_D}\left[1 + \frac{g_o}{g_D}\left(\frac{a_3}{a_2}\right)\right]}{\left(\frac{1}{a_2}\right) + \frac{g_o}{g_D}\left[2 + 3\left(\frac{a_3}{a_2}\right)\frac{g_o}{g_D}\right]} \tag{25}$$

2. AVAILABLE CONVERSION GAIN

The IF photocurrent generated in the photomixer is given (reference 12) by

$$I(\omega) = \eta q\, F_1 A \left(\frac{\tau_{het}}{T_r}\right) \frac{1}{1 + j\omega\tau_{het}} \tag{26}$$

where

$F_1 A$ = peak photon flux at IF

T_r = transit time of the carriers (= $L^2/\mu V$)

L = interelectrode spacing

A = illuminated area of the photomixer = L X W

The available conversion gain, or the ratio of the available IF output power to the available infrared signal power is,

$$G = \frac{P_{IF},\ \text{available}}{P_s} = \frac{|I(\omega)|^2}{8\left(g_o + g_D\right) P_s} \tag{27}$$

The LO-induced mixer conductance is

$$g_o = \frac{I_o}{V} = \frac{\eta q\ F_o\ A\tau_{LO}}{V\ T_r} = \frac{\eta q\ \mu\ F_o\ A\tau_{LO}}{L^2} \tag{28}$$

Substitution of equations 26 and 28 into 27 then gives

$$G = \frac{\eta\ q\ V\ \tau_{het}}{2h\nu_s\ T_r\left(1 + \omega^2\ \tau_{het}^2\right)} \left(\frac{\tau_{het}/\tau_{LO}}{1 + g_D/g_o}\right) \tag{29}$$

$$= \frac{\eta\ q\ \mu\ \tau_{het}}{2h\nu_s\left(1 + \omega^2\ \tau_{het}^2\right)} \frac{V^2}{L^2} \left(\frac{\tau_{het}/\tau_{LO}}{1 + g_D/g_o}\right)$$

In obtaining equation 29, use has been made of the relation for modulation index, namely,

$$\frac{F_1 A}{F_o A} \approx 2\sqrt{\frac{F_s A}{F_{LO} A}}, \quad F_{LO} \gg F_s \tag{30}$$

where the photon flux at signal frequency is

$$F_s A = \frac{P_s}{h\nu_s} \tag{31}$$

and the photon flux at LO frequency is

$$F_{LO} A \approx F_o A = \frac{P_{LO}}{h\nu_{LO}} \tag{32}$$

The conversion gain depends on the LO power directly through its effect on g_o and indirectly through effects on the lifetimes τ_{het} and τ_{LO} and the transit time T_r (through an effect on mobility μ).

An alternative expression for the conversion gain in terms of the absorbed bias power (P_{dc}) and the LO power (P_{LO}) is useful for gain calculations and for optimization of the ratio of bias to LO power. The total absorbed bias power is

$$P_{DC} = V^2 (g_o + g_D) \tag{33}$$

Since $\nu_s \approx \nu_{LO}$, substitution of equations 28, 32, and 33 into 29 gives

$$G = \frac{P_{DC}}{2P_{LO}} \left(\frac{\tau_{het}}{\tau_{LO}} \right)^2 \left(\frac{1}{1 + g_D/g_o} \right)^2 \frac{1}{1 + \omega^2 \tau_{het}^2} \tag{34}$$

If the carrier mobility is assumed to be independent of LO power, equation 34 shows that for $\omega\tau_{het} < 1$, the available mixer gain is independent of carrier mobility and depends only on the power, conductance, and lifetime ratios.

3. PHOTOMIXER NOISE

The overall mean-square noise current generator consists of three component noise generators

$$\overline{i_N^2} = \overline{i_{GR}^2} + \overline{i_G^2} + \overline{i_{IF}^2} \tag{35}$$

$\overline{i_{GR}^2}$ is the G-R noise given by (reference 12 and 17)

$$\overline{i_{GR}^2} = 4q\,\tau_{het} \left(\frac{1}{T_{r,e}} + \frac{1}{T_{r,h}} \right) \left(\frac{\tau_{het}}{\tau_{LO}} \right) \left[\frac{np}{n_e (n_o + p_o + n_e)} \right] \left(\frac{I_o B}{1 + \omega^2 \tau_{het}^2} \right) \tag{36}$$

$$\approx 4q \left(\frac{\tau_{het}}{\tau_{LO}} \right) \left(\frac{\tau_{het}}{T_{r,e}} + \frac{\tau_{het}}{T_{r,h}} \right) \left(1 + \frac{n_o}{n_e} \right) \frac{I_o B}{1 + \omega^2 \tau_{het}^2}$$

where

$T_{r,e}$, $T_{r,h}$ = transit time of electrons and holes, respectively, ($b = T_{r,h}/T_{r,e} \gg 1$)

n = total electron concentration = $n_o + n_e$

p = total hole concentration = $p_o + n_e$

$n_e = p_e$ and $p_o > n_o$

In equation 36 the local-oscillator induced, and dark contributions to G-R noise correspond to the terms 1 and n_o/n_e, respectively, in the factor $(1 + n_o/n_e)$. Qualitatively, $1 \gg n_o/n_e$ because the G-R noise is proportional to the minority carrier concentration, which increases much faster than the dc current (equivalently, majority carrier concentration) as hole-electron pairs are generated by the local oscillator. This statement is believed to have general applicability to HgCdTe intrinsic photodetectors although equation 36 was specifically derived for p-type HgCdTe with Auger band-to-band recombination dominant.

Using equation 18 an alternative form of the factor $(1 + n_o/n_e)$ in equation 36 is given by

$$1 + \frac{n_o}{n_e} = 1 + \left(\frac{g_D}{g_o} - \frac{p_o}{b\, n_e} \right) \approx 1 + \frac{g_D}{g_o}, \quad b\, n_e \gg p_o \tag{37}$$

$\overline{i_G^2}$ is the thermal noise of the total mixer conductance given by

$$\overline{i_G^2} = 4\,k\,T_M \left(g_o + g_D \right) B \tag{38}$$

where

k = Boltzmann's constant

T_M = physical temperature of mixer

$\overline{i_{IF}^2}$ is the IF amplifier noise referred to the output terminals of the mixer, and is

$$\overline{i_{IF}^2} = 4\,k\,T'_{IF} \left(g_o + g_D \right) B \tag{39}$$

where

T'_{IF} = effective input noise temperature of IF amplifier referred to the output terminals of the mixer = $(F'_{IF} - 1)\,T_o$

F'_{IF} = noise factor of IF amplifier referred to the output terminals of the mixer

T_o = reference temperature $\equiv$ 290 K

4. RECEIVER SENSITIVITY

The IF output signal-to-noise power ratio is

$$\left(\frac{S}{N} \right)_{POWER} = \frac{|I(\omega)|^2}{2\,\overline{i_N^2}} \tag{40}$$

Substitution of equations 27 to 29 and 35 to 39 into 40 then gives

$$\left(\frac{S}{N}\right)_P = \left(\frac{\eta P_s}{2h\nu_s B}\right) \frac{1}{\left(1 + \frac{n_o}{n_e}\right) + \frac{k\left(T_M + T'_{IF}\right)}{q\,V}\left(\frac{T_r}{\tau_{het}}\right)\left(\frac{\tau_{LO}}{\tau_{het}}\right)\left(1 + \frac{g_D}{g_o}\right)\left(1 + \omega^2 \tau_{het}^2\right)} \tag{41}$$

Thus, the NEP, or the value of signal power to give an IF S/N ratio equal to unity, is

$$\begin{aligned} NEP &= \frac{2h\nu_s B}{\eta}\left\{\left(1 + \frac{n_o}{n_e}\right) + \frac{k\left(T_M + T'_{IF}\right)}{qV}\left(\frac{T_r}{\tau_{het}}\right)\left(\frac{\tau_{LO}}{\tau_{het}}\right)\left(1 + \frac{g_D}{g_o}\right)\left(1 + \omega^2 \tau_{het}^2\right)\right\} \\ &= \frac{2h\nu_s B}{\eta}\left\{\left(1 + \frac{n_o}{n_e}\right) + \frac{1}{40V}\left(\frac{T_M + T'_{IF}}{T_o}\right)\left(\frac{T_r}{\tau_{het}}\right)\left(\frac{\tau_{LO}}{\tau_{het}}\right)\left(1 + \frac{g_D}{g_o}\right)\left(1 + \omega^2 \tau_{het}^2\right)\right\} \end{aligned} \tag{42}$$

with V in volts. In terms of the conversion gain (equation 29), equation 42 can be written

$$\begin{aligned} NEP &= \frac{2h\nu_s B}{\eta}\left(1 + \frac{n_o}{n_e}\right) + \frac{k\left(T_M + T'_{IF}\right) B}{G} \\ &\approx P'_{min} + \frac{k\left(T_M + T'_{IF}\right) B}{G} \end{aligned} \tag{43}$$

where $P'_{min} = 2h\nu_s B/\eta \cdot \left(1 + \frac{n_o}{n_e}\right)$ which reduces to the expression for extrinsic photoconductive photomixers (reference 2) when n_o/n_e is much less than unity. (The n_o/n_e term approach zero as the applied LO power is increased sufficiently to satisfy the condition of $g_o \gg g_D$.)

B. MEASUREMENT DATA

The following paragraphs present the results of detailed measurements which have been carried out on p-type HgCdTe mixer elements (reference 19). Data is presented on heterodyne receiver NEP, frequency response, power dissipation, mixer noise, and mixer conductance for various levels of dc bias and LO power.

The parameters of the single element photomixer at 77 K were:

Area	$A \approx 0.76$ mm^2
Peak Wavelength	$\lambda_p \approx 9.5$ to 10.5 μm
Dark Resistance	$R_D \approx 26\ \Omega$
Responsivity	$\mathcal{R} \approx 1$ V/W
D-star at 10.6 μm	$D^* \approx 3 \times 10^7$ W/Hz$^{1/2}$
Quantum Efficiency	$\eta \approx 25$ percent (estimate)
Hole Concentration	$p_o \approx 10^{17}$ cm^{-3}

1. MIXER CONDUCTANCE RATIO

The current-voltage characteristics of a p-type PC-HgCdTe photomixer was measured as a function of applied LO power and the results are given in Figure 50. The mixer conductance ratio varied linearly with applied LO power for g_o/g_D between 0.04 and 0.26, and the relationship became quadratic with LO power for g_o/g_D between 0.26 and the measurement extreme of 2.7. The measurement and calculated results were in good agreement (equation 24) and verified the fact that the photomixer was p-type (rather than n-type) HgCdTe. The second break point between the quadratic and cubic region, shown in Figure 49, is expected to occur at $g_o/g_D \approx b \approx 150$.

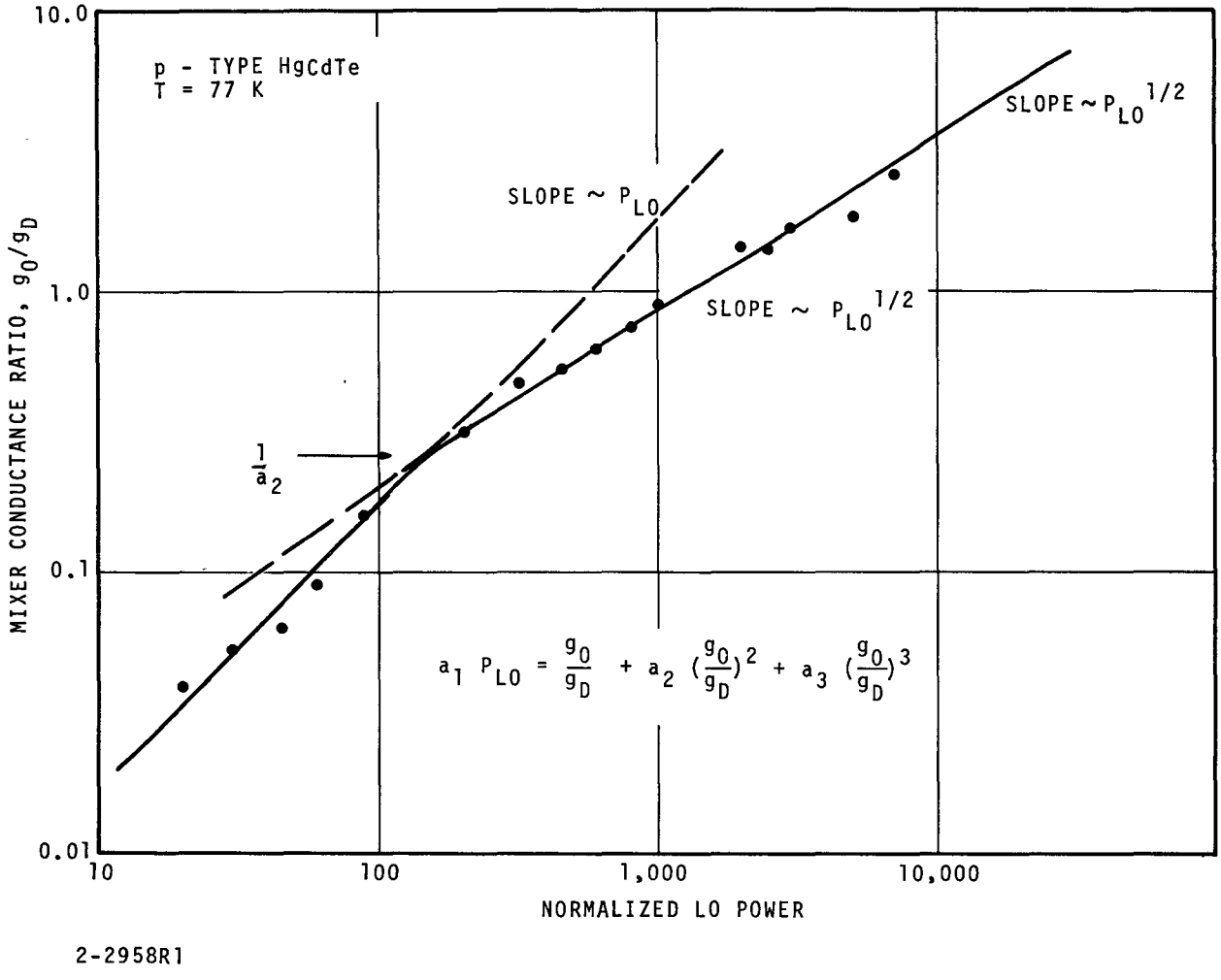

FIGURE 50. MEASURED MIXER CONDUCTANCE RATIO VERSUS APPLIED LO POWER IN p-TYPE HgCdTe

Using Figures 49 and 50, and equation 24, then

$$\frac{g_o}{g_D} = \frac{1}{a_2} = \left(\frac{K_{hh}}{K_{ee}} + \frac{n_o}{p_o}\right)\left(\frac{1}{b} + \frac{n_o}{p_o}\right)^{-1}$$

$$\frac{g_o}{g_D} \approx 0.26 \approx \frac{K_{hh}\, b}{K_{ee}}$$

$$K_{hh} \approx \frac{K_{ee}}{600}\ , \text{ for } b = 150$$

2. CONTACT (1/f) NOISE

Contact (1/f) noise was measured on the p-type HgCdTe photomixer at 77 K and IF frequencies between 10 kHz and 2 MHz for an applied bias voltage of 0.2 volts and $P_{LO} = 0$. The measured contact (1/f) noise (Figure 51) was relatively unaffected by applied laser LO power, but increased with increasing dc bias voltage and decreasing frequency as given by the expression

$$V_N^2 \approx \frac{K' V_{dc}^2 B}{f^{\alpha} \text{ Vol}} \tag{44}$$

where

K' = proportionality factor

V_{dc} = dc bias voltage

B = IF bandwidth

f = IF frequency

$\alpha \approx 0.8$

Vol = mixer volume

As can be seen in Figure 49, the contact (1/f) noise voltage was still decreasing at the highest IF frequency measured. The more rapid fall-off above 500 kHz is due to a decrease in the gain of the IF amplifier following the mixer element. In addition, noise measurements above 500 kHz become more difficult because of the low mixer element responsivity resulting in noise voltages which could not be accurately measured. This measurement uncertainty is denoted in Figure 51 by the bar-intervals shown between 500 and 2000 kHz.

Based on the contact and thermal noise measurements, the 1/f noise is expected to be essentially negligible at IF frequencies of 20 MHz and above.

3. PHOTOMIXER G-R NOISE

The measured photomixer noise as a function of applied dc bias power is given in Figure 52 with and without applied LO power. The system thermal noise dominates for $P_{dc} < 1$ mW and the photomixer G-R noise increased at the expected 3-dB per octave rate for $P_{dc} > 13$ mW.

4. MIXER FREQUENCY RESPONSE

A G-R noise measurement technique has been used to determine the frequency response of the p-type, intrinsic photoconductive HgCdTe photomixer. The technique was similar to the approach used to determine the frequency response of extrinsic photoconductive and photovoltaic photomixers (references 2 and 3 and Appendix I).

The G-R and thermal noise power were measured as a function of IF frequency and used to determine the resultant G-R noise spectrum given in Figure 53. The measured 3-dB cutoff frequency was (1) 32 MHz for an

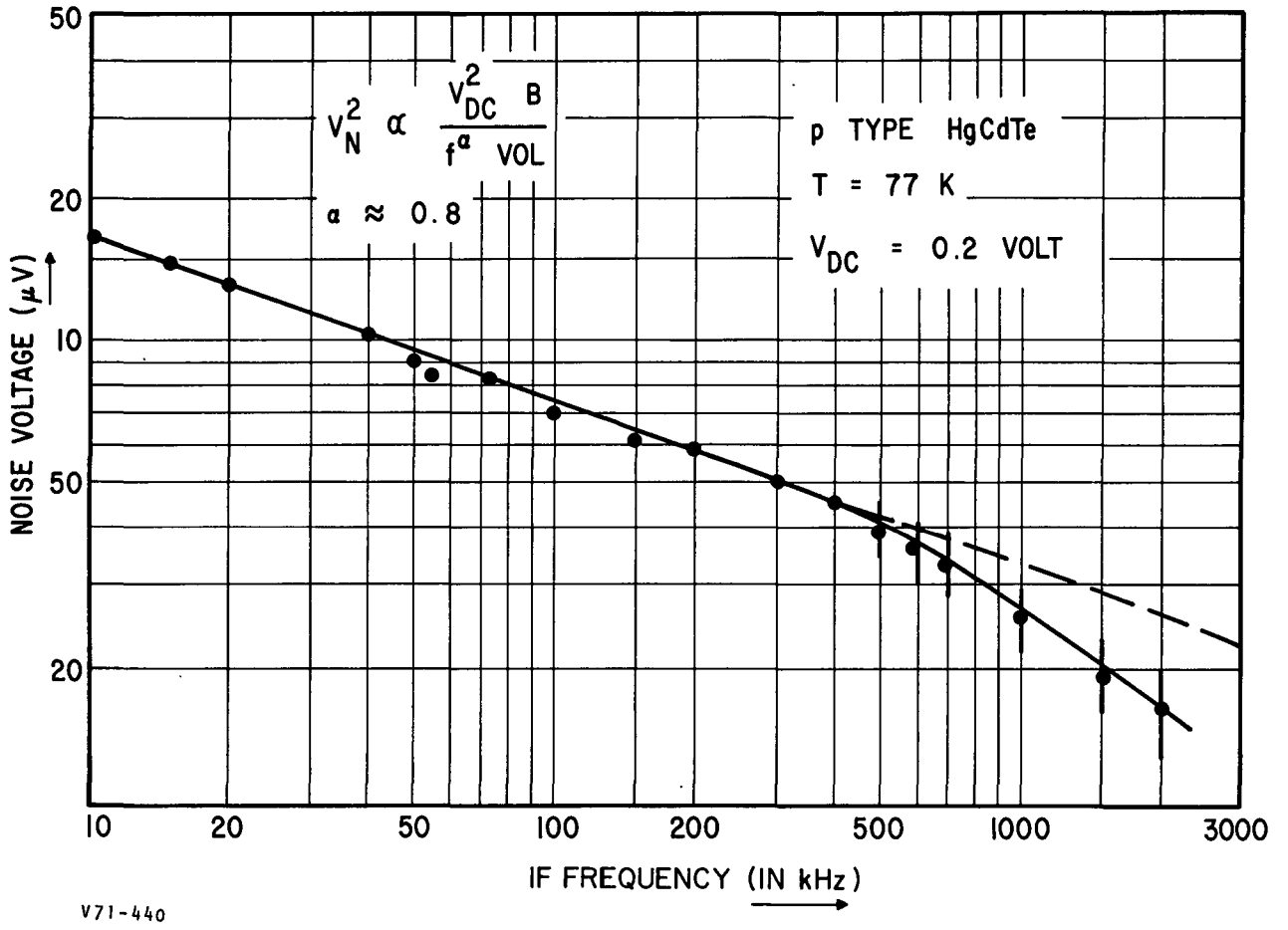

FIGURE 51. CONTACT (1/f) NOISE VERSUS IF FREQUENCY IN p-TYPE HgCdTe DETECTOR

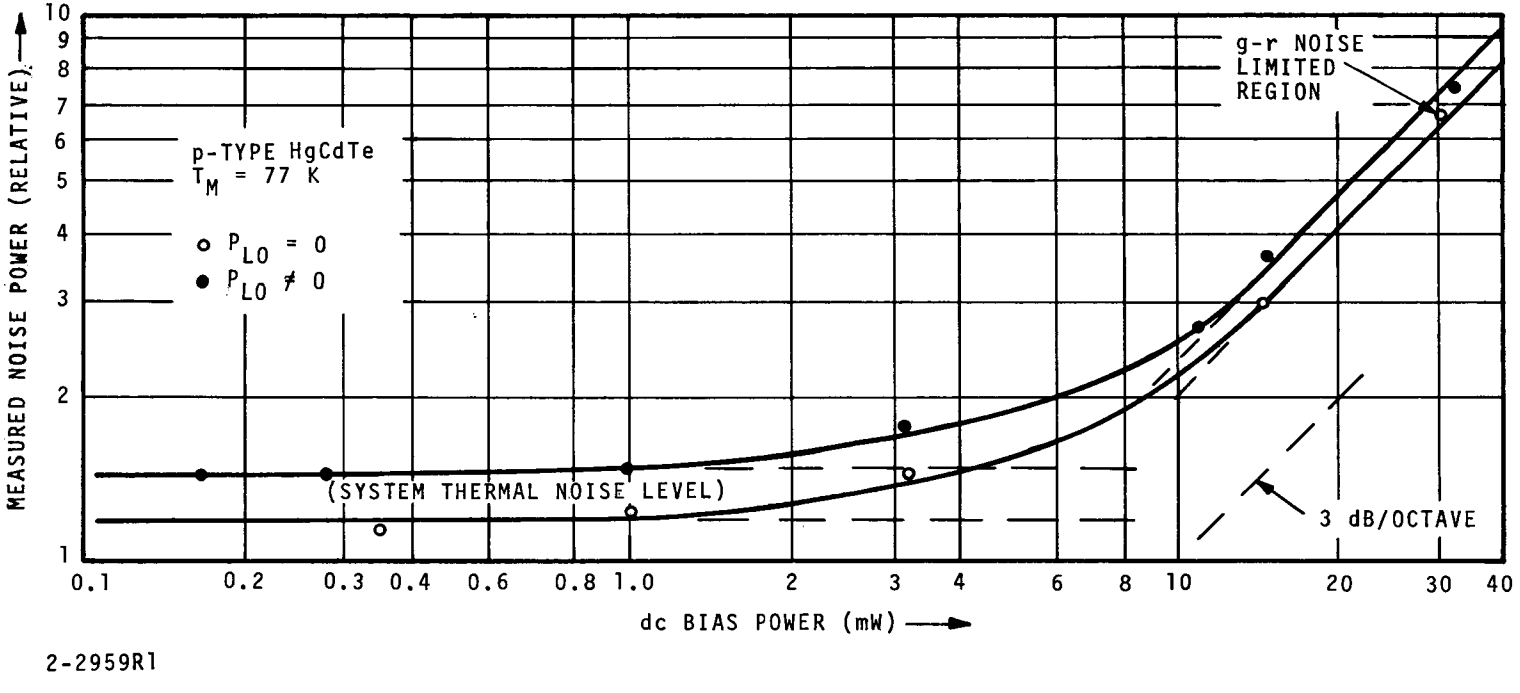

FIGURE 52. MIXER NOISE POWER VERSUS DC BIAS POWER IN p-TYPE HgCdTe PHOTOMIXER

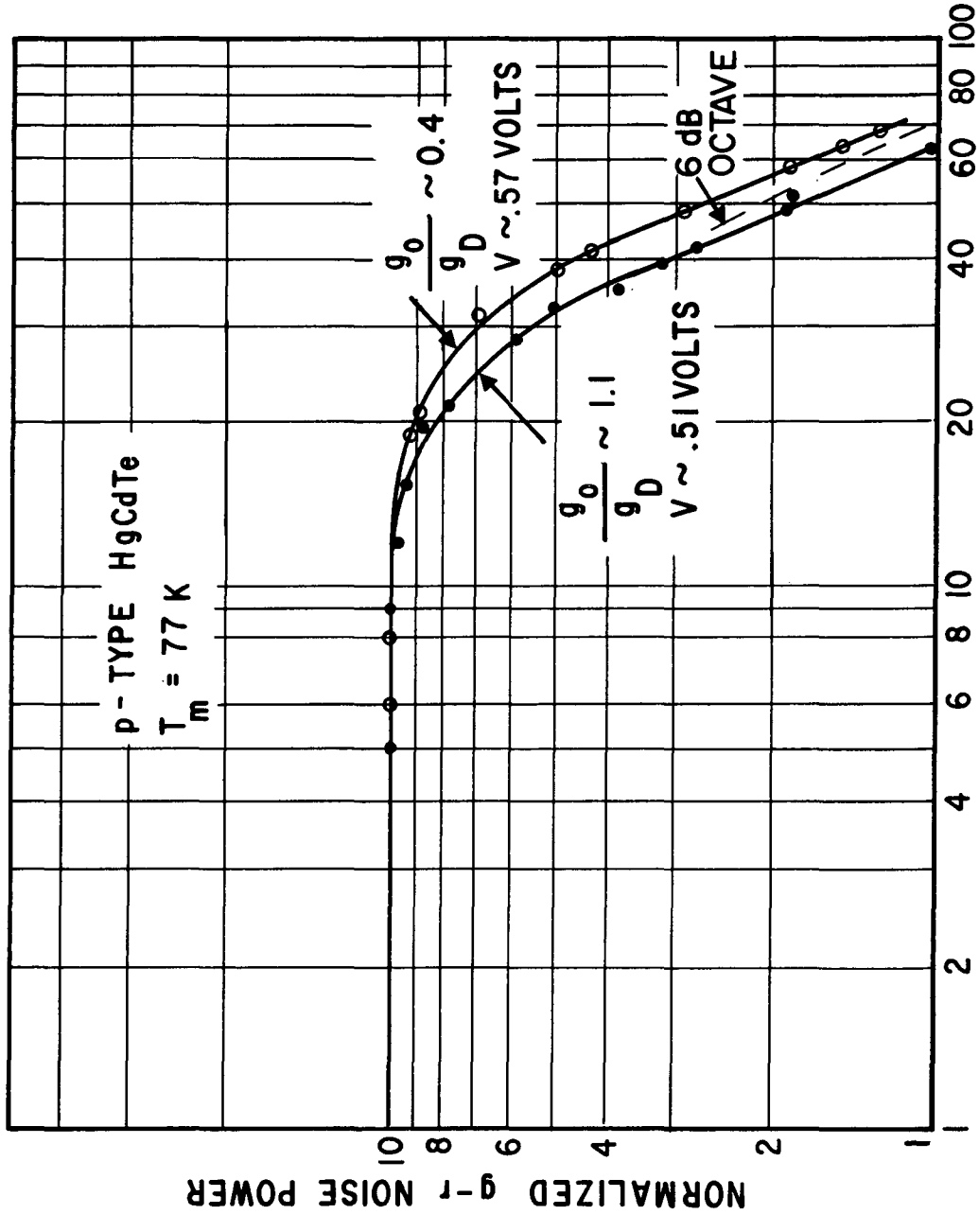

FIGURE 53. G-R NOISE SPECTRUM OF p-TYPE HgCdTe PHOTOMIXER

applied voltage of 0.51 volts and a conductance ratio of $g_o/g_D \sim 1.1$ ($P_{LO} \approx$ 70 mW) and (2) 38 MHz for an applied voltage of 0.57 volts and $g_o/g_D \approx 0.38$ ($P_{LO} \approx 20$ mW).

The G-R noise spectrum rolled off at the expected 6 dB/octave rate and the small change in frequency response with applied dc bias and LO power may be due to impedance changes, changes in carrier mobility or transit time effects. The measured 3-dB cutoff frequencies indicate that p-type HgCdTe may be a suitable photomixer for applications requiring a flat frequency response at IF frequencies of 20 MHz.

5. AVAILABLE CONVERSION GAIN

Using the measurement data reported in this section and equation 34, the available conversion gain of the p-type PC-HgCdTe photomixer was calculated and the results are summarized in Table V. The calculated conversion gain was (1) -15.7 dB (P_{LO} = 76 mW and P_{dc} = 21 mW) and (2) -14.3 dB (P_{LO} = 20 mW and P_{dc} = 17 mW).

TABLE V. MEASURED AND CALCULATED HETERODYNE PARAMETERS ON 10.6-MICROMETER p-TYPE HgCdTe PHOTOMIXER/IF PREAMPLIFIER FRONT-END

Case	g_o/g_D	P_{LO} (mW)	P_{dc} (mW)	V (Volts)	f_c (MHz)	τ_{LO} (ns) (Calc)	G (dB) (Calc)
1	1.1	76	21	0.51	32	5.0	-15.7
2	0.38	20	17	0.57	38	4.2	-14.3

6. NOISE EQUIVALENT POWER

The p-type HgCdTe photomixer was interfaced with a specially designed IF preamplifier and heterodyne NEP measurements were carried out as a function of applied dc bias power at an IF difference frequency of 30 MHz for $g_o/g_D \approx 0.14$. The results are shown in Figure 55.

The photoconductive gain increases linearly with applied dc bias (equation 34) thereby reducing the thermal noise term in the NEP expression (equation 43) until the receiver sensitivity approaches

$$\frac{P_{min}}{B} = \frac{2h\nu_s B}{\eta}\left(1 + \frac{n_o}{n_e}\right) \approx 1.4 \times 10^{-18} \text{ W/Hz for } P_{dc} > 40 \text{ mW}$$

For $g_D/g_o = 0.14$, $\eta = 25\%$ and $p_o < bn_e$, the calculated sensitivity limit is 1.2×10^{-18} W/Hz, in good agreement with the measured value of 1.4×10^{-18} W/Hz. It should be noted that there is some uncertainty in the photomixer quantum efficiency. The heterodyne receiver NEP can be further improved by increasing the applied laser LO power so as to reduce g_D/g_o and minimize the dark current contributions to the photomixer G-R noise term.

7. FOUR-ELEMENT SYMETRICAL ARRAY

A four-element (2×2) p-type photoconductive HgCdTe array was fabricated to AIL specifications. Each photomixer was 0.1 mm by 0.1 mm and the spacing between elements was 0.1 mm. The detectors exhibited a spectral peak at 11.8 μm when operated at 77 K, a D* (500,100,1) of approximately 10^8 cm $Hz^{1/2}$/cm, and a 3-dB frequency response near 30 MHz. The dark photoconductive resistance was 360 ohms, a very favorable value, and with laser LO power applied, the photomixer resistance dropped to 280 ohms ($g_D/g_o \approx 2.8$).

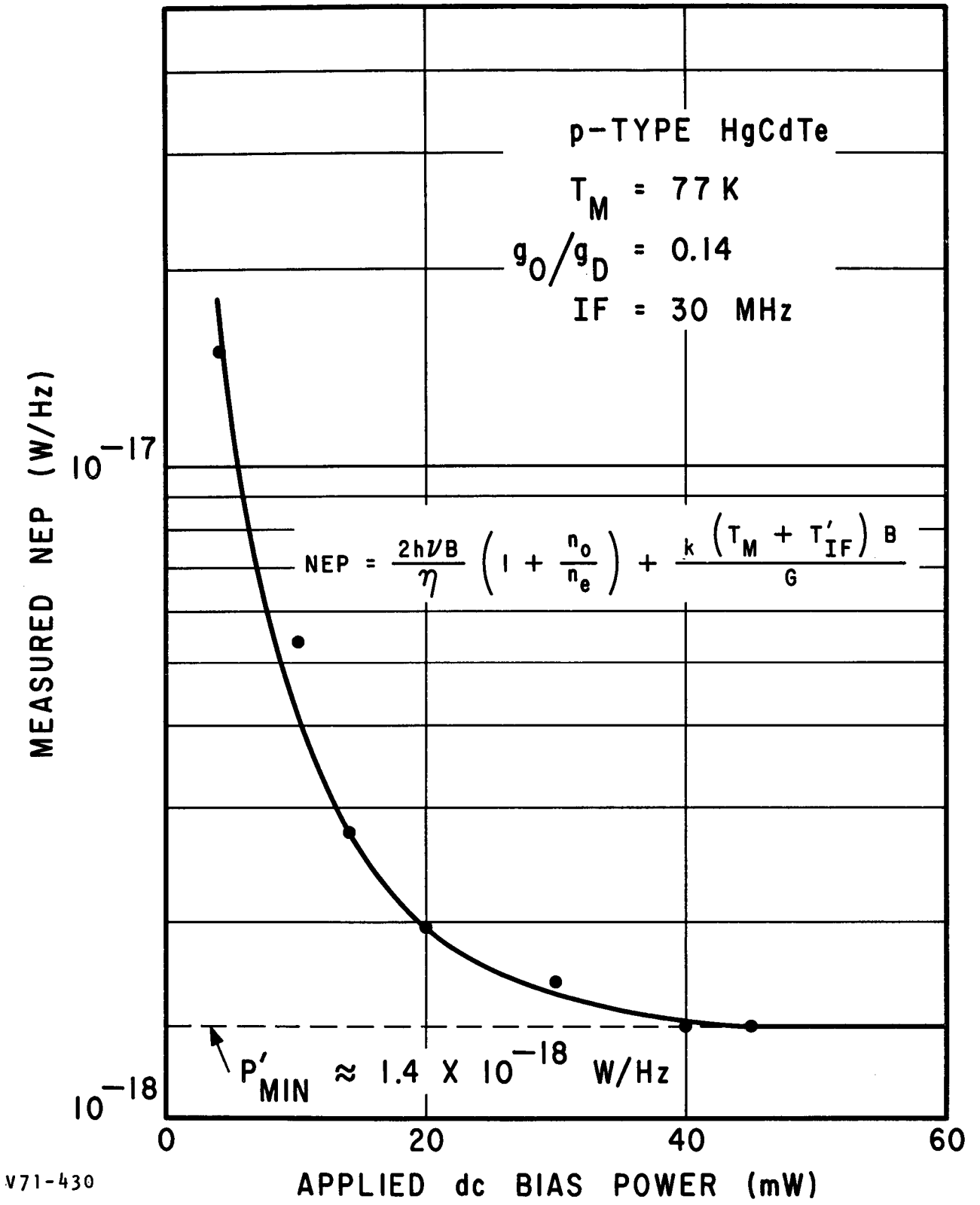

FIGURE 54. MEASURED NEP VERSUS APPLIED DC BIAS POWER IN p-TYPE HgCdTe PHOTOMIXER

The measured heterodyne noise equivalent power for the four-elements of the array at 77 K and an IF of 20 MHz were:

$$1.48 \times 10^{-18} \text{ W/Hz}$$

$$1.54 \times 10^{-18} \text{ W/Hz}$$

$$1.33 \times 10^{-18} \text{ W/Hz}$$

$$1.50 \times 10^{-18} \text{ W/Hz}$$

The measured NEP's for the four measured elements of the p-type HgCdTe array were reasonably close to the value (1.4×10^{-18} W/Hz) reported on the single element p-type HgCdTe photomixer. They are also limited by the dark current contributions to the photomixer G-R noise.

The HgCdTe array was operated as a coherent monopulse receiver with a 20 MHz offset between the incident signal and CO_2 laser local oscillator. The elevation difference channel and sum channel IF outputs were measured for various angles of arrival using a simulated optical antenna range. The results are shown in Figure 55. The resultant measurements were in good agreement with the expected classical monopulse patterns. However, the null between the sum and difference channels was limited by nonoptimized system noise. This type of coherent amplitude sensing monopulse receiver makes full use of the receiver aperture, provides greater angle error sensitivity than the conical scanner type tracker, and is relatively insensitive to atmospheric and target scintillations (references 20 and 21).

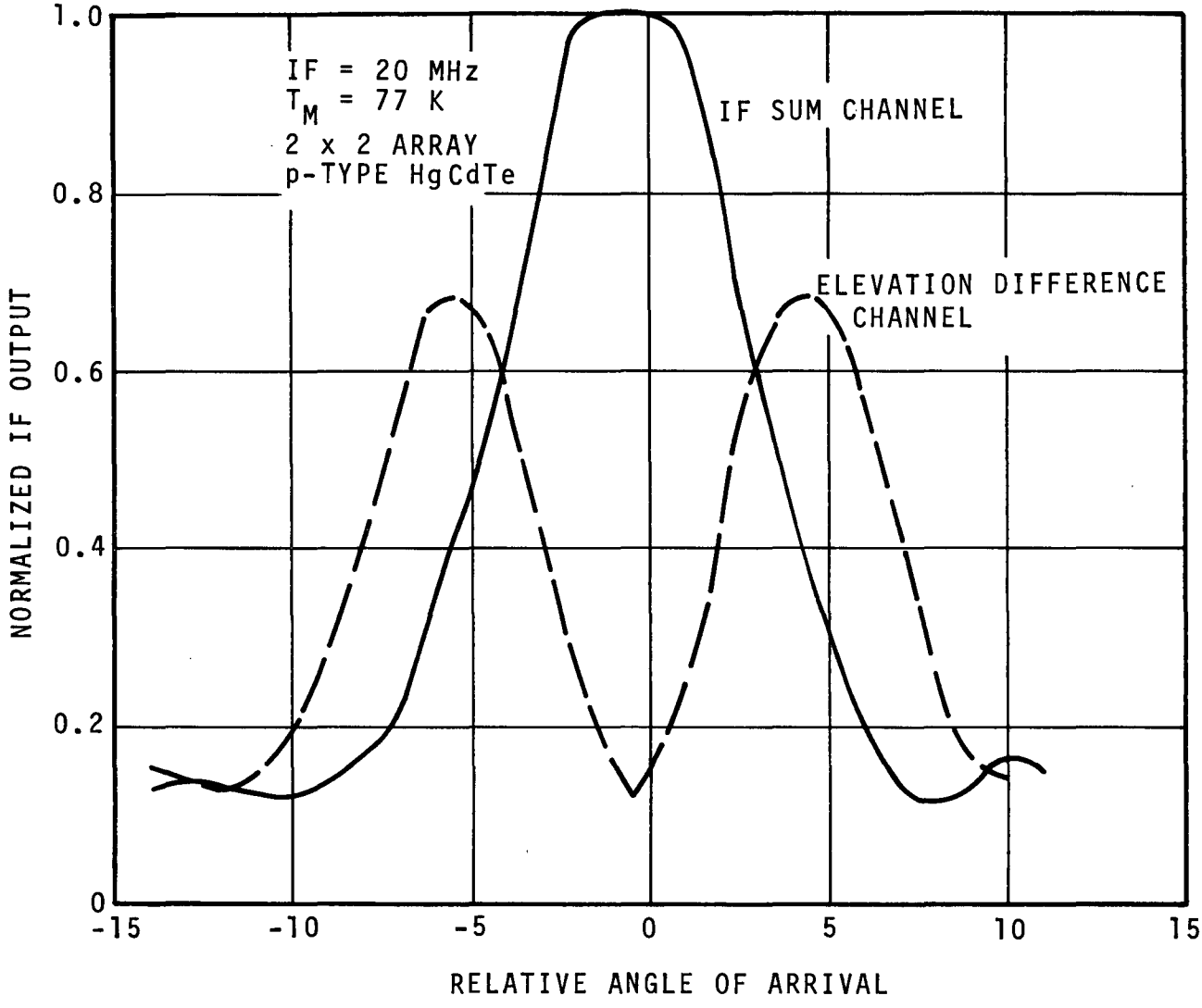

FIGURE 55. ELEVATION MONOPULSE ANTENNA PATTERNS FOR A 2 BY 2 p-TYPE HgCdTe PHOTOMIXER ARRAY

VII. CONCLUSIONS

Extensive analysis and measurements aimed at establishing the feasibility of designing and developing high-sensitivity, wide bandwidth 10.6 micrometer heterodyne receivers for a space-to-ground communications link has been completed.

An analysis and expressions have been presented for the engineering design of a quantum-noise-limited infrared receiver that uses a photovoltaic diode with finite dark conductance as the photomixer. The analysis considered such parameters as photomixer temperature, photomixer equivalent circuit, bias voltage, applied LO power, mixer conversion gain, and preamplifier source impedance. Measurements on the breadboarded receiver indicate that nearly quantum-noise-limited operation is achievable over a wide range of mixer temperature, IF, applied bias voltage, and incident LO power, and, in addition, the large frequency response of the HgCdTe mixer indicates the potential of applying this type of receiver to a satellite-to-satellite communications link where large Doppler offsets are encountered (reference 8). In addition, photomixing in photoconductive HgCdTe photomixers having a finite dark conductance was investigated. The feasibility of key receiver elements such as the photomixer, conical scanner acquisition circuitry, AFC loop and high fidelity communications channel has been demonstrated using the packaged breadboard shown in Figure 57. The pertinent receiver characteristics are as follows:

Sensitivity	less than 10^{-19} W/Hz (82 to 104 K) less than 1.8×10^{-19} W/Hz (77 to 140 K)
Photomixer temperature range	77 to 140 K
Photomixer power dissipation	<10 mW

Incident LO power	≈2 mW
IF bandwidth	>100 MHz (30 ±10 MHz selected)
Group-delay distortion (FM format)	< ±10 ns/10 MHz
AFC tracking	±6 MHz
Acquisition IF SNR	>-20 dB
Acquisition Time Delay	≈14 ms
Spatial Tracking	Conical scanner over >11 photomixer widths

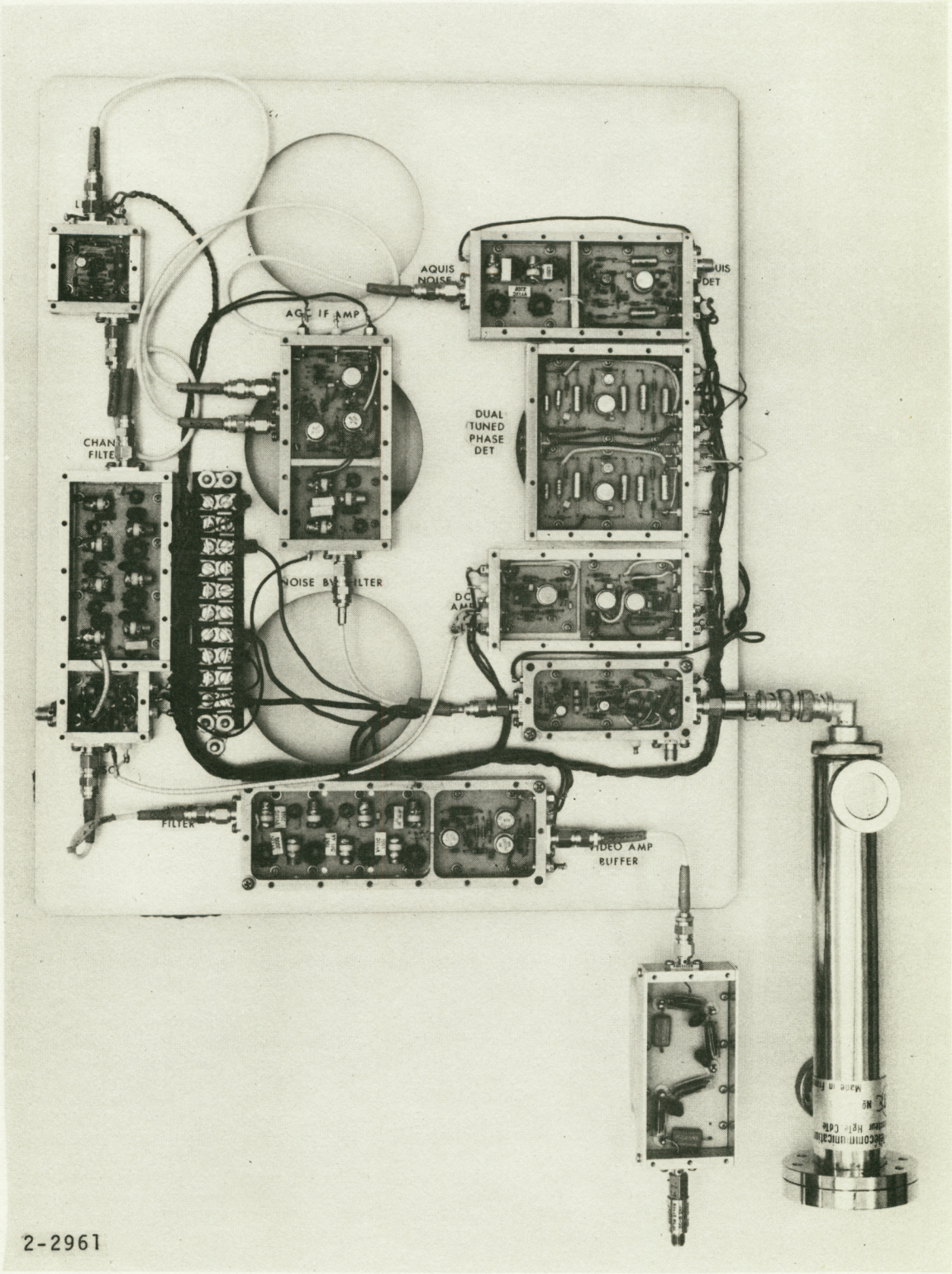

FIGURE 56. 10.6-MICROMETER OPTICAL RECEIVER SUBSYSTEM BREADBOARD

VIII. REFERENCES

1. H. W. Mocker, "A 10.6 μm Optical Heterodyne Communication System," Appl Opt, Vol 8, p 677-684, March 1969.

2. F. R. Arams, E. W. Sard, B. J. Peyton, and F. P. Pace, "Infrared 10.6 Micron Heterodyne Detection with Gigahertz IF Capability," IEEE Quantum Electron, Vol QE-3, p 484-492, November 1967. See also Infrared Detectors, Vol 5 of Semiconductors and Semimetals, A. Beer and R. Willardson, Eds., New York: Academic Press, Chapter 10, 1970.

3. B. J. Peyton, A. J. DiNardo, G. Kanischak, F. Arams, R. Lange, and E. Sard, "High Sensitivity Receiver for Infrared Laser Communications," IEEE JQE, Vol QE-8, No. 2, p 252-263, February 1972 (see Appendix I).

4. M. Teich, R. Keyes, and R. Kingston, "Optimum Heterodyne Detection at 10.6 Microns in Photoconductive Ge:Cu," Appl Phys Lett, Vol 9, p 357-360, November 1966.

5. C. Buczek and G. Picus, "Heterodyne Performance of Mercury-Doped Germanium," Appl Phys Lett, Vol 11, p 125-126, August 1967.

6. M. C. Teich, "Infrared Heterodyne Detection," Proc IEEE, Vol 56, p 37-46, January 1968. See also Infrared Detectors, Vol 5 of Semiconductors and Semimetals, A. Beer and R. Willardson, Eds., New York: Academic Press, Chapter 9, 1970.

7. B. J. Peyton, E. W. Sard, R. A. Lange, and F. R. Arams, "Infrared 10.6 μm Photodiode Heterodyne Detection," Proc IEEE, Vol 48, p 1769-1770, October 1970.

8. J. McElroy, N. McAvoy, H. Richard, T. McGunigal, and G. Schiffner, "Carbon Dioxide Laser Communications Systems for Near-Earth Applications," Proc of IEEE International Conference on Communications, p 22-27 to 22-37, San Francisco, June 8-10, 1970.

9. Private communication, T. McGunigal, J. McElroy, and N. McAvoy, Goddard Space Flight Center, NASA, and B. Walker and B. Wong, Aerojet General Corporation.

10. M. I. Skolnik, "Introduction to Radar Systems," McGraw-Hill Book Company, New York, 1962.

11. N. McAvoy, H. L. Richard, J. H. McElroy, and W. E. Richards, "10.6 Micron Laser Communications System Experiment for ATS-F and ATS-G," NASA Report X524-68-206, Goddard Space Flight Center, May 1968.

12. B. J. Peyton, "Phase One Design Report for High Sensitivity Infrared 10.6 Micrometer Heterodyne HgCdTe Receiver Development," AIL Report 8783-1 on Contract NAS-5-11665, September 1969.

13. B. J. Peyton, "Phase Two Design Report for High Sensitivity Infrared 10.6 Micrometer Heterodyne Receiver Development," AIL Report 8783-2 on Contract NAS-5-11665, March 1970.

14. J. Schmit and E. Stelzer, "Temperature and Alloy Compositional Dependences of Energy Gap of $Hg_{1-x}Cd_xTe$," Journal of Applied Physics, Vol 40, p 4865-4869, November 1969.

15. D. Long and J. Schmit, Infrared Detectors, Vol 5 of Semiconductors and Semimetals, A. Beer and R. Willardson, Eds., New York: Academic Press, Chapter 5, 1970.

16. K. M. Van Vliet, "Noise in Semiconductors and Photoconductors," Proc IRE, Vol 46, p 1004-1018, June 1958.

17. D. Breitzer, B. J. Peyton, E. Sard, and J. McElroy, "G-R Noise for Auger Band-to-Band Processes," Infrared Physics, Vol 11, p 237-239, 1971.

18. J. S. Balkemore, "Semiconductor Statistics," Pergamon Press, Oxford, 1962.

19. P. B. Pickar and A. T. Halpin, "Growth of HgCdTe by an Open Table Epitaxy Technique," presented at 1970 IRIS Detector Specialty Group, Santa Barbara, California, February 12, 1970.

20. F. P. Pace, R. A. Lange, F. R. Arams, and B. J. Peyton, "Spatially Coherent Array Technology for Wide-Band Infrared Heterodyne Receivers," IEEE Journal of Quantum Electronics, Vol QE-8, No. 2, February 1972.

21. R. A. Lange, F. P. Pace, and I. Rubinstein, "Coherent Heterodyne Monopulse Receiver at 10.6 Micrometers," presented at the Fifth DOD Laser Conference, Monterey, Calfornia, April 1972.

APPENDIX A

HIGH-SENSITIVITY RECEIVER FOR INFRARED LASER COMMUNICATIONS

High-Sensitivity Receiver for Infrared Laser Communications

BERNARD J. PEYTON, SENIOR MEMBER, IEEE, ANTHONY J. DiNARDO, GERALD M. KANISCHAK, MEMBER, IEEE, FRANK R. ARAMS, FELLOW, IEEE, RONALD A. LANGE, AND EUGENE W. SARD, SENIOR MEMBER, IEEE

Abstract—**The design of a high-sensitivity wide-bandwidth 10.6-μm heterodyne receiver has been established for space and ground operational use, and key elements for a satellite-to-earth communications link were demonstrated. The receiver includes a cooled HgCdTe infrared mixer diode, a conical scanner for spatial tracking, an acquisition channel for spatial search and station alignment, and an automatic frequency-control channel to maintain a fixed laser frequency offset. The infrared mixer is designed to provide nearly quantum-noise-limited operation over an extended range of mixer temperature, bias voltage, and IF.**

The resultant experimental receiver has a measured noise equivalent power of less than 10^{-19} W/Hz over the 15- to 40-MHz IF band for mixer temperatures from 85 to 115 K, and less than 2×10^{-19} W/Hz up to 140 K. Mixer 3-dB cutoff frequencies as high as 420 MHz were measured at a mixer temperature of 125 K.

An analysis and engineering equations are given for receiver noise components, noise equivalent power, available mixer conversion gain, mixer transducer gain, and quantum-noise factor in terms of such factors as mixer parameters, quantum efficiency, mixer temperature, dynamic conductance, bias voltage, LO power, and IF amplifier characteristics.

Manuscript received July 30, 1971; revised August 30, 1971. This work was supported by NASA Goddard Space Flight Center, Greenbelt, Md., under prime Contract with AIL and under Subcontract from Aerojet-General Corporation, Azusa, Calif.

B. J. Peyton, A. J. DiNardo, G. M. Kamischak, R. A. Lange, and E. W. Sard are with AIL, a division of Cutler-Hammer, Inc., Melville, N. Y. 11746.

F. R. Arams was with AIL, a division of Cutler-Hammer, Inc., Melville, N. Y. He is now with LNR Communications, Farmingdale, N. Y.

I. Introduction

ALTHOUGH direct detection is useful in 10.6-μm systems when simplicity is desired, in many applications heterodyne detection is preferred because it combines high sensitivity with wide electrical bandwidth, and preserves the phase and frequency char-

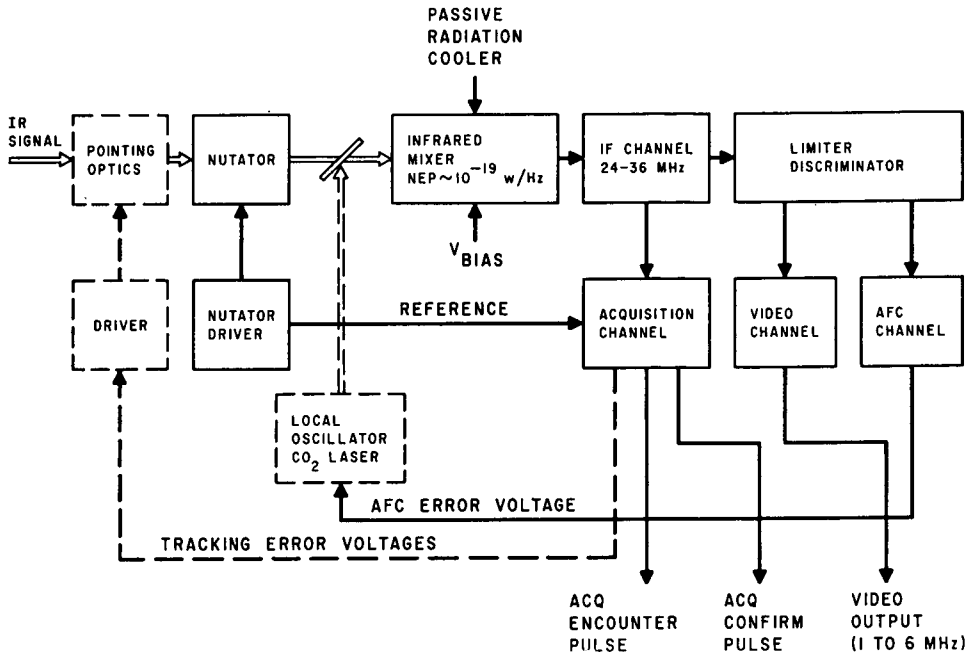

Fig. 1. Simplified block diagram of infrared communications receiver.

acteristics of the infrared signal. Coherent (heterodyne) detection is most practical at the long wavelengths due to reduced quantum noise, easier alignment of signal and LO, and greater diffraction-limited field of view [1]. Also, the CO_2 laser has proven practical as an efficient single-frequency stabilized source for the transmitter and LO [2], and operates in an atmospheric window. The potential of 10.6-μm heterodyne detection has been explored by a number of workers in several extrinsic [3], [4, ch. 10], [5], [6] and intrinsic [2], [4, ch. 9], [7]–[9] photodetector materials.

The design of a high-sensitivity wide-bandwidth 10.6-μm heterodyne receiver system suitable for use as a spaceborne and ground-based equipment for a two-way synchronous satellite-to-earth laser communications link [10] is established and the demonstration of key receiver elements is discussed. The receiver system to be described supplies all of the following functions.

1) Communications channel that provides heterodyne detection, amplification, and demodulation of frequency-modulated 10.6-μm signals with sensitivity near the quantum-noise limit.

2) Tracking channel that develops two orthogonal error voltages for spatial tracking using a conical scan of the heterodyne receiver field of view.

3) Acquisition channel that generates an x–y raster scan for spatial search during the acquisition mode and automatic transfer into the communications mode after acquisition encounter and confirm.

4) Automatic frequency control (AFC) channel that develops required error voltages to maintain a fixed frequency offset between incoming signal and LO laser.

5) Design that minimizes power dissipation in the infrared mixer element to permit passive radiation cooling in space.

6) Design toward fulfilling environmental, radio-frequency interference, and related space equipment requirements.

The resultant experimental receiver had a measured noise equivalent power of less than 10^{-19} W/Hz over the 15-to-40-MHz IF band using a reverse-biased HgCdTe photodiode for mixer temperatures from 85 to 115 K, and less than 2×10^{-19} W/Hz up to 140 K. The 3-dB cutoff frequency of the photodiode [11], [12] used was measured to be as high as 420 MHz over the 77- to 125-K range.

II. Receiver Description

The infrared receiver system (Fig. 1) consists principally of an infrared mixer/preamplifier, associated optical components, and signal-processing electronics. Its functions are described in the following paragraphs.

The communications channel includes all circuits from the IF preamplifier to the video output buffer amplifier. Due to the relatively narrow tuning range of the CO_2 LO laser, an IF center frequency of 30 MHz was used. The mixer, IF preamplifier, and postamplifier have a bandwidth exceeding 100 MHz. The system group delay for a high-quality 6-MHz video signal (IF from 24 to 36 MHz) was held to ± 5 ns using a delay equalizer. The FM signal is demodulated in an unusually wide (40-percent bandwidth) high-linearity limiter/discriminator. AFC error voltage is derived from the discriminator when the incoming signal and LO frequencies are not separated by exactly 30 MHz. The amplified error voltage is applied to a piezoelectric stack, which displaces one of the reflectors of the LO laser thereby changing its output frequency.

A key problem inherent in laser communications systems is accurate pointing and tracking due to their relatively narrow beamwidth. A conical scanner was demonstrated that nutates the received infrared beam so

as to develop east/west and north/south tracking-error signals that are fed to piezoelectrically driven pointing optics to maintain the receive beam (and the local transmit beam if a two-way link or a beacon is used) on boresight with respect to the received carrier. Unlike previous infrared trackers, this scanner operates in the heterodyne mode, where audio-frequency modulation on the carrier is compared to a reference from the nutator driver and separated into the two orthogonal error components in two phase detectors. The tracking-error voltages, together with a dc bias required for point-ahead correction, are then fed to the pointing optics to correct the spatial error.

A narrow-band acquisition encounter channel extracts a received signal pulse from noise under conditions of minimum signal-to-noise ratio when the scanning receiver beam intercepts the transmitter beam within the search volume dictated by the initial uncertainty of transmitter location. The encounter channel consists of a narrow IF bandpass filter, AM detector, matched filter, and threshold detector to trigger the acquisition pulse. An acquisition confirm channel is included, which operates at the second harmonic of the conical scan frequency. Measurement of probabilities of encounter versus video channel signal-to-noise ratio resulted in 100-percent probability of encounter for SNRs as low as -19 dB referenced to the IF bandwidth.

III. Choice of Infrared Photomixer

To minimize passive radiation cooler requirements aboard the spacecraft, the infrared mixer element must be capable of operating at as high a temperature as possible. This dictates the use of an intrinsic detector material using direct band-to-band excitation. The mixer crystal $Hg_{1-x}Cd_xTe$ was the only one sufficiently advanced in technological development to warrant consideration. The band gap in this ternary material can be tailored to the 10.6-μm wavelength by proper choice of molar content x [13]. The band-gap wavelength varies inversely with the temperature [4, ch. 5] so that the desired range of operating temperature also influences the optimum value of x.

For the communications application, an infrared mixer was required with a response that exceeds 60 MHz. Mixers with lower frequency response are not acceptable because of the reduced sensitivity and concomitant amplitude and phase variations [1] that can affect transmission fidelity. Matching networks designed to compensate for roll-off in mixer response were considered but rejected because of the change of mixer characteristics with temperature and bias.

Both photoconductive (PC), n and p types, and photovoltaic (PV) HgCdTe were considered in detail for the communications application and are briefly compared in the following paragraphs. Elements with response times as short as 50 ns have been reported using n-type PC-HgCdTe [2]. An analysis was carried out on the feasibility of reducing mixer lifetime with applied LO power. Expressions were derived for noise equivalent power (NEP) and mixer conversion gain that extend previously obtained expressions [14] by distinguishing between a small-signal (heterodyne) lifetime and large-signal (LO) lifetime. It was concluded that the increase in power dissipation was out of proportion to any obtainable increase in speed of response for n-type PC-HgCdTe.

A design analysis using p-type PC-HgCdTe was carried out and followed by experiments in which a heterodyne NEP at 30 MHz of 1.38×10^{-18} W/Hz was obtained using 30 mW of LO power and 40 mW of dc bias power [15]. Frequency response measurements yielded a 3-dB cutoff frequency of 38 MHz. It was concluded that the poor sensitivity, due to dark current-induced generation-recombination noise, in combination with large LO and dc power requirements, made the available p-type HgCdTe mixers unsuitable for this application.

The design analysis and subsequent experiments using PV-HgCdTe indicated that with proper design the receiver requirements could be almost completely satisfied using PV-HgCdTe in terms of operating temperature range, power dissipation, frequency response, sensitivity, and potential for future higher modulation rate systems. Hence, PV-HgCdTe was adopted for the receiver design. The results will now be discussed in further detail.

IV. Design Formulas for Photovoltaic Mixers

Following the approach used for photoconductive mixers [3], [4, ch. 10] expressions have been derived for reverse-biased photovoltaic mixer performance, expressed in terms of noise attributable to the mixer element itself and the IF amplifier; and the available conversion gain of the infrared signal power to the IF. The analysis is given in detail in Appendix I. It assumes a nonzero leakage conductance and neglects lead inductance. This is representative of present-day long-wavelength HgCdTe photovoltaic elements. The following is obtained for the available conversion gain:

$$G = \frac{\eta q I_0}{2h\nu G_D} \frac{1}{1 + (f/f_c)^2} \tag{1}$$

where

- η quantum efficiency,
- q electron charge,
- I_0 LO-induced dc photocurrent,
- h Planck's constant,
- ν infrared frequency,
- G_D small-signal shunt conductance,
- f intermediate frequency,
- f_c photodiode 3-dB cutoff frequency.

The photodiode cutoff frequency, defined as the IF at which the available mixer conversion gain is 3 dB down from its low-frequency value, is given by (Appendix I)

$$f_c = \frac{(1 + R_s G_D)^{1/2}}{2\pi C_D (R_s/G_D)^{1/2}} \approx \frac{G_D^{1/2}}{2\pi C_D R_s^{1/2}}, \qquad R_s G_D \ll 1 \tag{2}$$

where

R_s photodiode series resistance,
C_D photodiode junction capacitance.

If the available conversion gain is sufficiently large, the receiver sensitivity will remain nearly quantum noise limited even beyond the mixer cutoff frequency as has been demonstrated previously in extrinsic Ge:Cu mixers [3]. The receiver sensitivity is given by

$$\text{NEP} = \frac{h\nu B}{\eta} + \frac{k(T_M + T'_{\text{IF}})B}{G} \tag{3}$$

where

NEP noise equivalent power for SNR of 1, W,
B IF bandwidth,
T_M physical temperature of mixer,
T'_{IF} effective input noise temperature of IF amplifier.

As the first term on the right-hand side of (3) shows, the reverse-biased photovoltaic mixer has a quantum-noise sensitivity limit, which is a factor of 2 better than photoconductive mixers [3], [4, ch. 10].

The required LO power is obtained by combining (2) and (3) and using $I_0 = \eta q P_{\text{LO}}/h\nu$:

$$\frac{\text{NEP}}{B} = \frac{h\nu}{\eta}\left[1 + \left(\frac{2k(T_M + T'_{\text{IF}})G_D}{q}\right)\left(\frac{h\nu}{\eta q P_{\text{LO}}}\right)\right]. \tag{4}$$

The last term in (4) establishes an engineering criterion for the tradeoff between the fractional degradation in NEP as a function of LO power dissipation, using as parameters IF preamplifier characteristics T_M, G_D, and η. The calculated NEP is plotted in Fig. 2 as a function of applied LO power with η and $(T_M + T'_{\text{IF}})G_D$ as parameters. The optimum range for the applied LO power is dictated by considerations of sensitivity on one hand and of radiator cooler limitations on the other, and is indicated qualitatively in Fig. 2. As Fig. 2 shows, for $\eta = 30$ percent, $T_M = 100$ K, and an effective IF input noise temperature of $T'_{\text{IF}} = 140$ K, $G_D = 10^{-2}$ mho, NEP $\approx 6.8 \times 10^{-20}$ W/Hz, using an incident CO_2 LO power of 1.4 mW, corresponding to a photocurrent of 3.6 mA. These are favorable values.

It is instructive to recast (4) by defining a minimum detectable signal $P_{\text{min}} = h\nu/\eta$, available thermal noise power $P_{\text{th}} = k(T_M + T'_{\text{IF}})B$, and available shot noise power $P_{\text{sh}} = 2qI_0B$, to obtain in a manner similar to the photoconductive heterodyne receiver [3]:

$$\frac{\text{NEP}}{B} = P_{\text{min}}\left(1 + \frac{P_{\text{th}}}{P_{\text{sh}}}\right). \tag{5}$$

For best receiver sensitivity, the LO-induced shot noise is fixed to be much greater than the thermal noise so that

$$\frac{\text{NEP}}{B} \approx P_{\text{min}} = \frac{h\nu}{\eta}.$$

To obtain the desired infrared sensitivity, power dissipation, and other receiver performance goals, the following parameters must be considered:

130.4

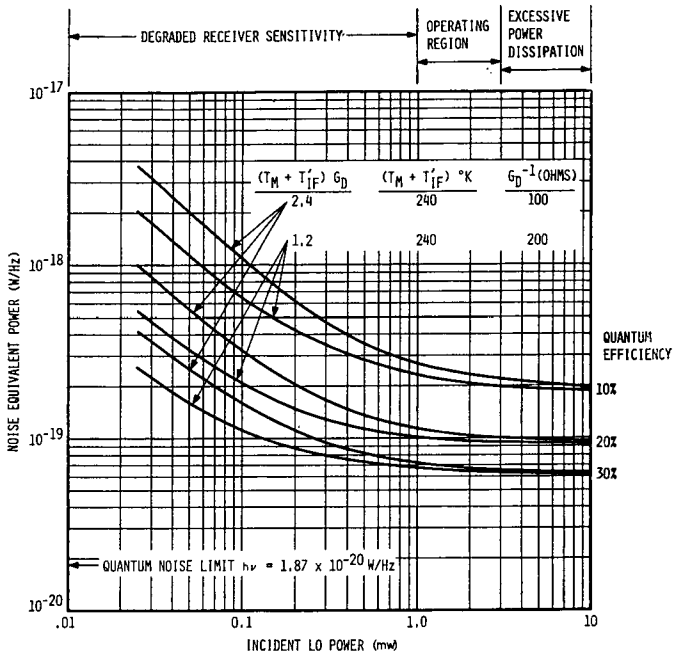

Fig. 2. Calculated receiver NEP versus incident LO power with quantum efficiency as parameters.

Parameter	Principal Constraint
T_M, P_{LO}, P_{dc}	spacecraft radiation cooler
G_D, C_D, R_s, f_c, η	detector
T'_{IF}, R_L, R_{IF}	electronics

The following values illustrate the results of a sample receiver design, the values of which were closely approached in practice (Section V):

effective IF input noise temperature T'_{IF}	148 K,
mixer temperature T_M	100 K,
$k(T_M + T'_{\text{IF}})$	3.42×10^{-21} W/Hz,
quantum efficiency	22 percent,
P_{min}	8.5×10^{-20} W/Hz,
G_D^{-1}	100 ohms,
f_c	200 MHz,
P_{LO}	2 mW,
mixer gain G	−5.3 dB,
thermal noise contribution	1.16×10^{-20} W/Hz,
NEP	9.7×10^{-20} W/Hz.

V. Infrared Mixer Measurements

A variety of measurements were carried out using both a homodyne and a heterodyne test setup. Two single-frequency cervit-cavity CO_2 lasers are employed that serve as signal and LO sources, respectively. They deliver about 1 W CW each, operate on the same vibrational rotational line, and are locked in frequency at the desired IF offset, for example, 30 MHz, by sampling the laser outputs by two beam splitters and mixing them in a separate p-type PC-HgCdTe detector. A 30-MHz discriminator generates an error signal, which is fed to the

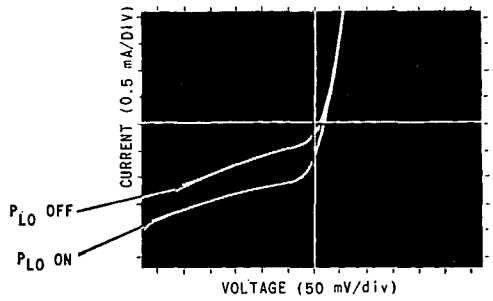

Fig. 3. Current–voltage characteristic of PV-HgCdTe mixer.

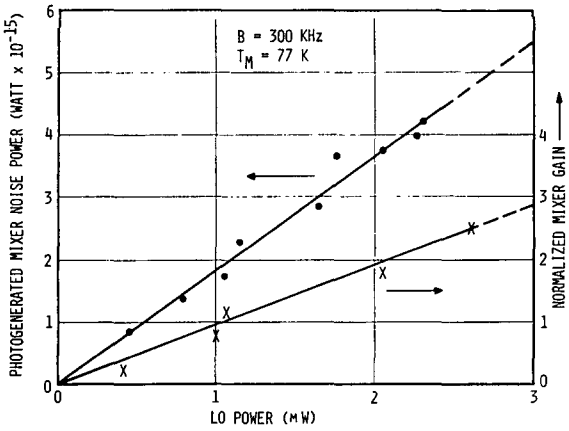

Fig. 4. Photogenerated shot noise and conversion gain versus LO power in HgCdTe photodiode.

piezoelectric tuning stack of one of the lasers. Other IFs were conveniently generated by adding an RF mixer and injecting an appropriate RF signal into the AFC loop. The main LO and signal beams illuminate the mixer element and are shaped individually by means of appropriate irises and lenses to obtain the desired diffraction-limited illumination.

A key consideration in receiver evaluation is the measurement of absolute infrared signal power. This was done by a substitution method whereby a high-reflectance mirror is inserted in the signal path to deflect the signal radiation to a room-temperature bolometer having a broad spectral response. The bolometer responsivity was calibrated using both a 500 K blackbody source and a thermopile. To ensure accuracy, the bolometer was located in the same focal plane as the mixer. To eliminate errors due to nonuniform illumination, the bolometer is physically smaller than the mixer and a relatively broad signal beam is employed.

A. Receiver Noise

For quantum-noise-limited operation, the mean-square shot noise current induced by the absorbed LO power must significantly exceed the sum of all other mean-square noise currents [(5), (16)]. This condition was achieved by proper infrared mixer and preamplifier design. The various noise contributions that had to be considered are discussed in the following.

1) Induced Shot Noise: The I–V characteristic of an HgCdTe diode, given in Fig. 3, shows an induced mixer current of about 0.5 mA when LO power is applied to the mixer element with only a small change in reverse dynamic resistance.

As expected from the analysis, the LO-induced shot noise varied essentially linearly with applied LO power for the case where G_D and η are independent of P_{LO} [(14), Fig. 4]. At higher IFs, the induced shot noise rolls off at 6 dB/octave due to the RC-limited frequency response of the HgCdTe photodiode.

2) Thermal Noise: The receiver thermal noise is determined by T_M, T'_{IF}, and Johnson noise due to load resistor R_L, if any. The preamplifier typically provides 25 dB of gain with an effective input noise temperature of 148 K ($F'_{IF} \sim 1.8$ dB) over an extended range of frequency and input impedances.

3) 1/f Noise: Since the mixer is normally operated with reverse bias, higher values of $1/f$ noise can be expected than for incoherent detection. The mean-square $1/f$ noise current falls off with increasing IF and decreasing bias current as given by [16]

$$\overline{i^2}_{1/f} = \frac{AI^2B}{f} \tag{6}$$

where

I dc bias current,
A proportionality factor, which includes mixer volume,
B bandwidth.

For heterodyne applications where the IF is normally in the megahertz range, the $1/f$ noise component can be expected to be negligible compared to other noise contributions.

4) Measured Data: The measured output noise voltage versus frequency is shown in Fig. 5. with reverse-bias voltage as the parameter. For the case where $P_{LO} = 0$ (no shot noise) and $V_B = -0.275$ V, the $1/f$ noise voltage rolls off at 3 dB/octave as expected from (6) and falls below receiver thermal noise voltage at approximately 3.5 MHz. As Fig. 5 indicates, the introduction of LO power increases the receiver noise level by a factor of about 6 (7.75 dB). Thus, for $P_{LO} \neq 0$ and the same bias voltage ($V_B = -275$ V), the IF noise voltage falls below the receiver (thermal plus shot) noise voltage at a lower frequency, that is, 60 kHz.

B. Mixer Conversion Gain

Measurements of the mixer conversion gain at an IF of 35 MHz are shown in Fig. 4. The results are consistent with (1). The mixer gain was found to increase linearly with LO-induced photocurrent (which is proportional to absorbed LO power).

C. Noise Equivalent Power

Mixer sensitivity measurements were made as a function of LO power and temperature with uniform-field

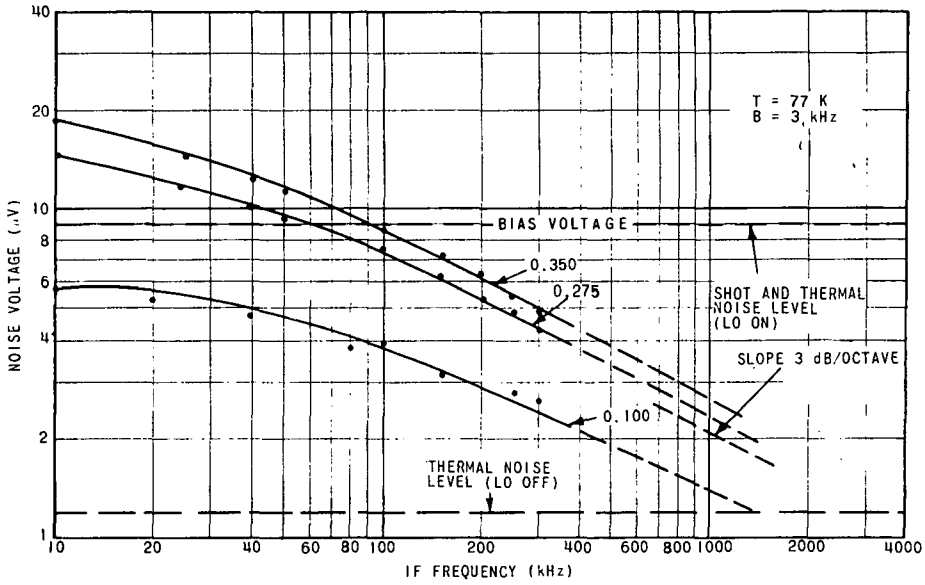

Fig. 5. Noise spectrum of PV-HgCdTe mixer.

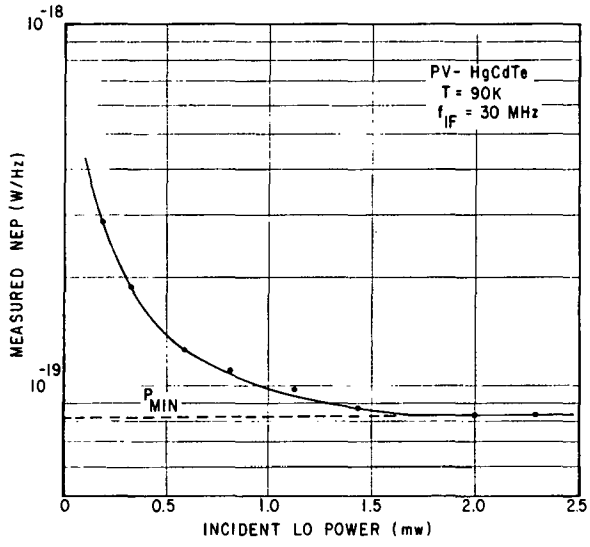

Fig. 6. Measured receiver NEP versus LO power.

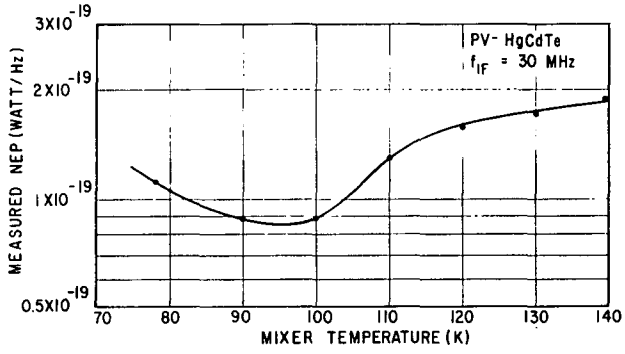

Fig. 7. Measured NEP versus mixer temperature.

plane-wave optical spots to ensure uniform energy distribution over the mixer surface. The NEP value thus obtained was within 1 dB of that obtainable with an optimumly focused beam (Appendix II).

Noise equivalent power at 30 MHz, as a function of LO power, is shown in Fig. 6 for T_M = 90 K. Use of LO power of 1.7 mW resulted in quantum-noise-limited operation with an NEP = 8.2×10^{-20} W/Hz. This value includes second-stage contributions, as well as losses in the antireflection-coated germanium entrance window of the mixer element. This NEP is reasonably consistent with a measured quantum efficiency at T_M = 90 K of about 22 percent.

Measured NEP at 30 MHz as a function of mixer temperature is shown in Fig. 7. The measured NEP was below 10^{-19} W/Hz for temperatures from 82 to 104 K, and below 2×10^{-19} W/Hz for all temperatures from 77 to 140 K. The absence of substantial NEP degradation at the higher temperatures is due in large part to the use of a mixer element having its peak spectral response at 12.7 μm at 77 K. As a result, the quantum efficiency increases at the higher temperatures due to shift of peak response toward 10.6 μm.

Another important parameter in obtaining low NEP values is maintaining reasonable values of dynamic mixer conductance to as high a temperature as possible. The dynamic resistance (G_D^{-1}) varied from 80 ohms at 77 K to 175 ohms at 140 K. Therefore, an IF preamplifier having a reasonably simple impedance matching network will permit nearly quantum-noise-limited operation over an extended temperature range.

Measurements of NEP for values of laser frequency offset from 15 to 45 MHz resulted in a constant value of NEP indicating that the mixer response exceeded 60 MHz.

D. Mixer Frequency Response

Due to the limited tuning range of the CO_2 laser, for measurement beyond 50 MHz, a noise-spectrum measurement technique was used similar to the one used for photo-

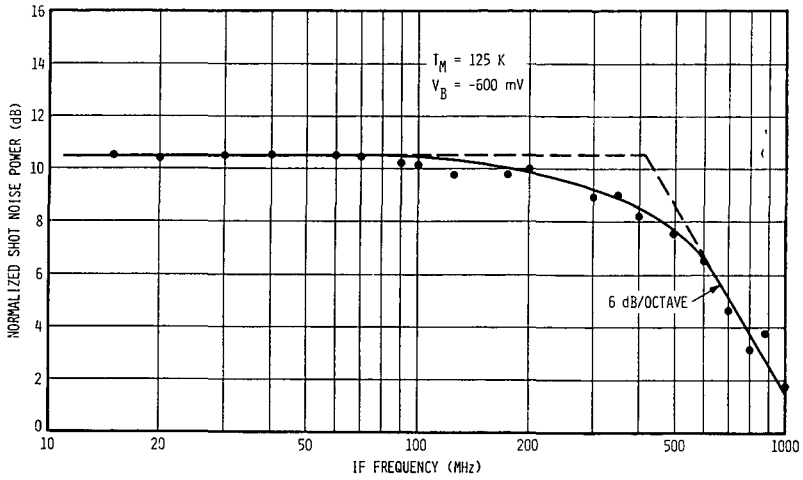

Fig. 8. Shot noise spectrum of HgCdTe photodiode.

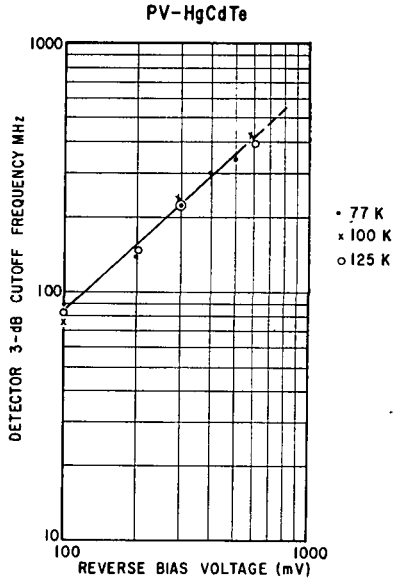

Fig. 9. Cutoff frequency versus bias voltage for HgCdTe photodiode.

conductive mixers [3]. The shot and thermal noise power are measured as a function of frequency. From these measurements, the receiver sensitivity can be inferred as shown in (5). The roll-off in shot noise then defines the mixer frequency response. The theoretical slope of the mixer roll-off is 6 dB/octave [(12)]. The spread in measured data was sufficiently small that the uncertainty in the cutoff frequency was estimated to be no greater than ±20 MHz. The resultant shot noise power spectrum is shown in Fig. 8. It was concluded that the 3-dB cutoff frequency of the particular HgCdTe photodiode was about 425 MHz under the measurement conditions $I_0 = 1.7$ mA and $V_B = -0.6$ V, values which are representative conditions of mixer operation. The roll-off experimentally observed is seen to closely approach the expected value of 6 dB/octave.

Measurements of the mixer cutoff frequency as a function of reverse-bias voltage is shown in Fig. 9 for mixer temperatures of 77, 100, and 125 K. The cutoff frequency versus bias voltage data fell on a straight line in the logarithmic plot and were essentially independent of temperature over the measured temperature range. For an ideal photodiode, G_D is independent of bias voltage, although in practice it may increase with V_B. For linear-graded and step-diffused junctions, C_D varies as V^{-n}, where $n = 1/2$ and $1/3$, respectively. Measurements on 2.5-μm HgCdTe photodiodes showed $n = 1/2$ dependence [17]. It was concluded that the diode frequency response was limited by the RC constant of the junction proper, rather than by the external-circuit transit-time limitations or diffusion effects [18]–[20].

VI. Conical Scanner

For station-to-station two-way communications, in order to maintain the local receive and transmit optics pointed toward each other, a means of generating tracking-error voltages must be employed. Although such systems are in existence for incoherent infrared detection systems, none had been demonstrated for coherent applications. In analogy to microwave systems [21], monopulse or conical-scan tracking techniques are potentially suitable. The use of a coherent infrared amplitude-sensing monopulse was considered [22]. However, the limitations on spacecraft complexity and cooling capacity precluded the use of a four-element mixer array. Therefore, the application of a conical scanner to an infrared heterodyne receiver was investigated and successfully tested. The two-laser heterodyne setup was modified to include a two-axis nutator, generating a 100-Hz circular scan. The 30-MHz IF output is amplified, detected, and fed to two phase detectors operating in quadrature to yield horizontal and vertical tracking error signals using a phase reference from the nutator driver (see Fig. 1). The field of view and hence the Airy disk of the receiver signal beam has an offset with respect to the boresighted nutation axis [Fig. 10(a)]. The LO beam is stationary.

With the target on boresight there is in principle no 100-Hz amplitude modulation superimposed on the IF signal. In practice, some AM is present due to mixer surface nonuniformity and other nonideal conditions [Fig.

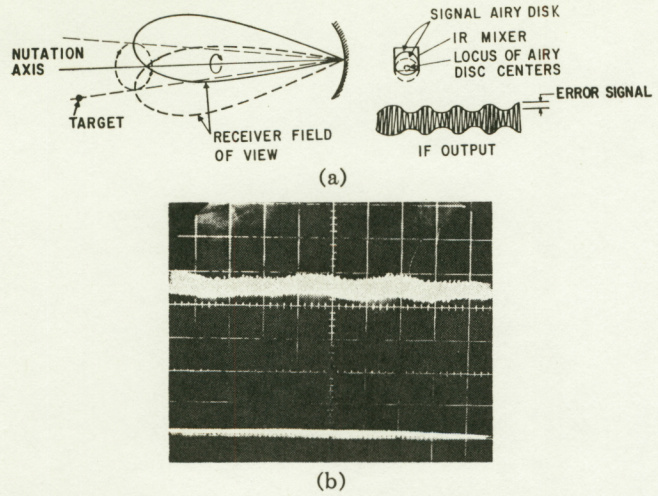

Fig. 10. Conical scan tracking for infrared heterodyne receiver. (a) Error-signal generation. (b) Detected IF signal.

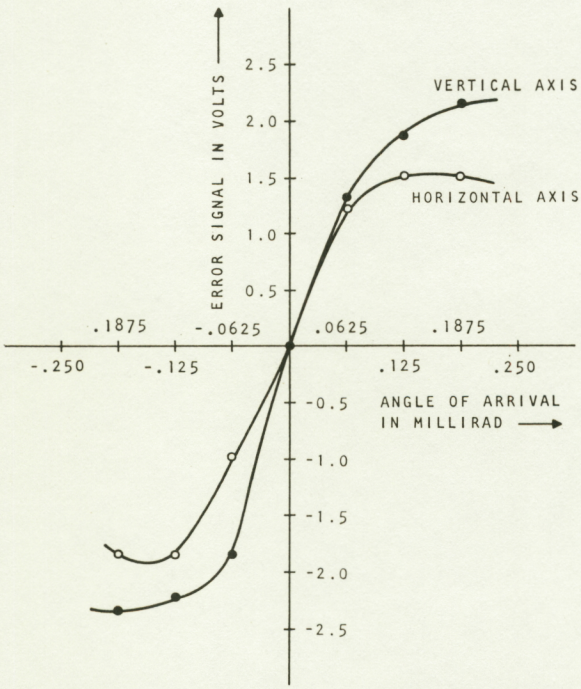

Fig. 11. Tracking-error voltage versus infrared signal angle of arrival.

10(b)], and is removed from the FM signal demodulation channel by the limiter. For the case of an off-axis target, north/south and east/west error voltages of appropriate polarity are generated to correct the pointing error. A nutation angle to decrease the signal level by 1 dB appeared to be a reasonable compromise to obtain sufficient tracking-error voltages. Fig. 11 shows the tracking-error S curve that was obtained. The difference in slope of horizontal and vertical error is due to gain a differential difference between the two channels.

VII. Acquisition

The uncertainty in attitude and position of the two stations requires an acquisition sequence whereby the optics in the two transceivers are aligned within some

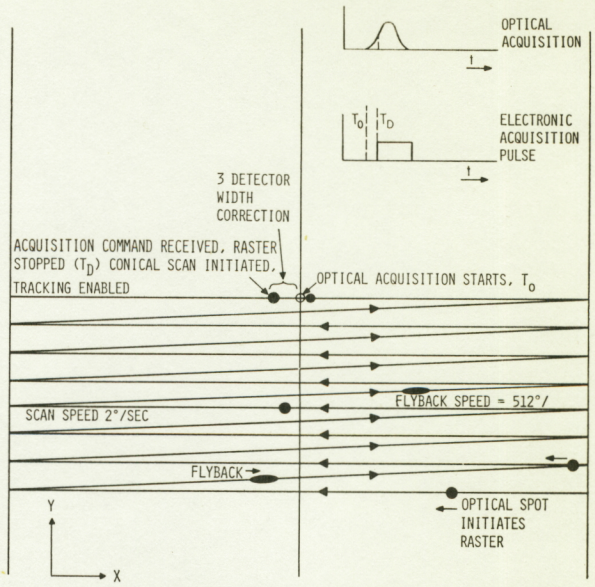

Fig. 12. Receiver acquisition search sequence.

specified time interval. The spatial search to achieve acquisition can take the form of an x–y raster scan pattern by the receiving optics of one station, while the transmit beam of the other station is broadened sufficiently to ensure illumination of the receive station consistent with uncertainty of location and attitude [10], [23]. The receiver acquisition channel's bandwidth is reduced to maintain a usable SNR in the presence of reduced signal level caused by transmit beam broadening. A matched filter following an AM detector is used to maximize SNR when acquisition is obtained by the receiver scanning optics sweeping through the transmit signal beam.

The acquisition sequence of the receiver is shown in Fig. 12 and was demonstrated in the laboratory. On receiving an acquisition encounter pulse, whose amplitude exceeds the predetermined comparator threshold, the raster scan is terminated and the 100-Hz conical scan is initiated. There is an overshoot of about three detector spot sizes, corresponding to 15 digital addresses, in the x-scan direction. The amount of overshoot depends on time constants within the required receiver and on the signal amplitude relative to the acquisition threshold setting. This overshoot is corrected by readdressing after acquisition. A 200-Hz dither modulation can be superimposed on one axis of the conical scan to generate an acquisition confirm signal. When acquisition is complete, the 100-Hz conical scan remains to maintain transmit/receive spatial tracking (Section VI).

Probability of encounter measurements were carried out by introducing 20 pulses into the IF channel over a 10-s interval. The probability of generating an encounter pulse was then measured as a function of encounter threshold voltage (V_T) for several SNRs. As Fig. 13 shows, V_T must be lowered as the SNR is reduced in order to maintain a given probability of encounter. For V_T = 1.5 V and SNR = −16 dB and larger (referenced

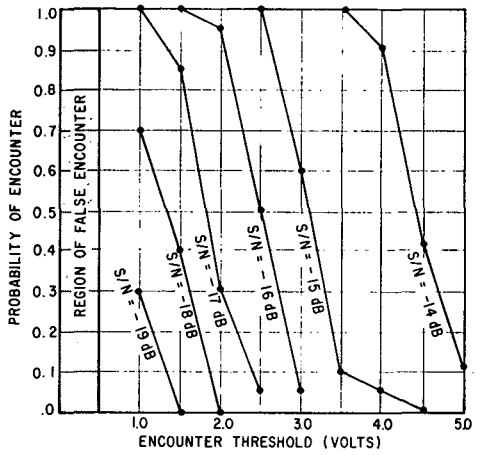

Fig. 13. Probability of encounter versus threshold level with IFSNR as parameter.

to the IF bandwidth), the probability of encounter is 1. For SNR = −17 dB, the probability of encounter is 0.85, and for SNR = −18 dB, the probability of encounter drops to 0.40. For a threshold setting of 0.5 V, baseline noise generates erroneous encounter pulses by false triggering of the threshold detector. From Fig. 13, a threshold voltage near 1 V is desired.

VIII. Signal-Processing Electronics

This section gives results on several portions of the signal-processing electronics of particular interest for the laser communication application.

A. Discriminator

The desired discriminator linearity is obtained by following the design procedure for a Foster–Seeley balanced discriminator. The Q of the tuned circuits and separation of the tuned frequencies are chosen to control the width and linearity of the discriminator characteristic. The two resonant circuits were separated by 29 MHz, resulting in a discriminator design of unusually wide fractional bandwidth [Fig. 14(a)]. The linearity of an input power level of +4 dBm is better than 2 percent from 24 to 36 MHz. There is very little degradation of linearity when the input power level changes ±1 dB, a change that is larger than expected since the limiter and automatic gain control circuits hold the power level constant to less than ±0.5 dB.

B. Nonlinear Phase Response

Nonlinear phase characteristics in any component will result in signal distortion and can be described by group-delay or envelope-delay distortion represented by a truncated Taylor series:

$$t(f) = t_0 + K_1 f + K_2 f^2 + t_r(f) \qquad (7)$$

where K_1 and K_2 are the linear and parabolic components of group-delay distortion, often given in ns/MHz, and ns/MHz^2, respectively.

The residual group-delay component $t_r(f)$ is generally given as a peak-to-peak value in nanoseconds. Fig. 14(b)

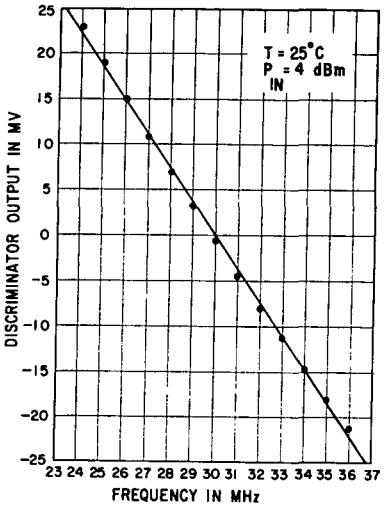

(a)

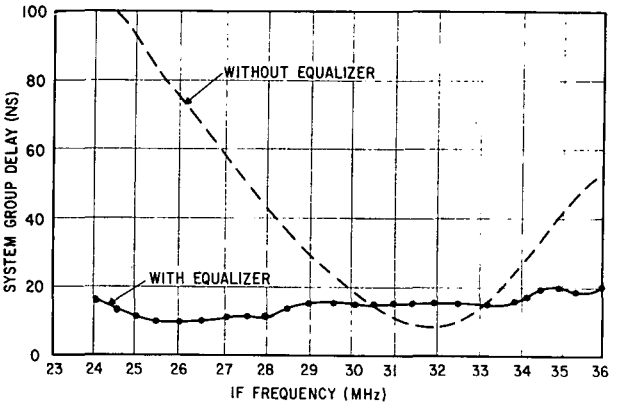

(b)

Fig. 14. Characterstics of signal processing components.

shows the measured group delay of ±50 ns/12 MHz for the IF and video channel (excluding the infrared mixer) without equalization. The amplifying circuits (preamplifier, postamplifier, and video amplifier) are all very broad-band so that their phase characteristics are very linear. The limiter is sufficiently linear so that its group-delay distortion is less than 1 ns/MHz. However, the phase characteristics of the filters require equalization. As a result of delay equalization, a group delay of ±5 ns/12 MHz was obtained, as shown in Fig. 14(b).

IX. Results and Conclusions

The design of a high-sensitivity wide-bandwidth 10.6-μm heterodyne receiver for space and ground operational use has been established, and key receiver elements were demonstrated. The heterodyne receiver was bread-boarded and tests were conducted in the communications, acquisition, and spatial tracking modes. The pertinent receiver characteristics are as follows:

sensitivity	less than 10^{-19} W/Hz from 82 to 104 K; less than 1.8×10^{-19} W/Hz from 77 to 140 K;

mixer temperature range	77 to 140 K;
mixer power dissipation	<10 mW;
spatial tracking	conical scanner;
IF bandwidth	3 to greater than 100 MHz, 30 ± 10 MHz selected;
group-delay distortion (FM format)	<±5 ns;
AFC tracking	±6 MHz.

An analysis and expressions have been presented for the engineering design of a quantum-noise-limited infrared receiver that uses a photovoltaic diode with finite dark conductance as the mixer element. The analysis considered such parameters as mixer characteristics, bias voltage, applied LO power, and mixer conversion gain.

Measurements on the bread-boarded receiver indicated that nearly quantum-noise-limited operation is achievable over a wide range of mixer temperature, IF, applied bias voltage, and incident LO power. The measurements demonstrate the suitability of this type of receiver for satellite-to-ground communication links, and the large frequency response of the HgCdTe mixer indicates the potential application of this type of receiver for a satellite-to-satellite communications link where large Doppler offsets are experienced [10].

Appendix I

Derivation of PV Mixer Design Equations

The analysis employs the same conversion gain approach used in the analysis of PC mixers [3], [4, ch. 10].

A. Available IF Signal Power

The equivalent circuit at IF for a PV infrared mixer consists of an ideal current source I_S in shunt with a leakage conductance G_D and junction capacitance C_D, and in series with a contact or material resistance R_S. The mixer analysis neglects any lead inductance that may be present.

The square of the peak IF signal current is given by

$$|I_S^2| = 4\left(\frac{\eta q}{h\nu}\right)^2 P_{sig} P_{LO} \tag{8}$$

where

- I_S peak IF signal current,
- ν signal frequency,
- η quantum efficiency,
- P_{sig} signal power,
- P_{LO} LO power $> P_{sig}$.

From the equivalent circuit, the ratio of the short-circuit current to the signal current is given by

$$\frac{I_{SC}}{I_S} = \frac{1}{(1 + G_D R_S) + j\omega C_D R_S} \tag{9}$$

where

- I_{SC} short-circuit current,
- G_D small-signal shunt conductance (slope of I–V curve),
- R_S series resistance,
- C_D shunt capacitance.

The real component of the output admittance is given by

$$G_{out}' = \frac{G_D + R_S(G_D^2 + \omega^2 C_D^2)}{(1 + G_D R_S)^2 + \omega^2 C_D^2 R_S^2}. \tag{10}$$

For most PV mixer elements $G_D R_S \ll 1$, so that

$$G_{out}' \approx \frac{G_D + \omega^2 C_D^2 R_S}{1 + \omega^2 C_D^2 R_S^2}. \tag{11}$$

The available output power from the PV mixer is

$$P_{IF\,(available)} = \frac{|I_{SC}|^2}{8G_{out}'} = \frac{|I_S|^2}{8[G_D(1 + G_D R_S) + \omega^2 R_S C_D^2]}. \tag{12}$$

The output power is 3 dB down at an IF given by

$$f_c = \frac{(1 + R_S G_D)^{1/2}}{2\pi C_D (R_S/G_D)^{1/2}} \approx \frac{1}{2\pi C_D (R_S/G_D)^{1/2}}. \tag{13}$$

B. Noise

The overall mean-square noise current generator is given by

$$\overline{i_N^2} = \overline{i_G^2} + \overline{i_{IF}^2} + \frac{\overline{I_S^2}}{(1 + G_S R_S)^2 + (f/f_c)^2 R_S G_D} \tag{14}$$

where

- $\overline{i_G^2}$ mean square thermal noise current, $= 4kT_m BG'_{out}$,
- $\overline{i_{IF}^2}$ mean square IF amplifier noise current, $= 4kT'_{IF} BG'_{out}$,
- $\overline{i_S^2}$ mean square shot noise current, $\approx 2qI_0 B$ for $f_{IF} < 1/(8T_r)$,
- k Boltzmann's constant,
- T_m physical temperature of mixer,
- B IF bandwidth,
- T'_{IF} effective input noise temperature of IF amplifier, which is a function of its source impedance,
- I_0 LO-induced dc photocurrent,
- T_r carrier transit time.

C. Mixer Gain

The available PV mixing gain, that is, the ratio of the available IF output power to the available infrared signal power, is given by

$$G = \frac{P_{IF\,(available)}}{P_{sig}} = \frac{|I_S|^2}{8P_{sig}[G_D(1 + G_D R_S) + \omega^2 R_S C_d^2]} \tag{15}$$

which can be written as

$$G = \frac{(\eta q/h\nu)^2 P_{LO}}{2[G_D(1 + G_D R_S) + \omega^2 R_S C_d^2]}. \tag{16}$$

For PV mixer $\tau/T_r = 1$. Therefore under the condition that $P_{LO} \gg P_{sig}$, the dc photocurrent is given by

$$I_0 = \frac{\eta q}{h\nu}\left(\frac{\tau}{T_r}\right)P_{LO} = \frac{q}{h\nu}\eta P_{LO}. \tag{17}$$

Combining these equations for $R_S G_D \ll 1$

$$G \approx \frac{\eta q I_0}{2h\nu G_D}\frac{1}{1+(f/f_c)^2}. \tag{18}$$

The available conversion gain is 3 dB down at an IF (f_c) previously defined.

It is interesting to note that the conversion gain varies with LO power through its effect on the photocurrent I_0.

D. Signal-to-Noise Ratio

The signal-to-noise ratio for the PV mixer is

$$\frac{S}{N} = \frac{|I_{SC}|^2}{2i_N^2}. \tag{19}$$

Substituting expressions for the noise current and the short-circuit current gives

$$\frac{S}{N} = \frac{(\eta q/h\nu)P_{sig}I_0}{I_0 qB + 2k(T_m + T'_{IF})B[G_D(1+R_S G_D) + \omega^2 R_S C_D{}^2]}. \tag{20}$$

Thus, the NEP, that is, the value of signal power to give an IF signal-to-noise ratio equal to unity, is

$$\text{NEP} = \frac{h\nu B}{\eta}\left\{1 + \frac{2k(T_m + T'_{IF})}{qI_0}\cdot[G_D(1+R_S G_D) + \omega^2 R_S C_D{}^2]\right\}. \tag{21}$$

This is reducible to

$$\text{NEP} = \frac{h\nu B}{\eta} + \frac{k(T_m + T''_{IF})B}{G} \tag{22}$$

which is the same expression as that derived for the PC mixing case [3], [4, ch. 10], with the exception of the factor of 2 in the quantum-noise term due to the generation-recombination noise in photoconductors.

Appendix II

Optimum LO Illumination

The NEP measurements reported were carried out with nearly plane-wave signal and LO illumination. Calculations were carried out on the optimum LO illumination for the case in practice where the Airy disk of the receive beam matches the diameter of the sensitive area of the mixer. The results are shown in Fig. 15 as a function of LO beam displacement from boresight with LO-beam f number as the parameter. Such a computation is of importance to minimize the heat load on the spacecraft radiation cooler due to LO power spillover. The case of plane-wave LO illumination (curve A) minimizes physical tolerance requirements in the LO but results in maximum LO power requirement and heat load. On the other hand, the case of an exact match of the LO and signal phase fronts (curve B) maximizes SNR and minimizes heat load, but creates LO alignment problems, and the improvement in SNR is only 1 dB, relative to curve A, for zero offset. The case of the LO beam 1.5 to 2 times the diameter of the signal beam appears to be a good engineering compromise (curve C) by combining good SNR, low heat load, and reasonable design tolerances.

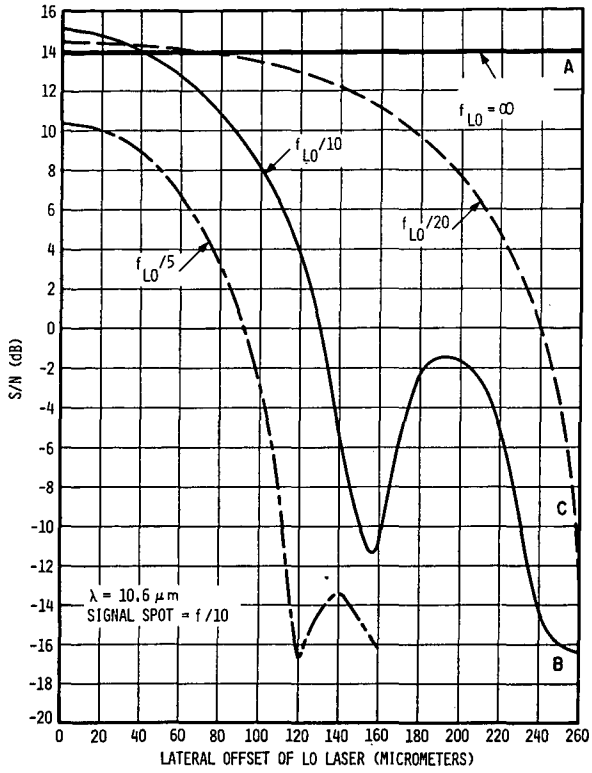

Fig. 15. Heterodyne signal-to-noise ratio as function of lateral displacement of LO laser beam in focal plane with f number of LO beam as parameter.

Acknowledgment

M. Aita and R. Cardwell of AIL contributed to the reported measurements.

References

[1] H. Melchior, M. B. Fischer, and F. R. Arams, "Photodetectors for optical communication systems," *Proc. IEEE*, vol. 58, pp. 1466–1486, Oct. 1970.
[2] H. W. Mocker, "A 10.6 μm optical heterodyne communication system," *Appl. Opt.*, vol. 8, pp. 677–684, Mar. 1969.
[3] F. R. Arams, E. W. Sard, B. J. Peyton, and F. P. Pace, "Infrared 10.6-micron heterodyne detection with gigahertz IF capability," *IEEE J. Quantum Electron.*, vol. QE-3, pp. 484–492, Nov. 1967.
[4] A. Beer and R. Willardson, Eds., *Infrared Detectors, Semiconductors and Semimetals*, vol. 5. New York: Academic, 1970.
[5] M. Teich, R. Keyes, and R. Kingston, "Optimum heterodyne detection at 10.6 microns in photoconductive Ge:Cu," *Appl. Phys. Lett.*, vol. 9, pp. 357–360, Nov. 1966.
[6] C. Buczek and G. Picus, "Heterodyne performance of mercury-doped germanium," *Appl. Phys. Lett.*, vol. 11, pp. 125–126, Aug. 1967.
[7] M. C. Teich, "Infrared heterodyne detection," *Proc. IEEE*, (Lett.), vol. 56, pp. 37–46, Jan. 1968.
[8] B. Peyton, E. Sard, R. Lange, and F. R. Arams, "Infrared 10.6-μm photodiode heterodyne detection," *Proc. IEEE*, vol. 58, pp. 1769–1770, Oct. 1970.
[9] E. D. Hinkley, T. C. Harman, and C. Freed, "Optical heter-

odyne detection at 10.6 μm of the beat frequency between a tunable $Pb_{0.88}Sn_{0.12}Te$ diode laser and a CO_2 gas laser," *Appl. Phys. Lett.*, vol. 13, pp. 49–51, July 1968.
[10] J. McElroy, N. McAvoy, H. Richard, T. McGunigal, and G. Schiffner, "Carbon dioxide laser communications systems for near-Earth applications," in *Proc. IEEE Int. Conf. Communications*, 1970, pp. 22-7–22-37.
[11] C. Vérié and J. Ayas, "$Cd_xHg_{1-x}Te$ infrared photovoltaic detectors," *Appl. Phys. Lett.*, vol. 10, pp. 241–243, May 1967.
[12] A. Sorrentino, "Infrared detectors, recent development at SAT," presented at the Infrared Symp., Malverne, England, Apr. 1969.
[13] J. Schmitt and E. Stelzer, "Temperature and alloy compositional dependences of energy gap of $Hg_{1-x}Cd_xTe$," *J. Appl. Phys.*, vol. 40, pp. 4865–4869, Nov. 1969.
[14] D. Breitzer, E. W. Sard, B. J. Peyton, and J. McElroy, "*G–R* noise for Auger band-to-band processes," *Infrared Phys.*, to be published.
[15] B. J. Peyton, "Infrared 10.6 μm heterodyne detection in p-type HgCdTe," presented at the Iris Detector Specialty Group Meeting, San Diego, Calif., Mar. 1971.
[16] K. M. van Vliet, "Noise in semiconductors and photoconductors," *Proc. IRE*, vol. 46, pp. 1004–1018, June 1958.
[17] E. N. Figurovskii, P. S. Kireev, A. V. Vanyukov, Yu. V. Evseev, and A. P. Korovin, "Some properties of p–n junctions in $Cd_xHg_{1-x}Te$ solid solutions," *Sov. Phys.—Semicond.*, vol. 3, pp. 1572-1573, June 1970.
[18] J. R. Biard and W. N. Shaunfield, Jr., "A model of the avalanche photodiode," *IEEE Trans. Electron Devices*, vol. ED-14, pp. 233–238, May 1967.
[19] C. Vérié and M. Sirieix, "Gigahertz cutoff frequency capabilities of CdHgTe photovoltaic detectors at 10.6 μm," this issue, pp. 180–184.
[20] I. Melngailis, T. C. Harman, E. D. Hinkley, and W. T. Lindley, "High speed $Hg_{1-x}Cd_xTe$ photodiode," presented at the Iris Detector Specialty Meeting, San Diego, Calif., Mar. 1971.
[21] M. I. Skolnik, *Introduction to Radar Systems*. New York: McGraw-Hill, 1962.
[22] F. P. Pace, R. A. Lange, B. J. Peyton, and F. R. Arams, "Spatially coherent array technology for wide-band infrared heterodyne receivers," this issue, pp. 246–252.
[23] T. McGunigal, J. McElroy, and N. McAvoy, NASA Goddard Space Flight Center, and B. Walker, R. Wong, and J. Cernius, Aerojet General Corp., private communication.

APPENDIX B
PHOTOMIXER HOUSING

A photomixer housing/coaxial adapter was designed and developed jointly by AIL and the photomixer manufacturer on a previous NASA sponsored program. The combined engineering effort resulted in a unit (Figure B-1) which considered such factors as:

- Hermetic sealing
- Thermal conductivity
- Transmission efficiency (at 10.6 micrometers)
- Size and weight
- Accurate location of mixer element
- Frequency response
- LO heating
- Coaxial output
- RFI immunity
- Environmental requirements

This appendix summarizes measurement data on the prototype photomixer housing.

A. ENVIRONMENTAL TESTS

A series of environmental tests have been carried out on the photomixer housing. For example: (1) 50 thermal shock cycles between -196^{o}C (liquid nitrogen temperature) and 30^{o}C were carried out, (2) normal (12 g) and reinforced (50 g) vibration levels were applied to the photomixer housing, and (3) a storage test at 60^{o}C was performed for 62 hours. At the conclusion of the environmental tests no physical damage was observed and the leak rate of the photomixer housing was measured to be less than 10^{-10} atm cm^3 sec^{-1}.

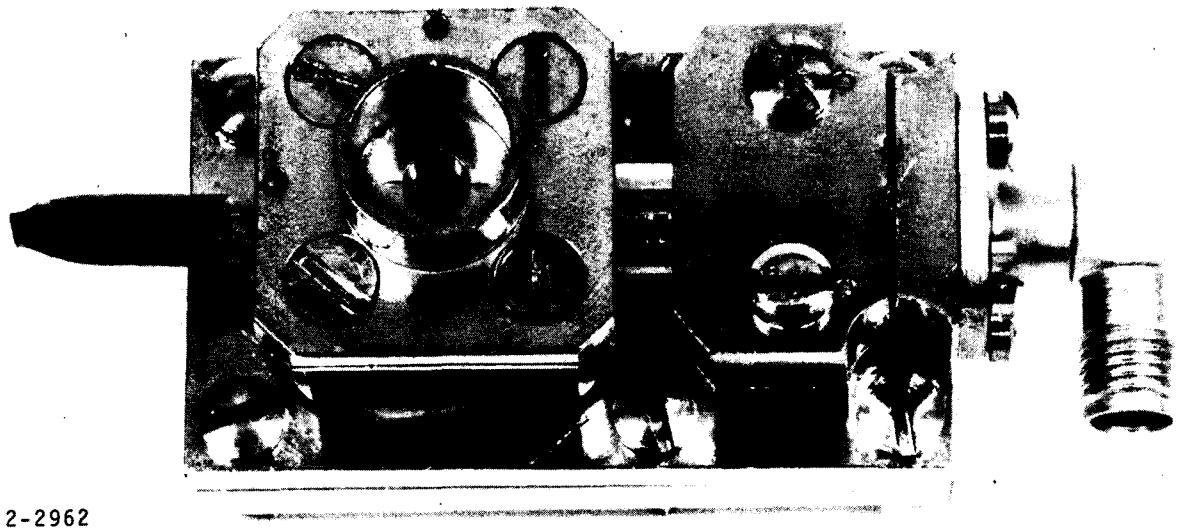

2-2962

FIGURE B-1. PHOTOMIXER HOUSING WITH COAXIAL ADAPTER

B. RFI IMMUNITY TESTS

A series of RFI immunity tests were conducted on the photomixer housing for the case of: (1) the photomixer housing mounted directly to a conducting plate and (2) the photomixer housing suspended one foot above a conducting plate.

The measured RFI data is summarized in Tables 1 and 2. Initial measurements were made for an RF level of 1 V/m generated by an antenna located 1 m from the housing under test. In general, no pickup exceeded the ambient level of the test receiver. The field intensity was then increased and the antenna was moved to within 1/2 m of the mount. The level of field intensity given in Tables 1 and 2 is the scaled value based on the power applied to the antenna.

TABLE B-1. SHIELDING EFFECTIVENESS OF PHOTOMIXER HOUSING

(Housing Bonded to Plate)

Frequency (MHz)	Polarization	Field Intensity V/m	Leakage 50 Ohm Receiver dBμV
20	V and H	1 to > 2.9	< -15
40	V and H	1 to > 2.4	< - 5
80	V and H	1 to > 10	< - 6
180	V and H	1 to > 17	< - 6
320	-	1 to > 20	< 6
500	-	1	< 11
500	-	> 4.7	17
600	-	1 to 13	< 9
1000	-	1	< 16
1000	-	> 8	31

TABLE B-2. SHIELDING EFFECTIVENESS OF PHOTOMIXER HOUSING

(Housing Suspended One Foot Above Plate)

Frequency (MHz)	Polarization	Field Intensity V/m	Leakage 50 Ohm Receiver dBμV
20	V and H	1 to > 3	< - 6
40	V and H	1 to > 2.4	< - 6
80	V and H	1 to > 11	< - 6
180	V and H	1 to > 17	< - 6
320	-	1	12
320	-	> 20	18
500	-	20	10
500	-	> 4.6	16
600	-	1	14
600	-	> 13	26
1000	-	1	15
1000	-	> 8	37

Probing measurements with a small loop antenna at 180 MHz, with the mount bonded to the table, indicated that the major areas of leakage in the photomixer housing were near connectors and coaxial cable braid. It should be noted that the cable used was RG9/U with an additional copper braid covering the cable and soldered over the connectors.

As shown in Table 2, the RFI leakage seemed to be greater when the detector mount was suspended above the table. At 320 MHz, the leakage was checked with the mount replaced by a 50-ohm termination. The leakage with the 50-ohm termination was 4 dB less than with the detector mount indicating that the mount was the major source of leakage.

The measured RFI leakage power of the photomixer housing as a function of frequency is given in Figure B-2. The mixer housing satisfies the requirements of MIL-STD-461 at frequencies up to 320 MHz (-100 dBm RFI level) and shows excellent RFI immunity (-92 dBm) out to 1 GHz.

C. HOUSING CUTOFF FREQUENCY MEASUREMENTS

The natural cutoff frequency of the photomixer housing was measured by measuring the VSWR at the coaxial output. The photomixer housing used for these measurements included a 50 resistive termination in place of the photomixer. An equivalent circuit for the photomixer housing is given in Figure B-3. The inductors are all short lengths of enameled wire having inductances of the order of nanohenries, the capacitors are strays associated with the proximity of the wires to ground planes and the capacitance of the hermetically sealed feedthrough ($\sim$ 2 pF). Measured VSWR data on the photomixer housing is given in Figure B-4. The housing

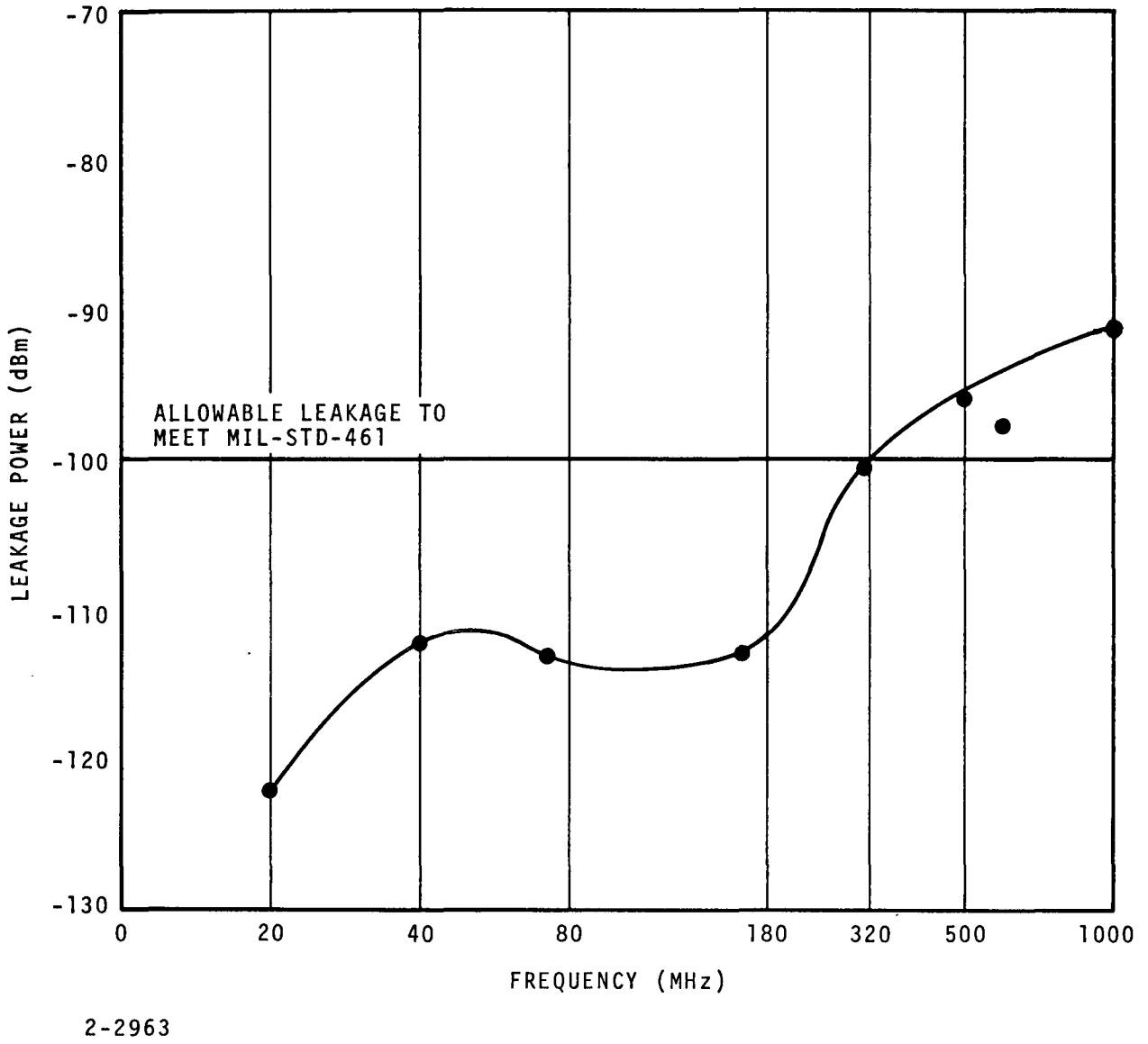

FIGURE B-2. MAXIMUM RFI LEAKAGE OF PHOTOMIXER HOUSING AS A FUNCTION OF FREQUENCY

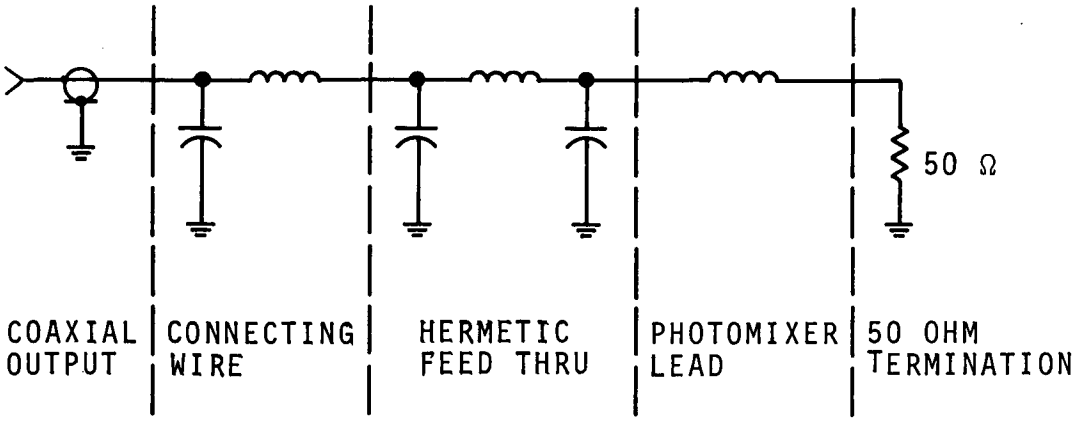

FIGURE B-3. EQUIVALENT CIRCUIT OF A PHOTOMIXER HOUSING

VSWR is approximately 1.4 up to 300 MHz and then rises to 1.75 at 900 MHz; a natural resonant frequency is obtained at 1300 MHz and above 1300 MHz the VSWR increases rapidly.

Based on the measurement data on the photomixer housing, it appears that it can be efficiently operated up to its design frequency of 1 GHz.

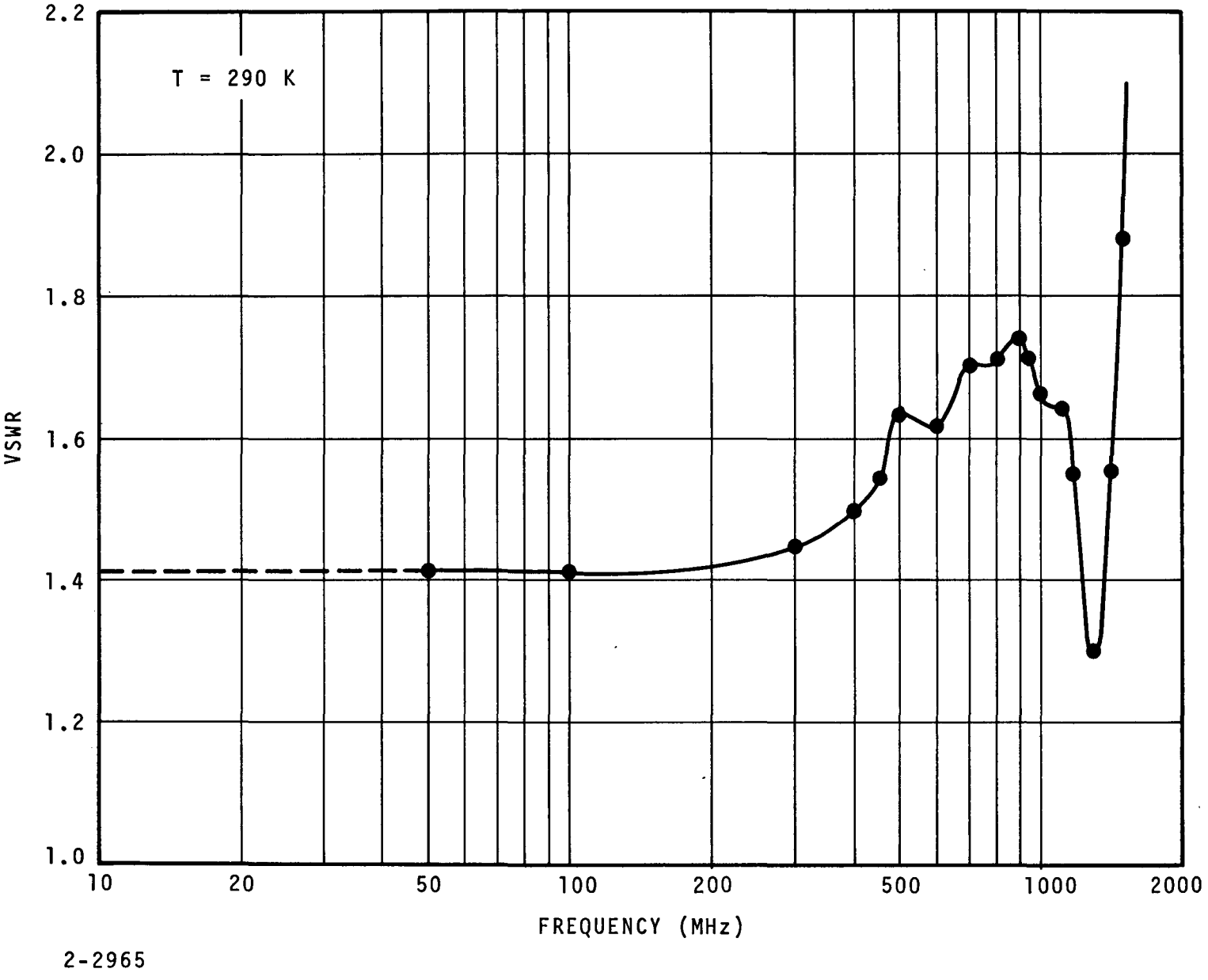

FIGURE B-4. MEASURED FREQUENCY RESPONSE OF A PHOTOMIXER HOUSING